GEO-3900

Master Thesis in Arctic Marine Geology & Geophysics

Late Cenozoic paleoenvironments in the Veslemøy High area, SW Barents Sea based on 3D- and 2D- seismic data

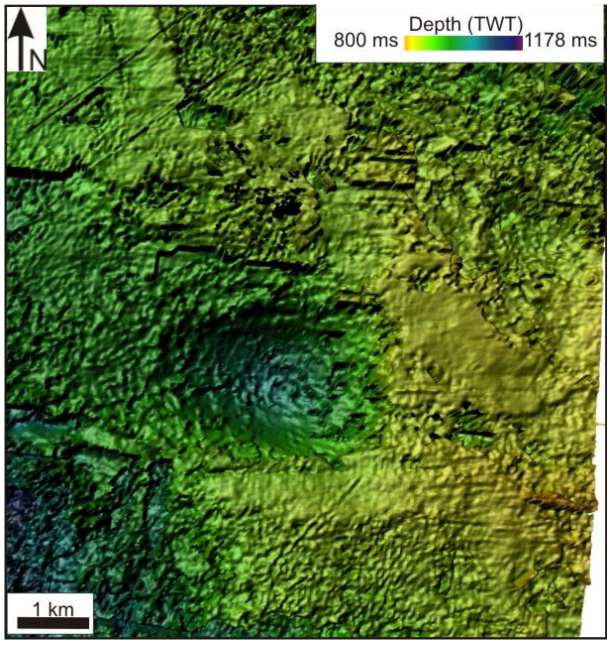

Jorge Sánchez-Borque

May 2009

Faculty of Science
Department of Geology

University of Tromsø

GEO-3900

Master Thesis in Arctic Marine Geology & Geophysics

Late Cenozoic paleoenvironments in the Veslemøy High area, SW Barents Sea based on 3D- and 2D- seismic data

Jorge Sánchez-Borque

May, 2009

ACKNOWLEDGE

First of all I want to express my gratitude to my supervisors Karin Andreassen and Jan Sverre Laberg for their comments, help and constructive criticism during this Master Thesis.

I also want to thank Monica Winsborrow and Lindsay Wilson for reading the manuscript and their corrections on the language and Carolina Pérez-García who has had a valuable input during the final stage of my work.

I have enjoyed the time I have spent with my fellow master students and PhD-students Gustav Pless, Iver Martens, Leif Egil Holbæk-Hanssen, Katarzyna Zamelczyna, Viktor Weibull and the rest of the students and staff at the “Brakka Sør” and especially to those who shared the office 9, Håkon, Birgit, Glennda and Matej.

Last but not least, I want to thank Christine, my fiancée, for convincing me that I could make it when I thought I could not and being there all the time, and also to my family who let me follow my dreams.

Tromsø 15.05.2009

Jorge Sánchez-Borque

Caminante, no hay camino,
se hace camino al andar.
Al andar se hace camino,
y al volver la vista atrás
se ve la senda que nunca
se ha de volver a pisar.

Wanderer, there is no road,
the road is made by walking.
By walking one makes the road,
and upon glacing behind
one sees the path that never
will be trod again.

Antonio Machado, Proverbios y Cantares XXIX, 1909

ABSTRACT

The aim of this master thesis has been to interpret the Late Cenozoic paleo-environments and the sedimentary processes in the Veslemøy High area, southwestern Barents Sea. Six seismic units and eight seismic unconformities, including the seafloor, are identified in the study area and correlated with previous work in the Sørvestnaget Basin. Submarine channels with a downslope (E-W) orientation suggest a glacimarine environment, i.e. the channels are inferred to have been formed by turbidity currents originating from glacial meltwater on the deepest reflector. On shallower reflectors, megascale glacial lineations, ridges and parts of hill-hole pairs indicate that grounded ice reached the paleo-shelf edge at least six times in the last 1.5 Ma. Moreover, two of the shallower seismic units show indications of sediment blocks that are inferred to have been subglacially eroded, transported and deposited by ice streams. The influence of the ice stream flowing from the Bjørnøyrenna in the last 330 ka is evident in the Veslemøy High; however, the origin of the ice streams is unclear on older paleo-surfaces.

INDEX

1. INTRODUCTION

1.1. Objectives

The main objective of this Master Thesis is to interpret the sedimentary processes and paleo-environments of the southwestern Barents Sea continental margin through the Late Plio-Pleistocene. The study is based mainly on a semiregional survey of three-dimensional (3D) seismic data supported by some industry two-dimensional (2D) seismic data. Previous studies in the area have revealed that the three main seismic reflectors, R1, R5, R7 (fig.1.1) can be correlated along the Western Barents Sea – Svalbard margin and separate the Plio-Pleistocene sediments into three main sediment packages (GI, GII, GIII; Faleide et al., 1996; Butt et al., 2000; Andreassen et al., 2008). The work on the 3D area has been carried out by interpreting the main regional reflectors (R1, R5 and R7) and four internal reflections in unit GIII and different 3D attributes maps have been used for the interpretation of the seismic units between the reflectors. Indicators of fluid migration and accumulation are observed in the seismic data; however, interpretation of such features is beyond the scope of this thesis.

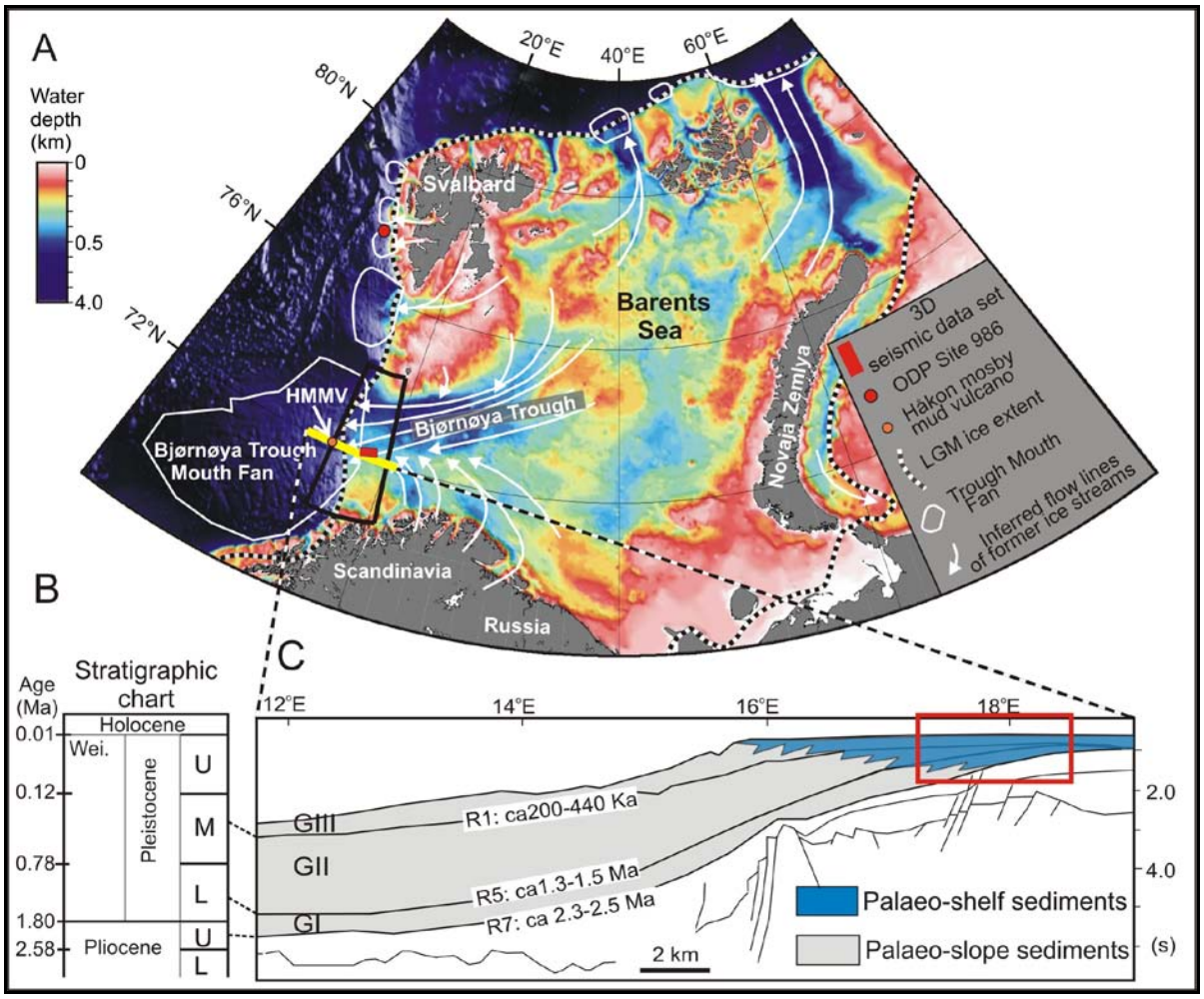

Figure 1.1: A Location of study area (black rectangle) on the western Barents Sea continental margin. The red box indicates location of the 3D study area. The red dot indicates the location of ODP site 986. LGM (Last Glacial Maximum). The map is constructed from the IBCAO grid of Jakobsson et al**. B** Stratigraphic chart. Wei: Weichselian glacial cycle. **C** Interpretation of regional seismic profile crossing the 3D seismic volume, indicated by the red rectangle. GI-GIII indicates main regional sequences, and R1, R5 and R7 main regional reflectors of the Plio-Pleistocene sedimentary succession Modified from Andreassen et al. 2007a.

1.2. Barents Sea bathymetry

The Barents Sea is an epicontinental sea located at the north-western flank of the Eurasian continent fig.1.2). It is delineable by the Norwegian-Greenland Sea in the west, Novaya Zemlya in the east, the Arctic Ocean in the north, and northern Norway and the Kola Peninsula in the south. The Barents Sea

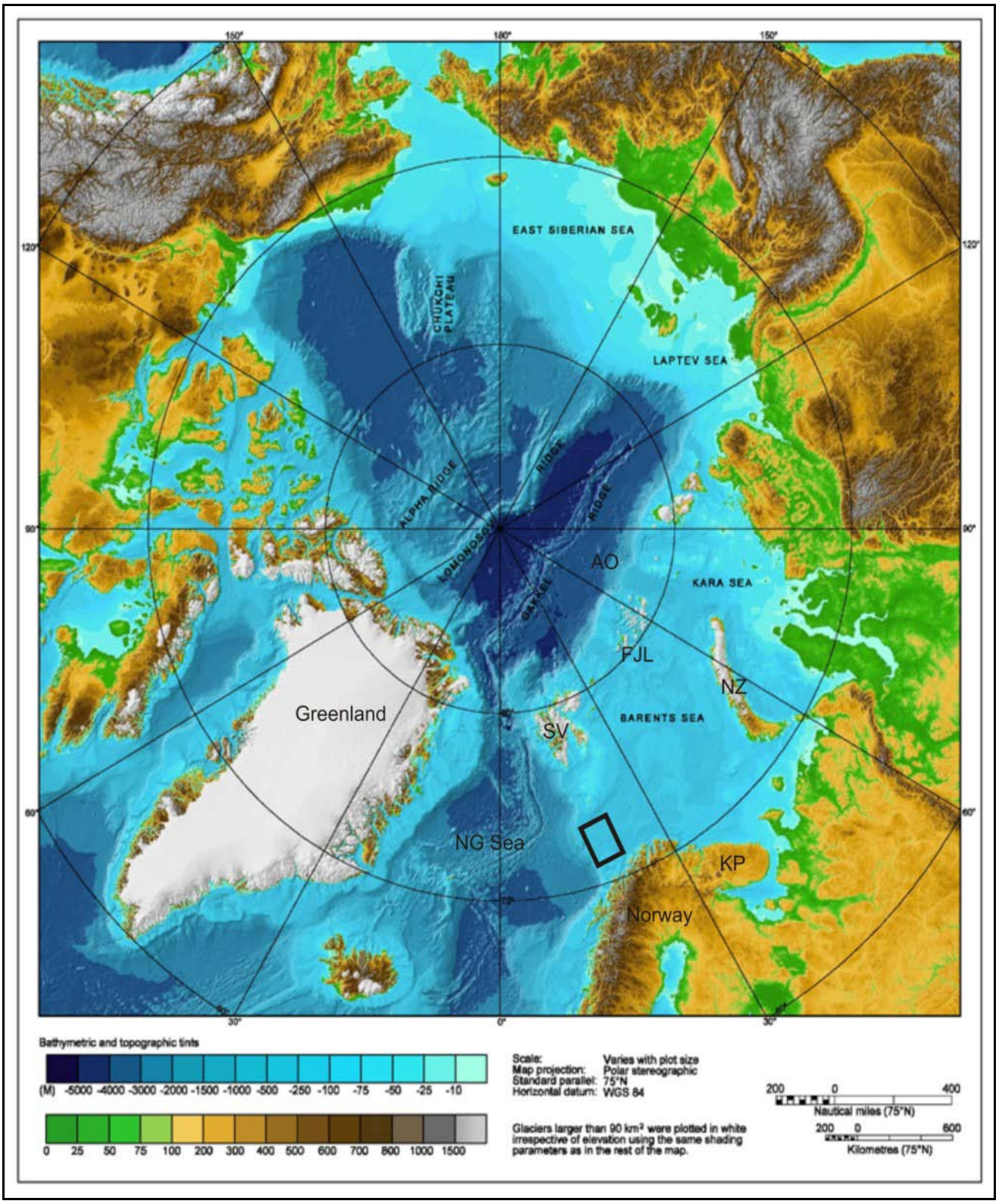

Figure 1.2: Location of the Barents Sea on the IBCAO map from Jakobsson et al. NG Sea: Norwegian-Greenland Sea, KP: Kola Peninsula, SV: Svalbard, NZ: Novaya Zemlya, AO: Arctic Ocean, FJL: Frank Josef Land. Rectangle shows the location of the study area.

covers an area of about $1.2 \cdot 10^{6}$ km^2. It is a shallow ocean which deepest area is the Bjørnøyrenna, a large W-E/NE oriented glacial trough with a depth of more than 500 meters. North of the Bjørnøyrenna, we find shallow banks with depths of 100 meters or less, and in the south, banks have water depths between 200-300 meters. Another deep area is Ingøydjupet, which reaches water depths of 400 m (fig.1.1). The western Barents Sea continental slope has a gentle slope which ranges between 1º and 4º (Vorren et al., 1989; Laberg & Vorren, 1995; 1996; Solheim et al., 1998), and it is dominated by fan-shaped geomorphic features at the mouth of the Bjørnøyrenna and Storfjordrenna (fig.1.1), called Trough Mouth Fans (TMF, Vorren et al. 1991; 1998). The Bjørnøyrenna TMF is comparable in size to the Mississippi and Amazon River fans (Vorren et al. 1991; Fiedler & Faleide, 1996; Faleide et al. 1996; Elverhøi, et al. 1998). The Bjørnøyrenna fan is considered to be from Tertiary and Quaternary origin and represents a depocenter for erosion products from Cenozoic uplift and erosion, much of which is late Plio-Pleistocene glacial erosion, of the Barents Shelf area (Spencer et al., 1984; Nøttvedt et al., 1988; Vorren et al., 1991; Eidvin et al., 1993; Faleide et al., 1996, 2008; Svendsen et al., 2004; Dahlgren et al. 2005).

The 3D study area is located on the Veslemøy High. The Veslemøy High is located at 72ºN and between 17ºE and 18 ºE. The Veslemøy High (fig.1.3) is located between the Bjørnøy Basin in the north and the Tromsø Basin in the south and it is partly separated from the Sørvestnaget Basin by west-stepping normal faults (Gabrielsen et al., 1990; Faleide et al., 1993; Breivik et al., 1998).

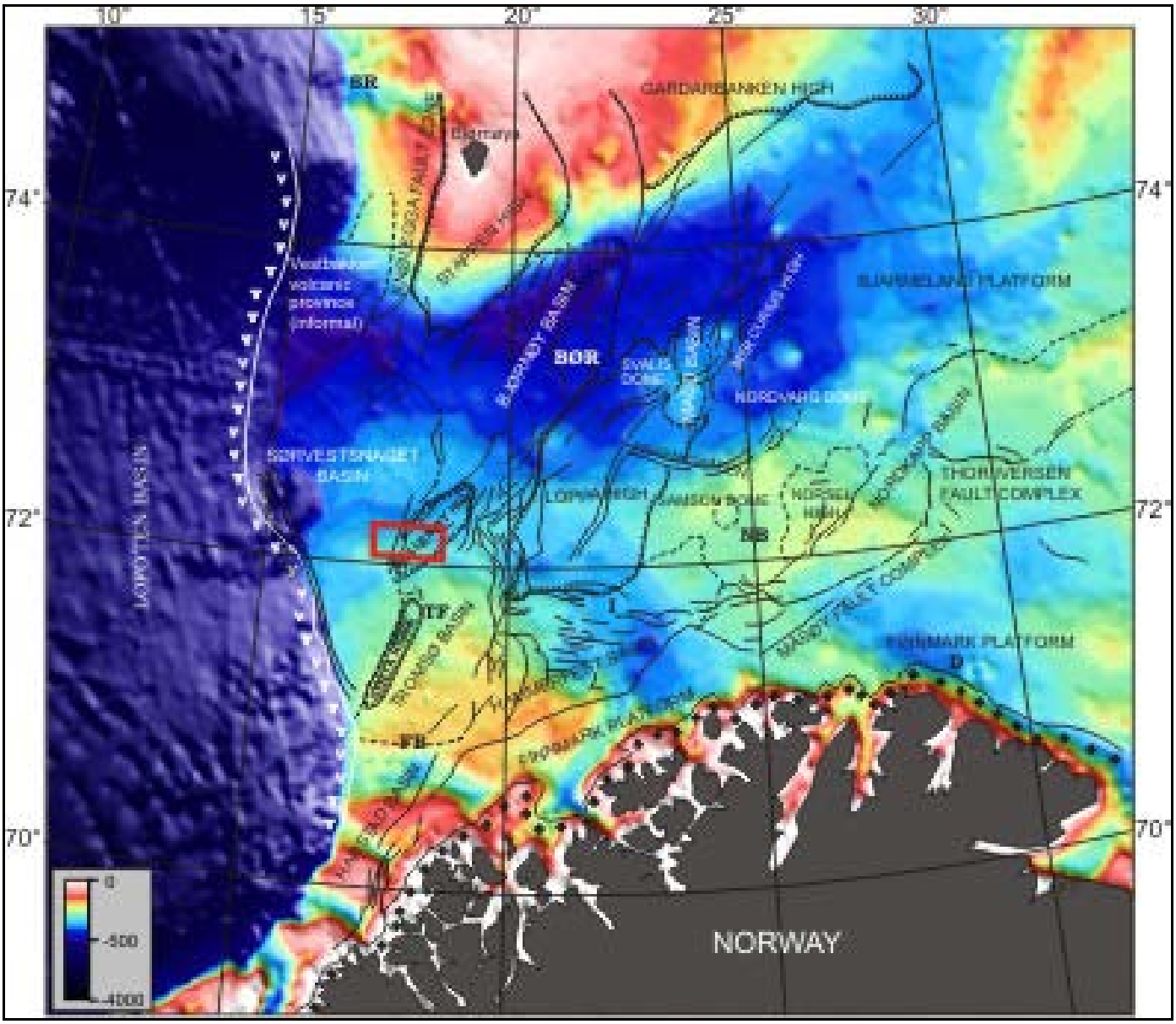

Figure 1.3: Main structural elements in the southwestern Barents Sea (after Gabrielsen, et al. 1990). Red box indicate location of 3D seismic EL0001. FB: Fugløybanken; TF: Tromsøflanket; BØR: Bjørnøyrenna; I: Ingøydjupet; NB: Nordkappbanken, SR: Storfjordrenna, D: Djuprenna. Figure is modified from Larsen et al. (2003).

1.3. Geological history of the Barents Sea

Development of the present morphology of the Barents Sea area has been related both to the opening of the Norwegian-Greenland sea and Late Cenozoic glacial history (Vorren et al. 1991; Riis & Fjeldskaar 1992; Eidvin et al. 1993; Fiedler & Faleide, 1996; Faleide et al. 1993, 1996, 2008; Elverhøi et al. 1998; Butt et al. 2000). The Western Barents Sea is underlain by large thicknesses of Upper Paleozoic to

Cenozoic deposits (Faleide et al. 1993; 2008). On the basis of sedimentary fill, tectonic style and crustal structure, Faleide et al. (1993; 2008) divides the West Barents Sea in three regions (1) the oceanic Lofoten Basin which formed during the Cenozoic opening of the Norwegian-Greenland Sea and the Vestbakken Volcanic Province; (2) the south-west Barents Sea basin province of deep Cretaceous and Early Tertiary basins (Harstad, Tromsø, Bjørnøy and Sørvestnaget Basins) separated by intrabasinal highs (Senja Ridge, Veslemøy High and Stappen High); and (3) Mesozoic basins and highs further east between 20º and 25º E which have not experienced the pronounced Cretaceous-Tertiary subsidence (Finnmark Platform, Hammerfest Basin, and Loppa High).

The post-Caledonian geological history of the western Barents Sea is dominated by three major rift phases, Late Devonian?-Carboniferous, Middle Jurassic-Early Cretaceous and Early Tertiary, each comprising several tectonic pulses.(Faleide et al. 1993; 2008). Structurally, the Barents Sea continental shelf is dominated by ENE-WSW trends with local influence of WNW-ESE striking elements. The western Barents Sea has been the tectonically most active sector throughout Mesozoic and Cenozoic, while the east has been dominated since Late Carboniferous by stable platforms (Gabrielsen et al., 1990).

1.3.1. Paleozoic

During the Paleozoic, broad subsidence of the Barents Sea and the continental shelf off northeast Greenland formed a large epieric basin (Nøttvedt et al. 1988). In the early Devonian, the young Caledonides were eroded and molasse sediments were deposited in East Greenland and Svalbard. It is believed that arid continental conditions where dominant here while carbonates and evaporites were dominant in the East (Faleide et al. 1984; 2008). In the late Devonian the compressional system changed to a left-lateral shear regime and strike-slip movements took place in the Arctic-North Atlantic region (Harland, 1965; Ziegler, 1978; Faleide et al. 1984; 2008). Transpression and transtension during the Svalbardian phase in this area led to the formation of Spitsbergen (Faleide et al. 1984; 2008).

During the Carboniferous, continental clasts and coal from the Sverdrup basin to the Franz Josef Land, dominated in the west and Svalbard, while carbonates dominated in the east. In the Middle Carboniferous, tectonic activity recommenced. After a break in sedimentation in the Bashkirian-

Namurian period, a transgression led to marine conditions. Thick carbonates and evaporites associated with clastic sediments were deposited in the Barents Sea (Faleide et al. 1984; 2008).

At Early Permian Svalbard and Bjørnøya were stabilized and a carbonate shelf extended from Sverdrup basin to Pechora. Evaporites dominated both in Svalbard and Pechora Basins during the Artinskian and Kungurian periods. During the Late Permian a continuous seaway was opening and connected Greenland and the North Sea. Clastic sedimentation is characterized at this stage (Faleide et al. 1984; 2008).

1.3.2. Mesozoic

During the Triassic, the connection to the south was closed and the tectonic conditions were quiet. Clastic marine sedimentation predominated in all the Barents Sea. During the Early Jurassic, a major break in sedimentation occurred in areas bordering the Barents Sea, followed by regional transgression in Bathonian-Callovian (Faleide et al. 1984). Tectonically, the Triassic and Jurassic were quiet periods in the Barents Sea (Gabrielsen et al. 1990).

During the Jurassic-Cretaceous rifting, a series of sedimentary basins (Faeroe-Møre-Vøring) formed by subsidence. This expansion was linked to the De Geer Zone (Faleide et al. 1984; 1993; Rowley & Lottes, 1988). In this period, a series of extensional faults deformed the basins fills during the Middle Jurassic (Faleide et al. 1993). There was a main period of subsidence which started in the Late Jurassic and lasted until the Middle Cretaceous (Aptian-Albian) times (Faleide et al. 1993). Reactivation of the faulting happened in the Late Cretaceous until the Early Tertiary (Gabrielsen et al. 1990). During the Cretaceous, the Harstad, Tromsø and Bjørnøya Basins underwent large scale subsidence and sedimentation (Faleide et al. 1993). The development of the Norwegian-Greenland Sea is schematically shown in figure 1.4.

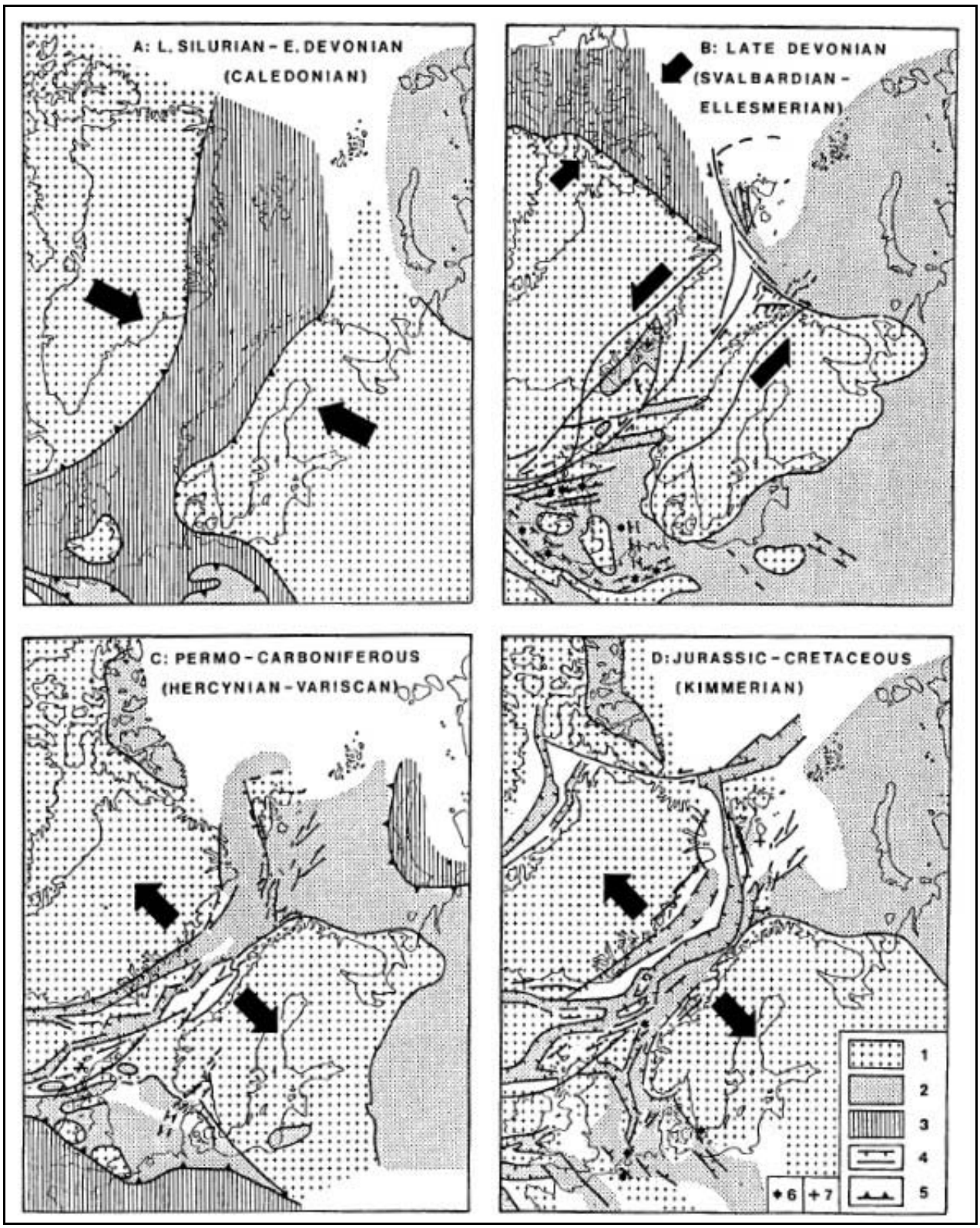

Figure 1.4: Main stages in the evolution of the western Barents Sea and surrounding areas. Continental fit after : **A,** Harland, 1969; **B** and **C**, Le Pichon, 1977; **D** Ziegler, 1978. **1**, Stable elements – continental cratons and intrabasinal highs; **2**, sedimentary basins; **3**, active foldbelts; **4**, normal and wrench faults; **5**, deformation front of active foldbelts; **6**, intrusions: **7**, volcanics. From Faleide et al., 1984.

1.3.3. Cenozoic

The western Barents Sea continental margin and the adjacent Lofoten Basin have evolved in response to the opening of the Norwegian-Greenland Sea starting ca 55 Ma ago (Vorren et al., 1991; Faleide et al., 1993, 1996, 2008; Fiedler & Faleide, 1996; Dahlgren et al., 2005). The western Barents Sea evolved as a passive shear margin during these periods (Tawani & Eldholm, 1977; Myhre et al., 1982; Eldholm et al., 1987).

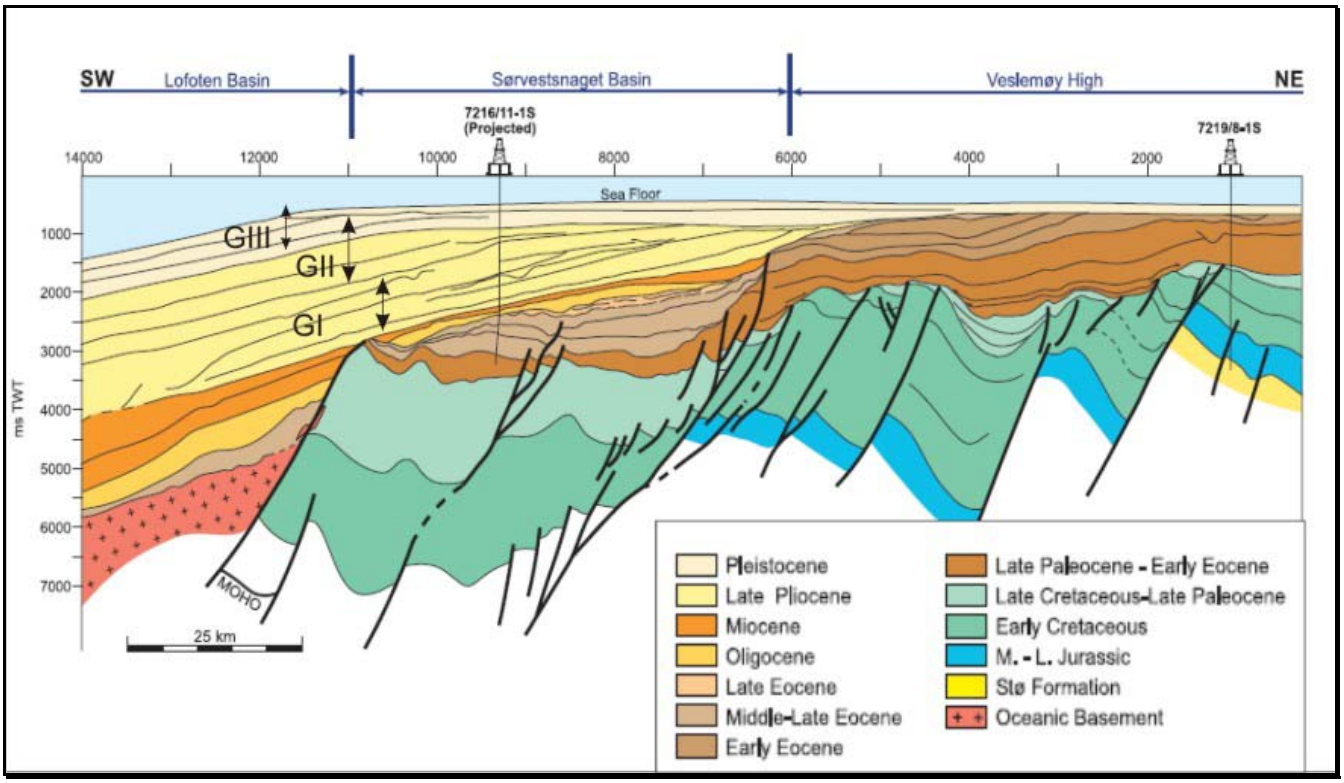

Figure 1.5: Geoseismic cross-section showing the Cenozoic succession from the Lofoten Basin to the Veslemøy area through the Sørvestnaget basin. Modified from Ryseth et al. (2003).

During the Eocene, rift basins adjacent to the Stappen High were formed to the west and southwest, these are the Sørvestnaget and the Bjørnøya Basins and the Vestbakken volcanic province (Faleide et al. 1988). Extensive erosion in the Bjørnøya shed sediments into these basins during the Early Tertiary (Sættem et al., 1994; Nøttvedt et al. 1988; Faleide et al., 1988; Wood, 1990; Vorren et al., 1990; Richardsen et al., 1991; Nyland et al. 1992).

Other basins such as the Tromsø, Bjørnøya, Harstad Basins underwent large subsidence and

sedimentation. Finally, the area suffered uplift in the Late Oligocene which affected most of the Barents Sea (Faleide et al. 1993). Butt et al. (2002) inferred by numerical models that the Barents Sea was subaerial in the earliest Late Pliocene, becoming a submarine platform at about 1 Ma.

The Cenozoic in the Barents Sea has been influenced by extensive erosion of the shelf region and redeposition on the slope and in the basins of the evolving Norwegian-Greenland Sea to the west. This erosion in the Stappen High-Spitsbergen area is about 3 km and the rest of the Barents Sea is on average about 1 km. (Wood et al. 1990; Riis & Fjeldskaar, 1992; Sættem et al. 1994; Wood et al., 1990).

The erosion in the Barents Sea during the Cenozoic is divided by Rasmussen & Fjeldskaar (1996) into two main episodes:

1.- After continental rifting in the Early Tertiary, there is subaerial erosion due to tectonic uplift. Deposition of these erosional products filled the basins on the south and southeast of the Barents Shelf.

2.- During the Plio-Pleistocene the Barents Sea was characterized by glacial erosion and transport towards the present margins. Isostatic uplift happened subsequently.

The Late Cenozoic sediments on the margin (fig.1.5) were mostly eroded from the Barents shelf areas and deposited as thick fan deposits located on the edge of the continental margin along the newly formed western margin (Spencer et al., 1984; Nøttvedt et al., 1988; Vorren et al., 1991; Sættem et al., 1994; Laberg & Vorren, 1996). These prograding wedges consist of sediments from the Naust Formation of the Nordland group (Larsen et al., 2003; Dahlgren et al., 2005; Andreassen et al., 2007).

1.4. Glacial History in the Barents Sea

The Norwegian-Barents Sea-Svalbard continental margin is classified as a glacial margin that periodically has been impacted by grounded ice sheets on the continental shelf. The ODP sites (fig.1.1 and fig.1.6) on the Vøring plateau shows that the onset of the main Northern Hemisphere Glaciations occurred at about 2.6 Ma (Thiede et al., 1989; Jansen et al., 1991). The ODP site 986 (fig.1.1) has been

a key location for estimating the chronology of the Plio-Pleistocene units along the western Barents Sea-Svalbard margin (Table 1.1). Paleomagnetic, biostratigraphic and Sr-isotopes analysis (Butt et al. 2000) have been used to establish this chronology. Faleide et al. (1996) has estimated similar ages for these reflectors by seismic correlation with commercial boreholes. Sættem et al. (1992) estimated that R1 is younger than 440 ka. Extrapolation of calculated sedimentation rates in piston cores on the Svalbard margin has given an approximate age of 200 ka in this area . R1 thus has a likely age between 440 ka and 200 ka. R5 is assigned interpolated ages of 1.3-1.5 Ma at Site 986, supported by biostratigraphic and Sr. data. Faleide et al. (1996) suggested a likely age of about 1.0 Ma for R5. This sequence boundary was interpreted to represent a hiatus resulting from the most significant change in sedimentation patterns during the R7-R1 time. The erosion was suggested result from increased glacial activity on the shelf, and correlated to increased amounts of IRD and oxygen- isotope measurements showing a shift in climatic cyclicity and amplitudes in the time period 1.2-0.8 Ma. R7 has been established by interpolating linearly between the maximum age of 2.6 Ma at the base of ODP Site 986 borehole and the base of the Olduvai paleomagnetic event gives a tentative age of 2.3–2.5 Ma for R7, supported by biostratigraphic and Sr data. Although uncertain, this is compatible with age estimates of 2.3–2.5 Ma from seismic correlation to commercial wells in the southwestern Barents Sea.

The stratigraphy of the glacigenic sediments of the Western Barents Sea is divided in three main sedimentary units (GI, GII and GIII), where GI is the oldest. Within these units, 7 correlatable reflectors are identified. These are R1 through R7, where R1 is the youngest (Faleide et al., 1996, Andreassen et al., 2004). Deposition of glacigenic sediments became dominant at about 2.3 Ma, represented by the Reflector R7, which is also the base of the western margin trough mouth fans (Faleide et al. 1996).

A correlation between the regional reflectors according to different authors is displayed in table 1.1. The boundaries were assigned ages from sequence pinch-out on dated oceanic basement, seismic facies and ties to shallow boreholes and commercial exploration wells in the SW Barents Sea (i.e. Vorren et al., 1991; Eidvin & Riis, 1989; Laberg & Vorren, 1995; Sættem et al. 1991; Rafaelsen et al., 2002; Faleide et al., 1996; Butt et al., 2000). The seismic structure of the northwestern Barents Sea margin suggests at least sixteen glacial advances during the last 1 Ma. (Solheim et al., 1996), while Sættem et al. (1992) and Laberg & Vorren (1996) have found indications of eight major ice advances in the

southwestern part over the last 0.44 ka. Andreassen et al. (2004), evidence of grounded ice reaching the western Barents Sea shelf edge at least eight times during the last 1.5 Ma is provided.

In a recent study based on revised chrionostratigraphy, recompilation of borehole data from the Barents Sea continental margin, Knies et al. (2009) propose a glaciation model over the past 3.5 Ma where three different phases of growth are inferred.

An initial phase (~3.5-~2.4 M), glaciations would be limited to Svalbard and northern parts of the Barents Sea (fig.1.6a) and most part of the Barents Sea would be sub-aerially exposed between ~3.5 and ~ 2.4 Ma (Rassmussen & Fjeldskaar, 1996; Butt et al. 2002; Knies et al. 2009)**.** Junttila et al (2008) suggests that there is glacial erosion of Mesozoic sediments in the central/northern Barents Sea during ice sheet advance and subsequent release at the coastline. The lack of glacially eroded material further than the Fram Strait indicates the ice sheet was of limited extent. At ca 2.7 Ma, a period of ice growth on the uplifted Barents Sea beyond the coastline (Knies et al., 2009) is suggested by the glacial intensification in the circum-Atlantic region and a distinct supply of IRD-rich sediments in the Yermak Plateau between (~2.7 and ~2.4 Ma).

The transition phase (~2.4-1.0 Ma) commenced with a partial disintegration of the outermost ice margins leading to a more stable position at the coastline. In this phase, a terrestrial glacial build up is inferred by low smectite values along the western Barents Sea and the occurrence of turbidites and debris flows (Forsberg et al., 1999; Knies et al. 2002; 2009). The lower input of smectite declines due to (1) the blocking of the transport pathways of sediments entrained in the sea ice on the Siberian shelves due to the expanding Barents Sea ice sheets (fig.1.6b), (2) a change from a rather distal source of smectite to increased local sediments supply associated with the onset of glacigenic wedge growth or (3) a combination of both.

In the third phase or final growth phase (fig.1.6c) started at ~1.0 Ma, finding of high-amplitude short-term kaolinite pulses (<20%) in Holes 911A/910A and 986C indicates erosion and meltwater outwash of Mesozoic sediments underlying the ice sheet in the Central Barents Sea. Evidence (megascale glacial lineations) that grounded ice reached the shelf break in the southwestern Barents Sea since ~1.5 Ma (Andreassen et al., 2004) supports Knies et al (2009) glaciations model.

On the continental shelf, the glacigenic deposits are recognized as an erosional unconformity, the Upper regional unconformity (URU in Solheim & Kristoffersen, 1984). Sediments in the west part are described as large prograding fans located at the mouth of glacially-eroded troughs. The Bjørnøya TMF consists on 3-4 km thick of glacigenic deposits and covers an area of 280000 km^2 (Laberg & Vorren, 1996). These are interpreted as depocenters of sediments transported by ice streams (Laberg & Vorren, 1995; Dowdeswell et al., 1998, Elverhøi et al.; 1998; Vorren et al., 1998; Andreassen et al. 2007a).

Large glaciations (fig. 1.7) have been present three times in the Eurasian and Arctic area during the Weichselian Glacial Maximum (Mangerud, 1998; Svendsen, 2004; Larsen et al. 2006). Early Weichselian (90-80 ka), Middle Weichselian (60-50 ka) and Late Weichselian, LGM (25-10 ka). Ice coverage in the Early Weichselian is unsure, but probably reached Norway, Finland and Sweden (Svendsen et al., 2004). It was followed by a large deglaciation in the period at about 85-75 ka.

According to Mangerud (1998), the ice during the Middle Weichselian covered Svalbard and the continental margin. After this, the deglaciation led to a period where the Barents Sea was ice free. LGM started probably at 28 ka and it covered Scandinavia and the Barents Sea and probably it extended to the northernmost part of the Barents margin, western Barents Sea and northern parts of Great Britain and Ireland, as well as Scandinavia (Elverhøi et al. 1995; Mangerud et al. 1996). At around 15 ka, the deglaciation started, uncovering the deepest oceanic parts first with Bjørnøyrenna one of the main drainage areas (Larsen et al., 2006; Andreassen et al. 2008). At 12 ka, most part of the central Barents Sea was ice free (Larsen et al., 2006; Andreassen et al. 2008).

Ice streams are corridors of fast ice flows (ca.0.8 km/year) within an ice sheet and are the responsible for discharging the majority of the ice and sediments within them (Bennett, 2003). The existence of a major ice stream in Bjørnøyrenna that during glacial maxima delivered sediments to the fan at its mouth (fig.1.1), has been inferred from bathymetry and ice sheet geometry (Denton & Hughes, 1981, Stokes & Clark, 2001), glacial flutes on the seafloor (Solheim et al., 1990), investigations of the Bjørnøyrenna (Vorren & Laberg, 1997) and from megascale glacial lineations on several buried surfaces and the seafloor (Andreassen et al., 2004, 2007, 2008).

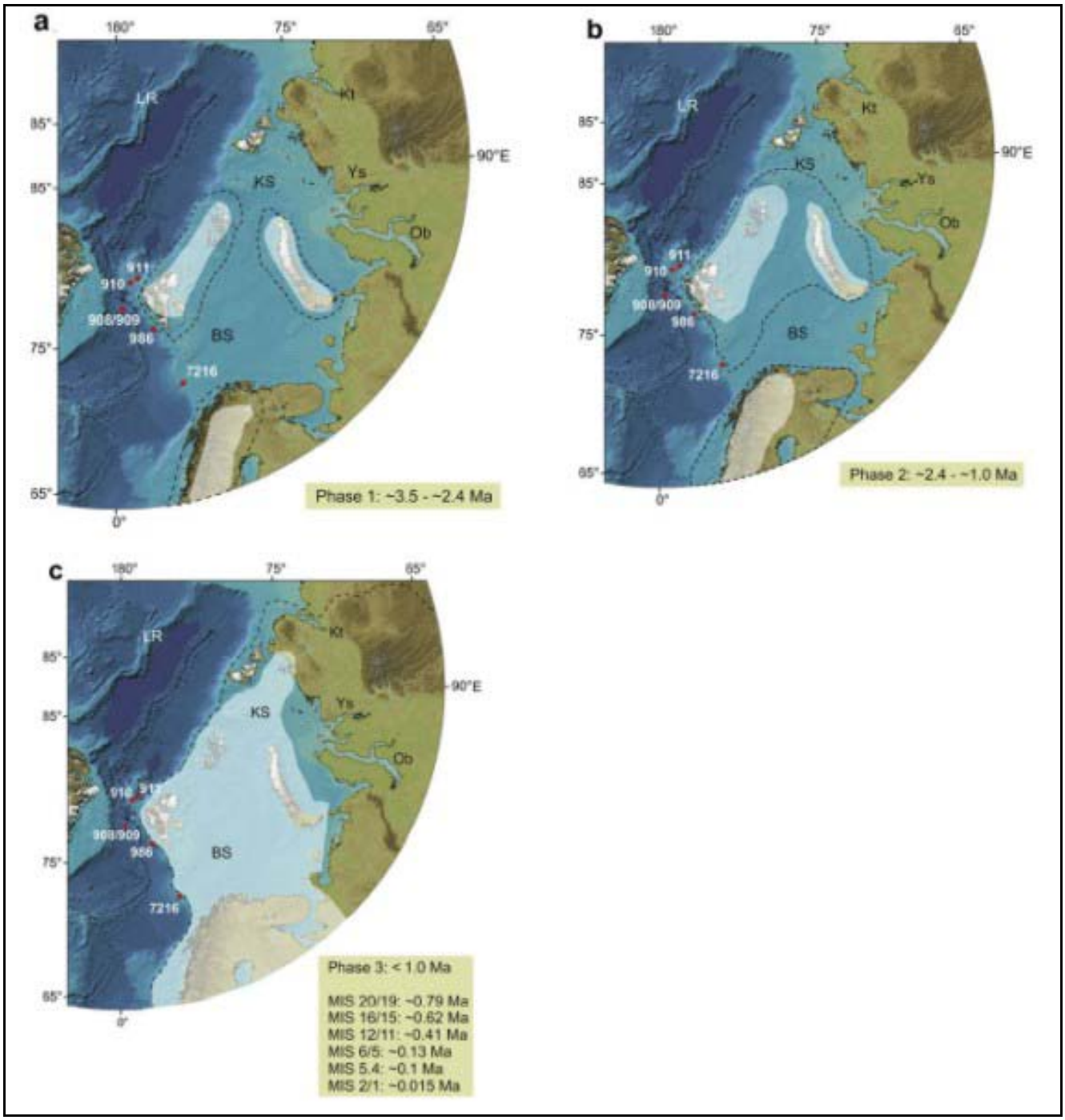

Figure 1.6: Schematic (min/max) model of lateral ice extension in the Barents Sea region during the Late Plio-Pleistocene time period (black stippled lines = maximum; white transparent polygons = minimum). **a.** Phase 1 (~3.5-2.4 Ma) **b.** Phase 2 (~2.4-1.0 Ma). The style of glaciations during both phases is conceptual and based on data and reasoning discussed in Knies et al. (2009). **c.** Phase 3 (< 1.0 Ma) is represented by the reconstructed Saalian (maximum) and LGM (minimum) glaciations (Svendsen et al. 2004) (modified from Knies et al., 2009).

Table 1.1: Correlation of seismic sequences along the western Barents Sea – Svalbard margin with suggested ages for the main sequence boundaries, and comparison with previously published stratigraphies. Modified from Larsen et al. (2003).

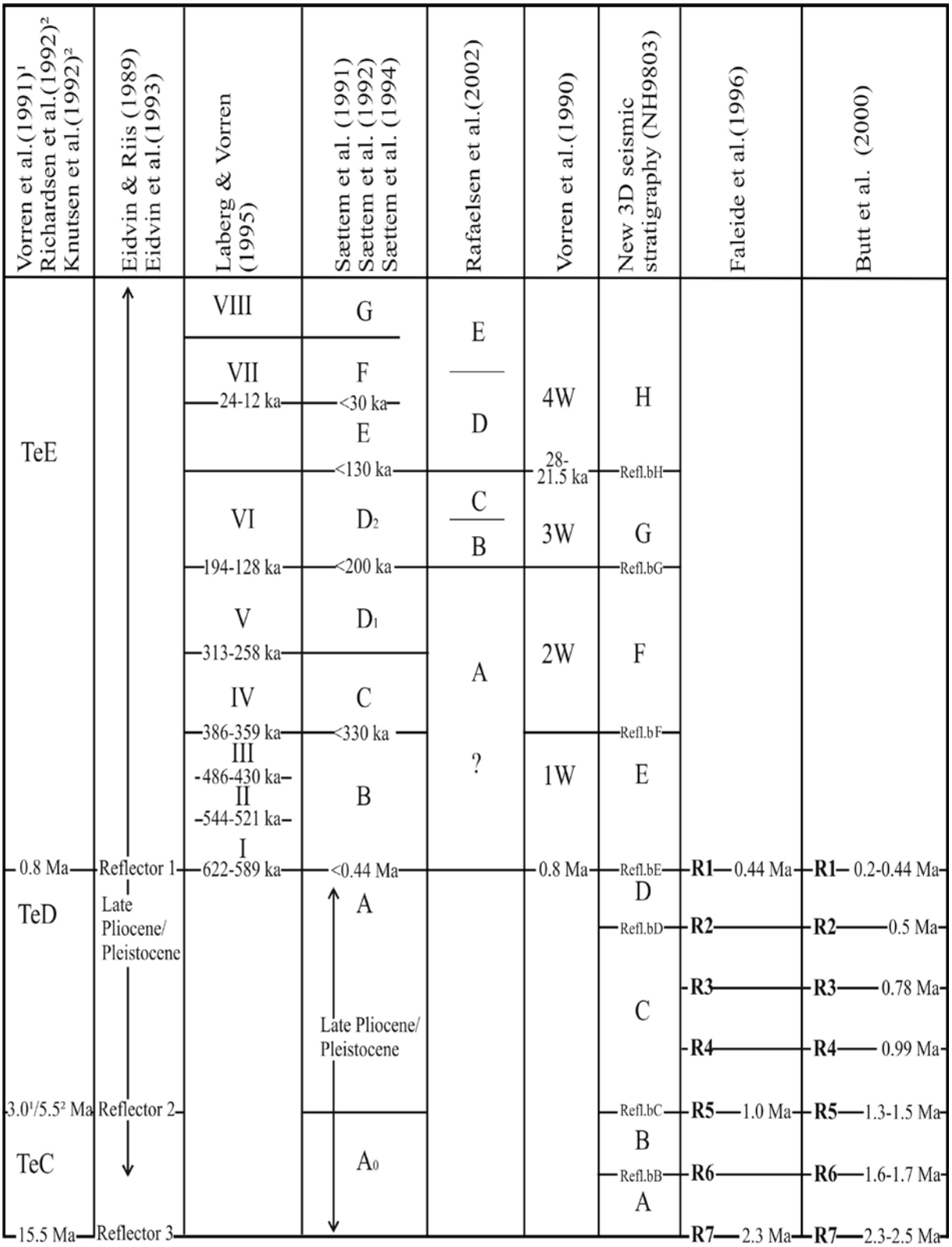

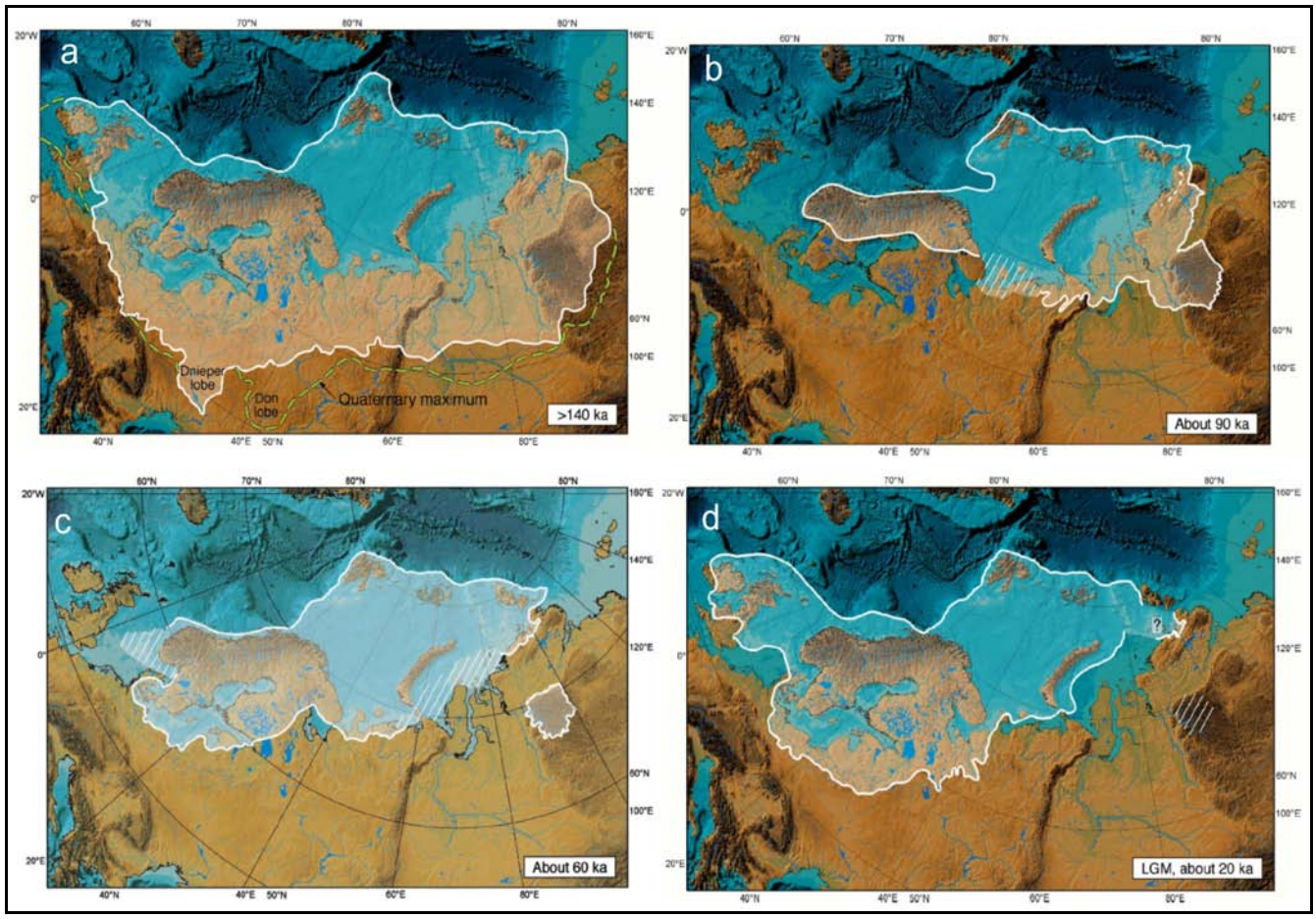

Figure 1.7: a. Reconstruction of the maximum ice-sheet extent in Eurasia during the Late Saalian (ca. 160-140 ka). **b.** Reconstruction of the maximum ice-sheet extent in Eurasia during the Early Weichselian glacial maximum (ca. 90-80 ka). **c.** Reconstruction of the ice-sheet extent during the Middle Weichselian glacial maximum (60-50 ka). **d.** Reconstruction of the maximum ice-sheet extent in Eurasia during the Late Weichselian Glacial Maximum (LGM). From Svendsen et al. (2004).

Megascale glacial lineations are morphological features attributed to fast flow of grounded ice. These features can be seen on the seafloor along the major troughs in the Barents Sea (fig.1.8). Andreassen et al. (2008) groups them into five different sets: mfs1 to mfs5. Mfs1 and mfs2 are inferred to be generated during the Last Glacial Maximum, while msf3 are associated to the deglacial Bjørnøyrenna Ice Stream and mfs4 and mfs5 are associated to deglacial ice flows from the Scandinavia mainland and the eastern Barents Sea.

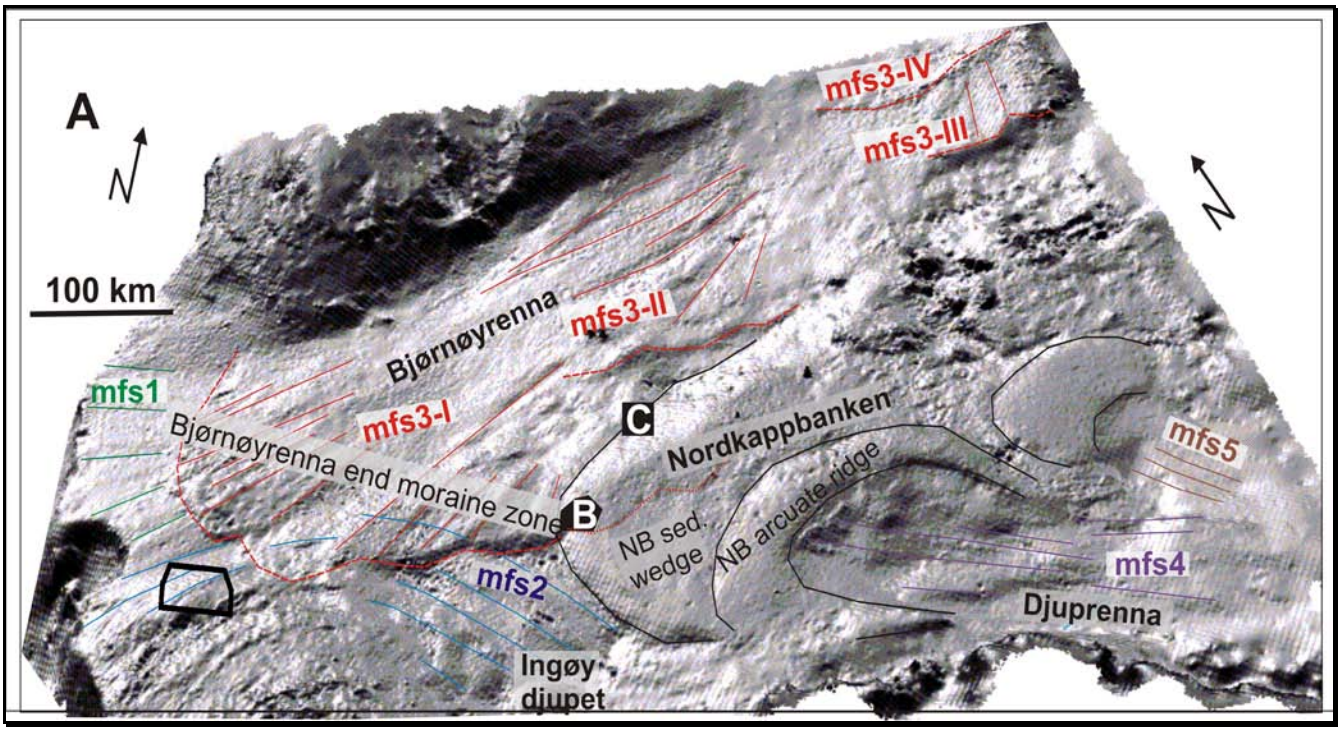

Figure 1.8. Image of the major mega-scale lineation flow sets msf1 to msf5 overlaid on a grey-scale perspective view of the study area, constructed from 2D seismic data. The black rectangle represents the 3D seismic data set used in this work. Mfs: Mega-scale lineation flow sets. Modified from Andreassen et al. (2008).

MATERIAL AND METHODS

2.1. Dataset

This Master Thesis is based on a semi-regional 3D seismic data set and a regional grid of 2D seismic data from the southwestern Barents Sea continental margin (fig.2.1).

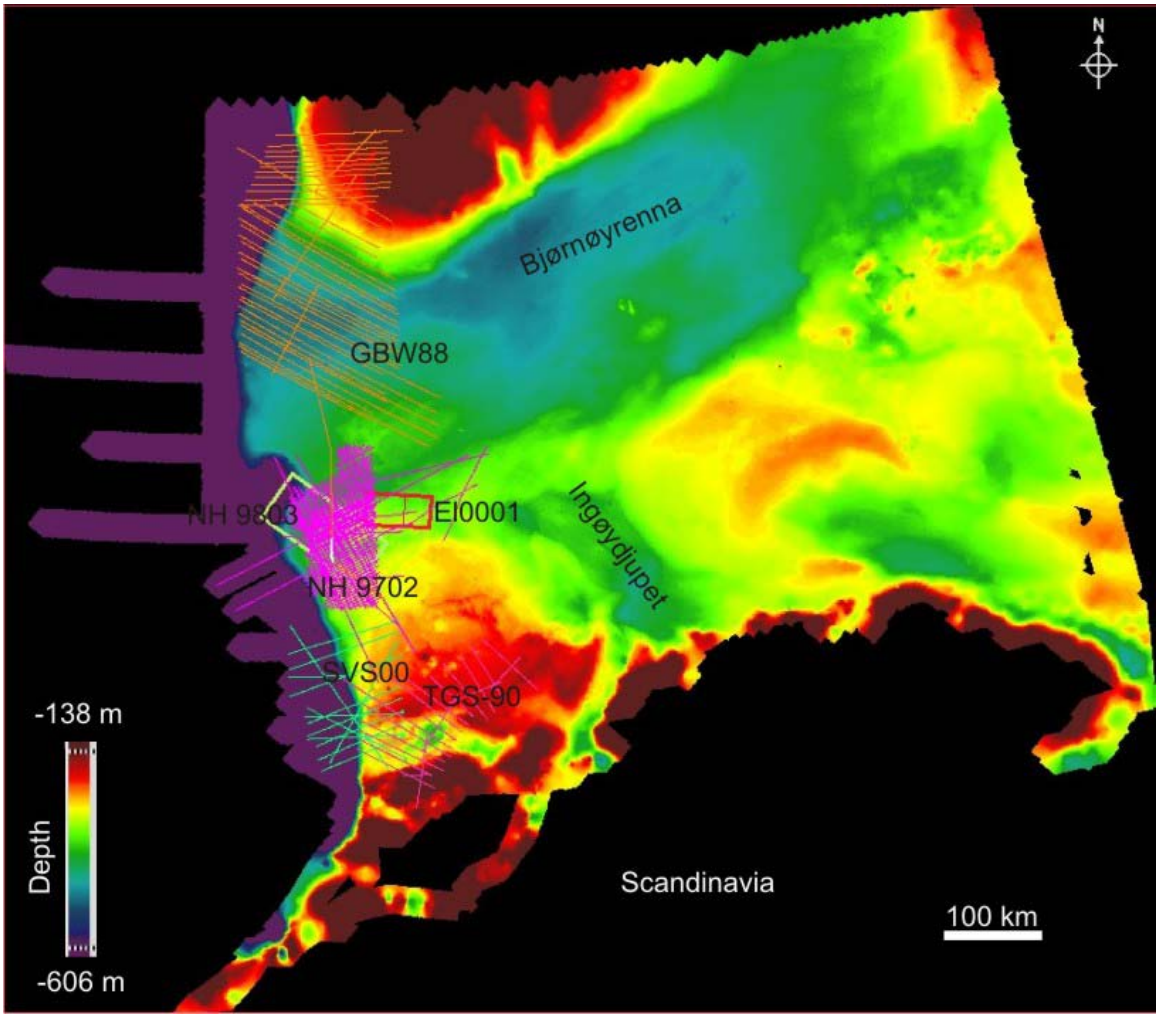

Figure 2.1: Time-depth map to the seafloor in the SW Barents Sea showing the location of the 2D seismic data sets. The red box shows the location of the 3D seismic data set. Map is generated from a 2D seismic lines grid from the Barents Sea.

3D data interpretation made it possible to see features that previously were too small to be seen. 3D seismic data gives a much better horizontal resolution and it allows a better understanding of the processes which happened in the past. Figure 2.2, an illustration

from Cartwright and Huuse (2005), shows the significant difference in interpretation of the same area with 2D and 3D seismic data. 2D seismic lines have much larger distance between them and many features cannot be seen or only poorly mapped. Distance between lines in 2D grids can be of some kilometers, while the distance between lines in 3D surveys can be of 25 m or less.

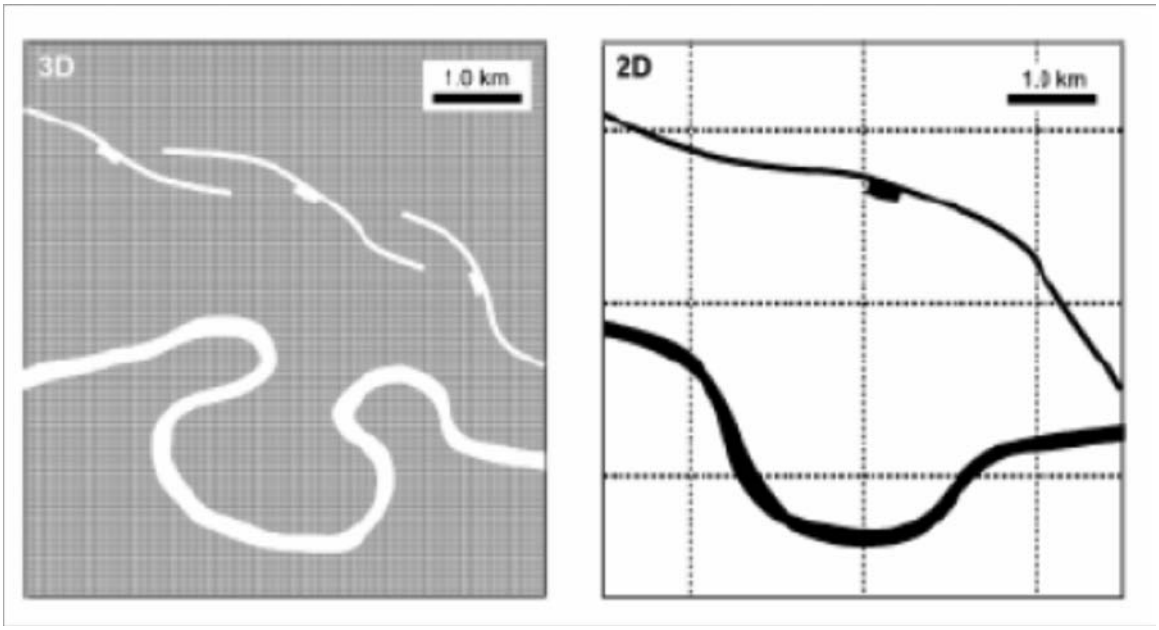

Figure 2.2: Illustration showing the difference in spatial resolution of 2D and 3D seismic data. The area to the left shows a channel and faults mapped with line spacing of 12.5-50 m whereas the map on the right shows the same structures with a line spacing of 2 km (Cartwright and Huuse, 2005).

2.1.1. 2D dataset

Several 2D surveys have been used to carry out a regional study of the area. The surveys used are NH9703, TGS-90, SVS00 and GBW-88 (fig.2.1). These surveys have been acquired by different companies and together cover a large area of the southwestern Barents Sea continental margin.

NH9702 was acquired in 1997 and 1998 by a group of companies with Norsk Hydro as the operator. It comprises around 5752 km of reflection seismic data, with a line spacing of 1-2 km. TGS-90 and SVS00 were acquired in 1990 and 2000 by TGS-NOPEC. They comprise around 1000 km of reflection seismic data each, with line spacing of 1-8 km,

and up to 10 km spacing to the east of TGS-90 and north of SVS00. GBW-88 was acquired in 1988 by GECO. It comprises around 4800 km of reflection seismic data, with line spacing of 1-2 km and 1-4 km. GBW-88 will be publically released in 2009 and SVS00 in 2011.

2.1.2. 3D dataset

The Veslemøy 3D survey, EL0001 (fig.2.1), covers an area of 990 km^2. Geographical localization of the 3D area is indicated in table 2.1. The dataset was acquired for Total and processed by CGG Norge in 2001. It has two hundred east-west oriented inlines sampled in intervals of 4 ms, and the total depth is 8000 ms (TWT). Distance between inlines is 12.5 m. Inlines were acquired in a direction of 92.854º (clockwise from the North). The interpretation is carried out on final migrated stack data. The dataset used in this study was cut at 3000 ms TWT.

Table 2.1: Geographical coordinates for Veslemøy 3D area.

Latitude	Longitude
72º 11’ 57.76” N	18º 39’ 22.57” E
72º 11’ 56.29” N	17º 20’ 31.59” E
72º 00’ 6.59” N	17º 20’ 58.21” E
72º 00’ 6.56” N	18º 38’ 58.04” E

2.2. Frequency analysis

A frequency analysis was carried out at two different depths to know the resolution at different depths (fig.2.3). To calculate the dominant frequency in the 3D seismic area, a representative seismic line (inline 100) in the study area was exported to proMAX. The analysis showed that the dominant frequencies are between 10 and 60 Hz for both depths, with peaks around 25 Hz and 30 Hz for the deepest and shallowest areas, respectively (fig.2.3).

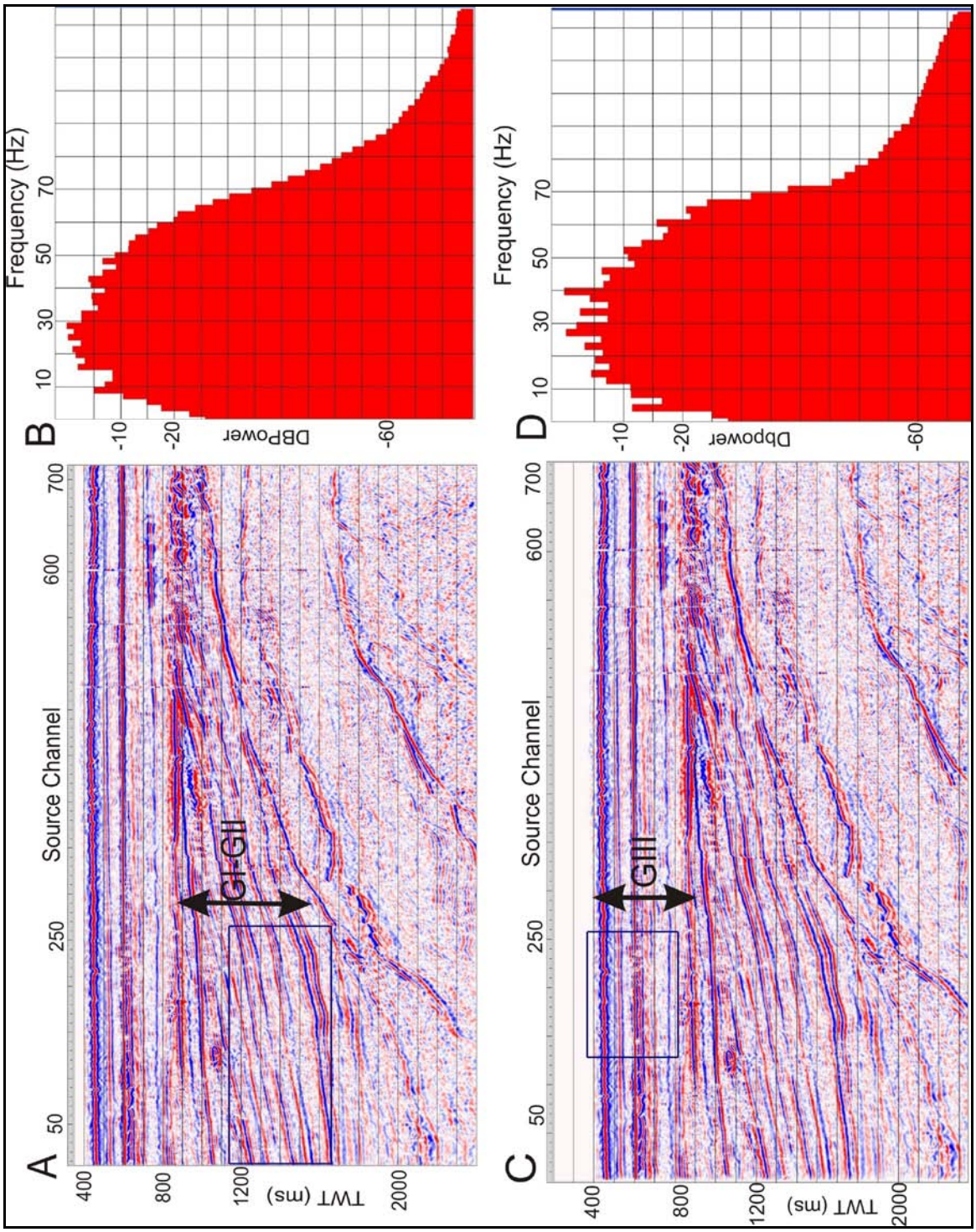

Figure 2.3: Frequency analysis in units GIII and GI-GII. **A.** The area of the seismic line used to do the analysis in unit GI-GII. **B.** The frequency spectrum from units GI-GII. **C.** The area of the seismic line used to do the analysis in GIII. **D.** The frequency spectrum from unit GIII.

2.3. Limitations in seismic interpretation

In a typical sequence of sedimentary rocks, seismic reflections will arise at each lithological boundary across which the acoustic impedance changes. All the acoustic impedances have the potential to produce reflections. However, whether or not these changes are significant enough for their reflections to be recognized and recorded will depend upon the sensibility of the seismic recording and processing system. Many reflections from the acoustic impedance are too small to be recorded by the methods currently available (Badley, 1985).

2.3.1. Resolution

"Resolution" is defined as the minimum distance between two features so that one can tell that there are two features and it is measured in wavelength (λ). Resolution varies with the velocity of the wave and the frequency (fig.2.4). Seismic velocity increases with depth due to compaction of the sediments and frequency decreases with depth because the higher frequencies are easily absorbed and attenuated so only high frequencies will be available in shallow areas. As a combination of these two factors, we can state that resolution decreases with depth (Brown, 2003). We can distinguish between horizontal and vertical resolution.

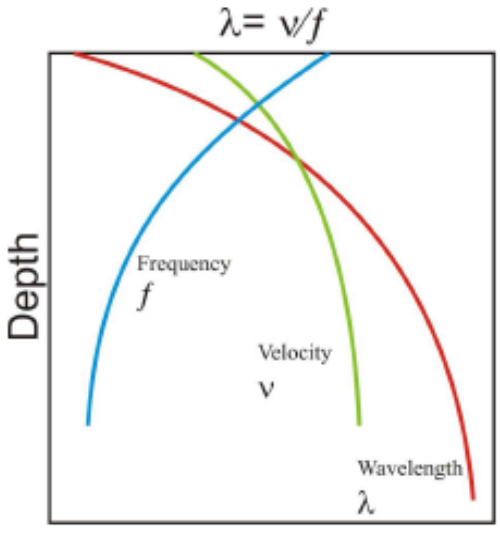

Figure 2.4: Relation of variation of frequency, velocity, and wavelength with depth and how resolution changes with them. From Brown (2003).

2.3.2.Vertical resolution

The vertical resolution refers to the ability to identify the top and the bottom of a thinning sedimentary bed (Bulat, 2005). Vertical resolution is determined by the seismic source signal and the way it is filtered by the Earth (Bacon et al., 2007). It is in theory a quarter of the dominant wavelength (Brown, 1996; Bulat, 2005). When the thickness of a sedimentary package is thinner than this, the reflection will be reflected as one and not as a package with a top and a bottom (Sheriff, 1980, Badley, 1985).

Fiedler & Faleide (1996) calculated the average P-wave velocities in the seismic unit GIII in the southwestern Barents Sea based on a large number of seismic refraction profiles. The velocities are 1970 m/s in seismic unit GIII, 2400 in seismic unit GII, and 2680 m/s in GI. To calculate the vertical resolution in the study area, those velocities have been used.

Average vertical resolution in GIII: ¼ λ = V/4f = 1970 / 4·30 = 16m.
Average vertical resolution in GII: ¼ λ = V/4f = 2160 / 4·25 = 21m
Average vertical resolution in GI: ¼ λ = V/4f = 2400 / 4·25= 24 m.

2.3.3. Horizontal resolution

The horizontal resolution refers to the minimum distance between two features that can be separated laterally. For unmigrated data, the horizontal resolution will be determined by the Fresnel Zone (fig.2.5), which is the portion of the reflector from which energy returns to the hydrophone within a half-cycle (λ/4) after the onset of the reflection.

Migration is the principal technique for improving the horizontal resolution. After this process, the Fresnel Zone will be reduced to an ellipse perpendicular to the line for 2D migration and to a small circle for 3D migration (fig.2.5). The diameter of this Fresnel Zone is λ/4 (Brown, 1996), but Bulat (2005) explains that for this to happen the migration has to be perfect and that is something that does not always happens.

Horizontal resolution after migration in the 3D area will be λ/4.

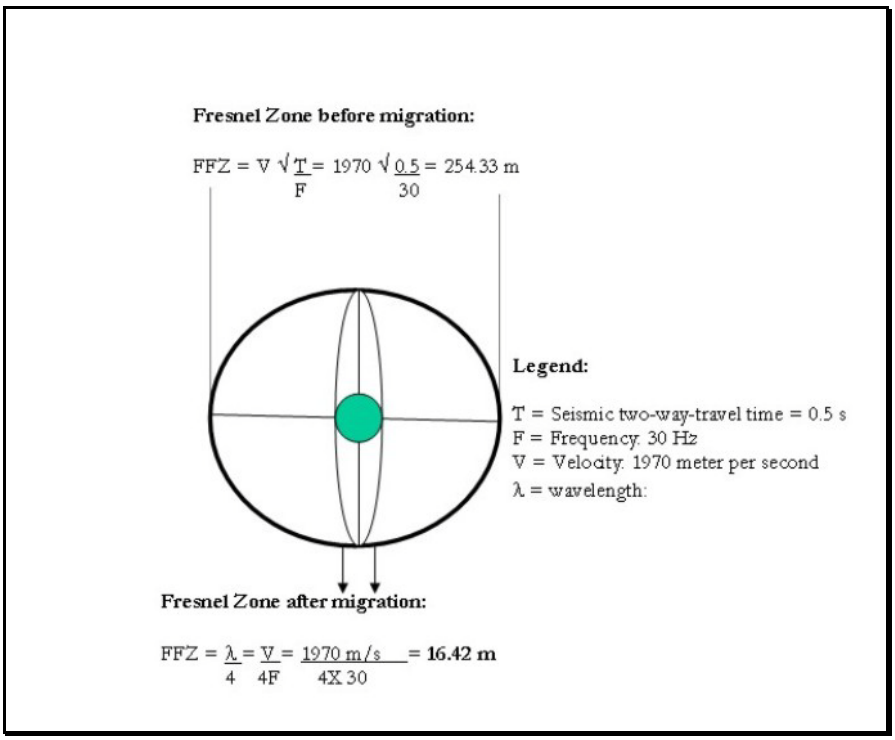

Figure 2.5: Illustration of the effect in Fresnel Zone size and form after 2D and 3D migration. The circle represents the Fresnel Zone before migration, the cigar shape is after 2D migration, and the green dot is after 3D migration (modified from Brown, 2003).

Average horizontal resolution for GIII: $\lambda/4 = V/4f = 1970 / 4 \cdot 30 = 16$ m

Average horizontal resolution for GII: $\lambda/4 = V/4f = 2160 / 4 \cdot 25 = 21$ m

Average horizontal resolution for GII: $\lambda/4 = V/4f = 2400 / 4 \cdot 25 = 24$ m

2.4. Seismic interpretation

Seismic interpretation has been carried out using the Software Charisma from Schlumberger. There the reflections have been followed through different parts of the signal (fig.2.6) depending on the continuity of the reflections, strength of the signature and the disturbance of the different parts in the signal. The interpretations which show better details are used to illustrate the geological features in this Master Thesis.

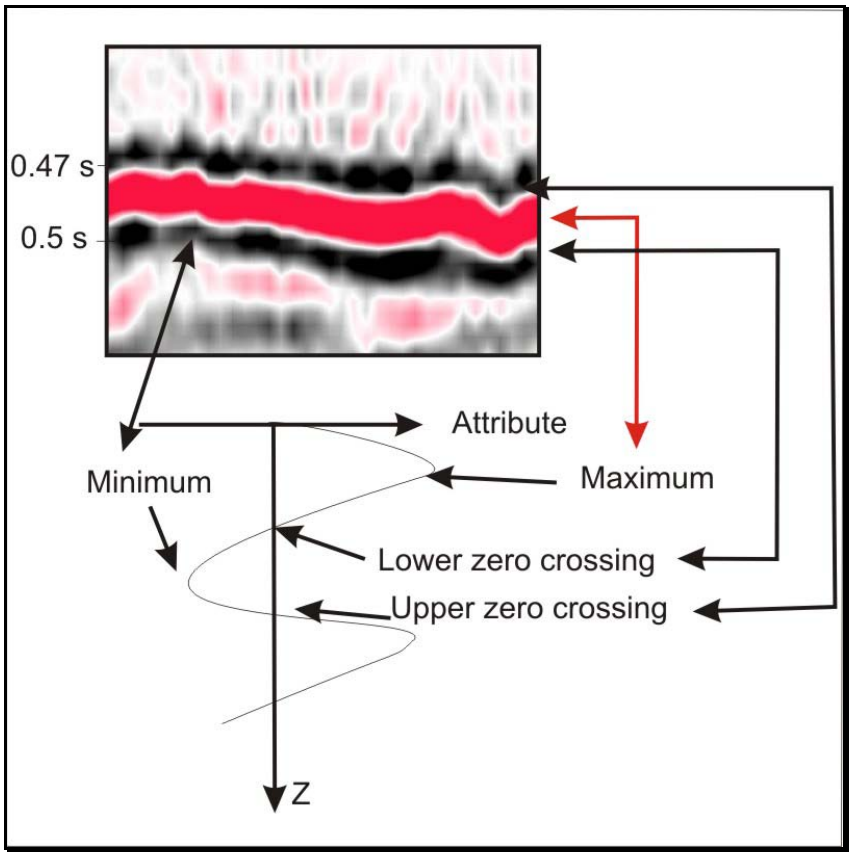

Figure 2.6: Figure showing the different parts of the seismic signal that have been used to interpret reflections in this work.

2.4.1. Seismic interpretation of 2D lines

Areas covered only by 2D lines have been interpreted automatically following regional high amplitude reflections or unconformities, and manually in more complex areas. In order to create maps of paleo-surfaces, the function "gridding" has been of great utility.

2.4.2. Seismic interpretation of 3D lines

The 3D area has been interpreted automatically by the "Automatic Seismic Area Picker (ASAP) Paintbrush Tracking" function. There are areas where the program does inaccurate interpretations and a more accurate manual interpretation is required.

2.4.3. 3D seismic attributes

A great number of 3D seismic attributes can be generated. These can be divided into three main groups, surface based, volume based and grid based attributes.

2.4.3.1. Surface based attributes

Seismic Amplitude: It reads the trace's amplitude value at the horizon pick, at a fixed time offset from the horizon surface, or by adjusting the horizon to an event (peak, trough, zero crossing). The scale is dependent on the input format of the seismic. Amplitude maps can help to identify bright spots, dim spots and faults.

Reflection Strength: It is a description of the waveform shape and corresponds to the total envelope of energy at any given instant along seismic trace. It is measured in decibels (dB). High reflection strength is associated with major lithological changes between adjacent rock layers such as unconformities, sequence boundaries, gas accumulations and gross porosity.

2.4.3.2. Volume based attributes

This calculates the attribute in each sample in an interval between a horizon and a set time (volume window) or between two horizons. They can be divided into two main groups, integrated and heterogeneity attribute computation.

Integrated computation: It is the sum of the attribute values for all the samples between two horizons or volume window. Variations can be related to density variations, porosity, and lithology.

Seismic Amplitude: It is the sum of all the amplitude values between two horizons. It helps to identify bright spots and faults.

Reflection Strength: High reflection strength is associated with major lithological changes between adjacent rock layers like unconformities, sequence boundaries, gas accumulation and gross porosity.

Magnitude Seismic Amplitude: It is the sum of the absolute values of the amplitudes along the seismic trace from a given volume of data. The changes in amplitude can be helpful in detection of buried channels and subtle faults.

Heterogeneity computation: It is the sum of the absolute difference in attribute value from sample to sample. It displays changes in the internal reflection patterns within a specified volume. It is important to detect shale layers in sand bodies for example.

RMS: It calculates the square root of the integral of the squared seismic amplitude, divided by the number of samples, for each trace in the defined volume, and displays that value in the corresponding grill cell.

2.4.3.3. Grid Attributes

These attributes depend on the grid, not on the seismic data. It can be useful to detect anomalies due to acquisition, processing, miss-picks and so on. These attributes are dip, azimuth, and illumination. These anomalies can also be detecting in other visualization tools.

2.4.4. Visualization tools

Surface map: This map is grid based and it is a three-dimensional map where the z-axis is zero. Z is represented by a color scale which gives a three-dimensional image of the area.

Attribute maps: These maps can be used to visualize different morphologic features which will not easily be seen on a surface map or Geoviz. This kind of maps will show the volume of a sedimentary package.

Geoviz: This is a three-dimensional map. This map allows the interpreter to visualize the surface from different angles and with different lights. It is common to exaggerate the vertical axis to highlight features of interest.

2.5. Main artifacts in the seismic data

Artifacts are features that are considered unlikely to be geological in origin and artifacts have to be taken into account when interpreting (Bulat, 2005). In this section, the artifacts that occur in the 3D seismic dataset will be described.

2.5.1. Survey footprint

Survey footprint is described as systematic noise that correlates with the acquisition geometry. It is observed as minor time shifts between lines giving rise to a corrugated effect (Marfurt et al., 1998; Bulat & Long, 2001; Bulat, 2005). They look like lineations which are parallel to the acquisition direction. By adjusting the light, the interpreter can shade the visual impact of the noise (fig.2.7).

2.5.2.- Migration artifacts

A number of features which resemble seismic masking due to vertical fluid flow or gas chimneys to gas chimney (fig.2.8) can be followed in parallel lines from the NE to the SW of the study area. On seismic profiles, these features are followed from the surface to the deepest part of the dataset and they look like pinnacles, which can give a false topography of lineations on different surfaces (fig.2.8). These artifacts are interpreted to be formed during processing due to their unusual and vertical geometry and the linearity of the features (Bulat & Long, 2001; Bulat, 2005). Migration and several other common

processing algorithms spread noise throughout the time section, it is common practice to apply cosmetic mute to remove the noise. Mutes are specified at times and locations and are linearly interpolated between these. Mutes are also defined with a mute time ramp so that they are not abrupt applied. The quality of the control point's assignment can influence the attenuation of the noise and topographic level can be attenuated or even muted, resulting in data gaps.

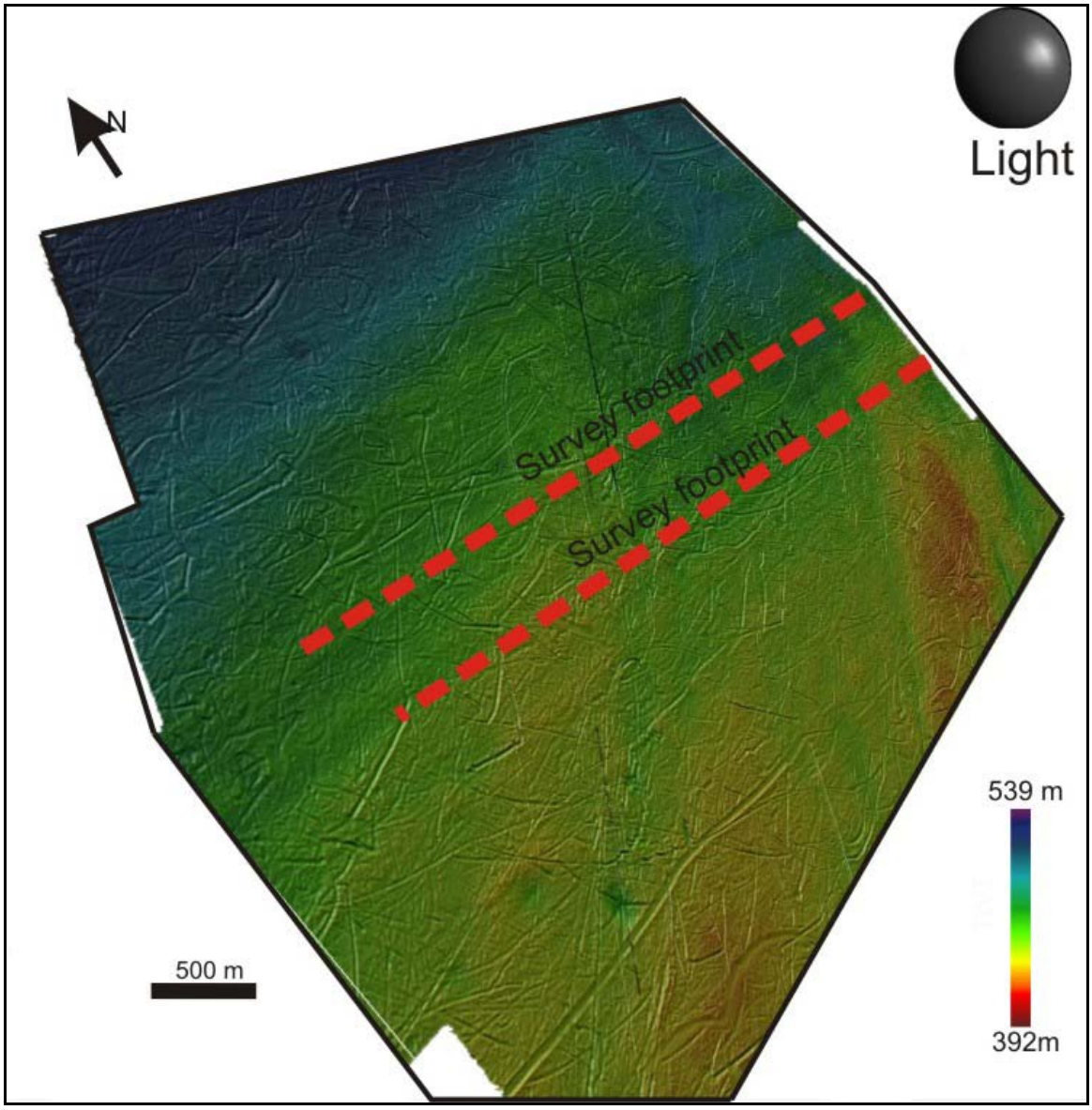

Figure 2.7: Shaded relief map of the seafloor on the study area. Red dotted lines indicate the survey footprints which appear as sets of lineations.

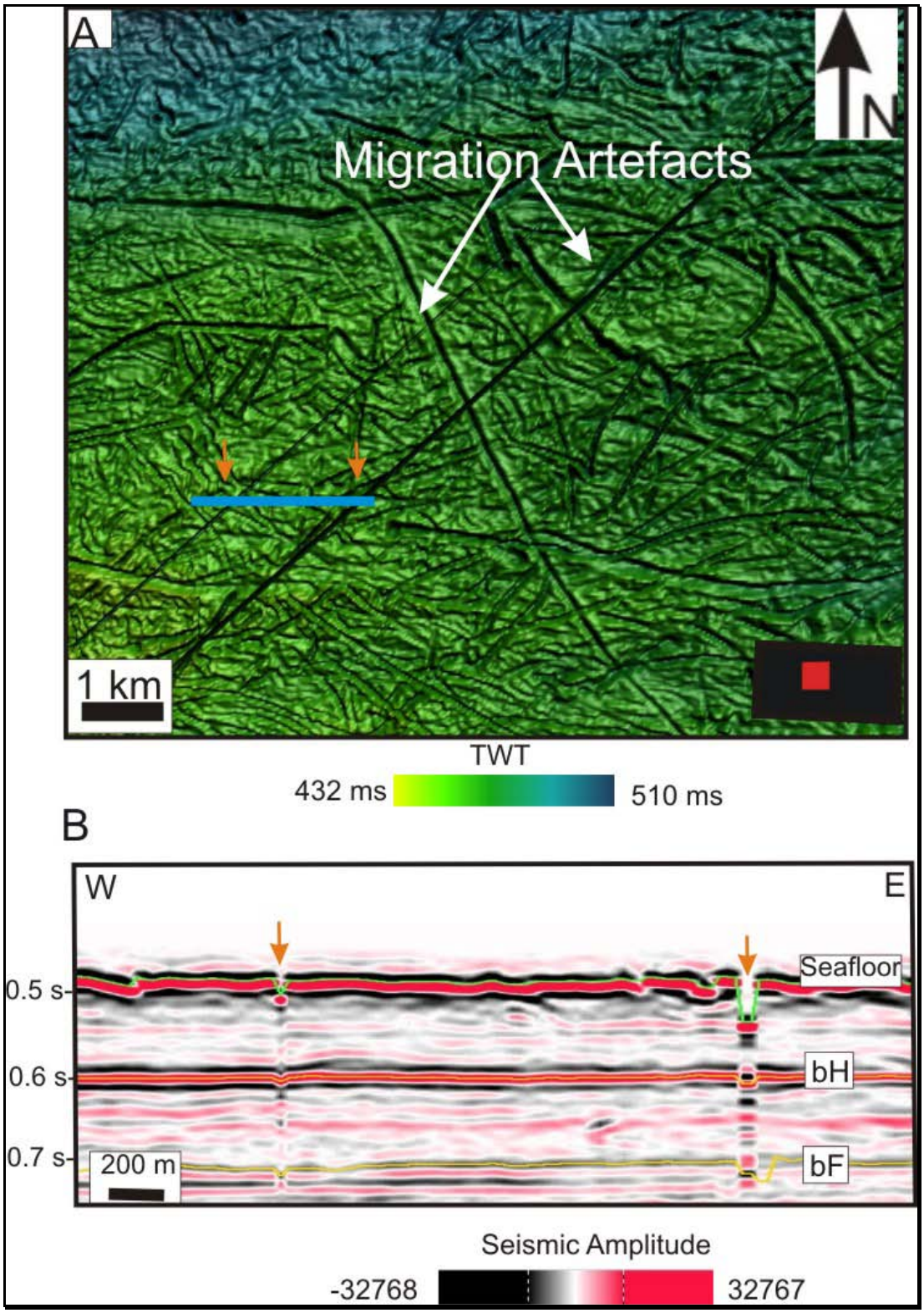

Figure 2.8: A. Shaded relief image of the seafloor. The black parallel lines show the lineation-like structures. Blue line is the seismic profile shown in B. The red box in the lower right corner shows the location of the figure within the dataset. **B.** Seismic profile across the lineation-like structures, which can be followed to the bottom of the data set.

2.5.3. Imbricate structures

Imbricate structures disturb the upper part of seismic unit H in the study area. They are found on vertical seismic profiles as dipping and obliquely imbricate stacked reflections (fig.2.9). These dipping reflections have lengths between 700 m and up to 3 km long, from 200 to 500 m wide, and up to 130 m deep. The angle of inclination varies from 10º to 52º. Most part of the features dip towards the west (fig.2.9), although some in some seismic lines they dip towards the east. On a time slide, a clear U-shape of the feature can be inferred (fig.2.9b).

Similar imbrications have been described by Rafaelsen (2007) in the Nordkappbanken area. They have been interpreted to be related to sailing direction during data acquisition. Due to the imbricate character and U-shape of the features, these reflections can be misinterpreted to be glaciotectonic imbricate structures (Rafaelsen et al., 2007). These imbricate features are therefore interpreted to be artifacts.

2.5.4. Terracing effect

The northwest part of the study area is dominated by a series of north to south oriented troughs and ridges (fig.2.10 and 4.25). These features occupy an area of about 360 km^2. Their main orientation is north to south and they are perpendicular to an E-W axis. They are between 5 and 15 km long. The spacing between ridges is between 300 and 400 m and width of the ridges is about 300 m. The ridges present heights up to 10 ms (TWT). The ridges are quite parallel to each other and appear at quite constant distances and the wiggle display of the reflector show that that the amplitude of some traces has been clipped (fig.2.11).

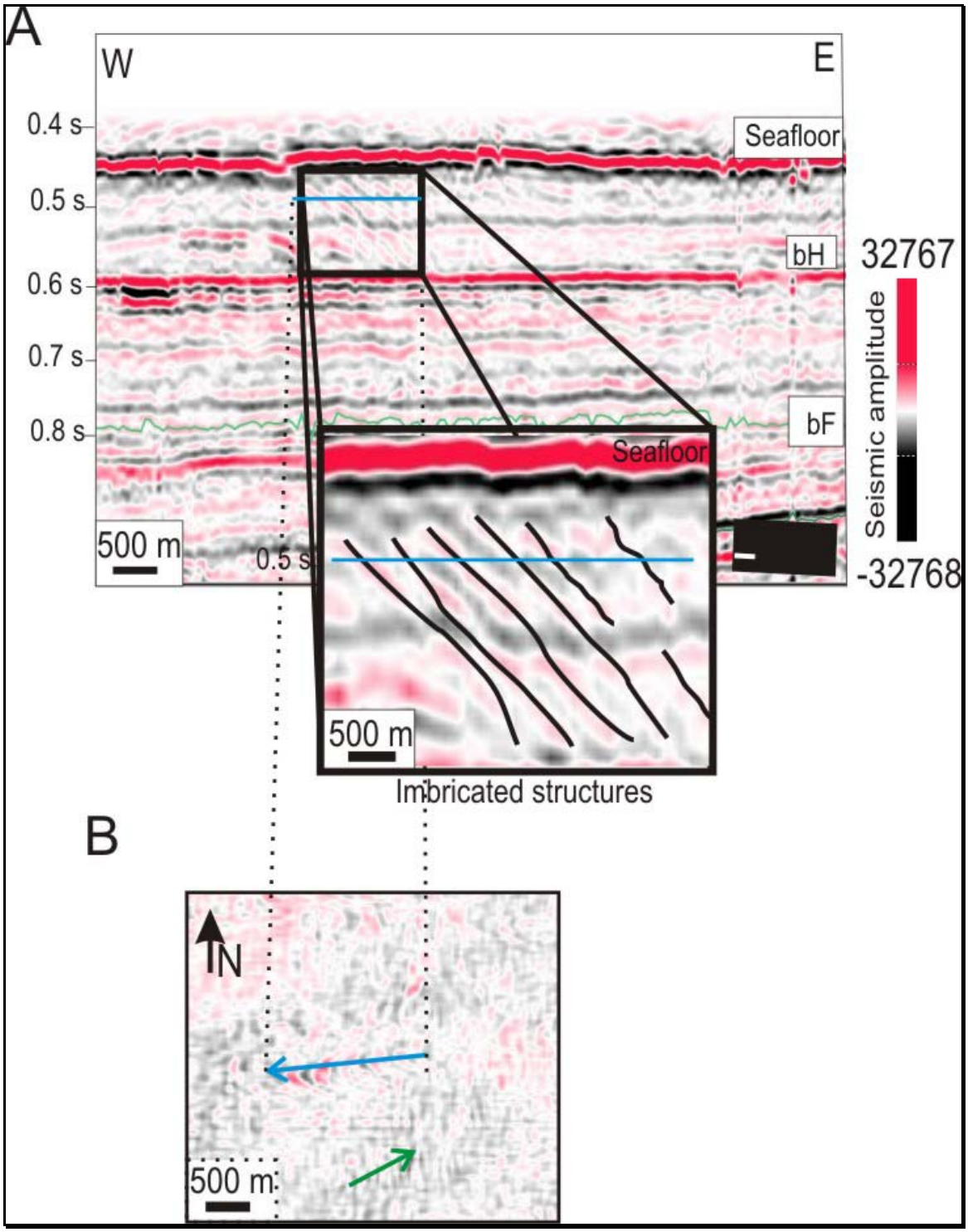

Figure 2.9: A. Seismic profile showing a series of imbricate structures at the top of seismic unit H. The blue line represents the location of the time slide. **B.** Time slide of the structure showing the characteristic U-shape of the feature. The blue arrow shows dipping reflection towards the WSW, while the green arrow indicates other structures dipping towards the ENE.

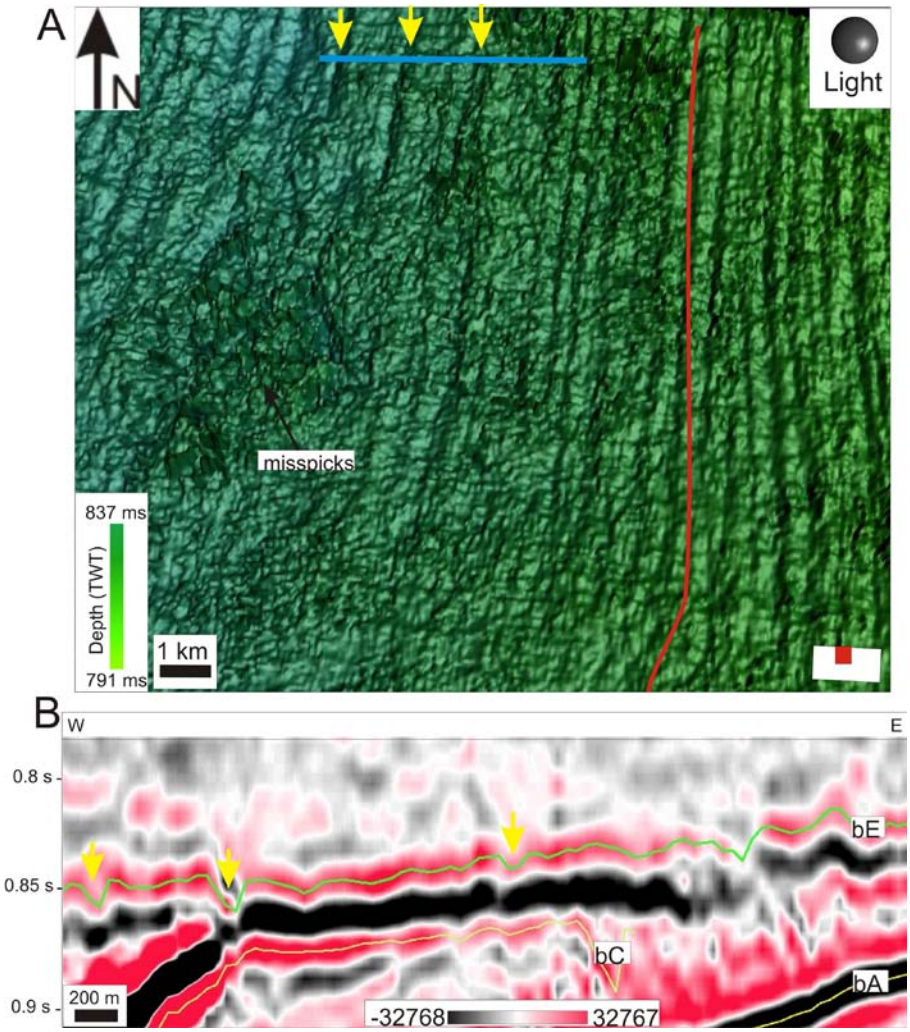

Figure 2.10: **A.** Shaded relief map of the horizon bE focusing on the ripple-like features to the NW (red lines). The blue line shows the location of the seismic profile in **B**. The yellow arrows show the location of the troughs of the undulations. **B.** Seismic profile across the undulations.

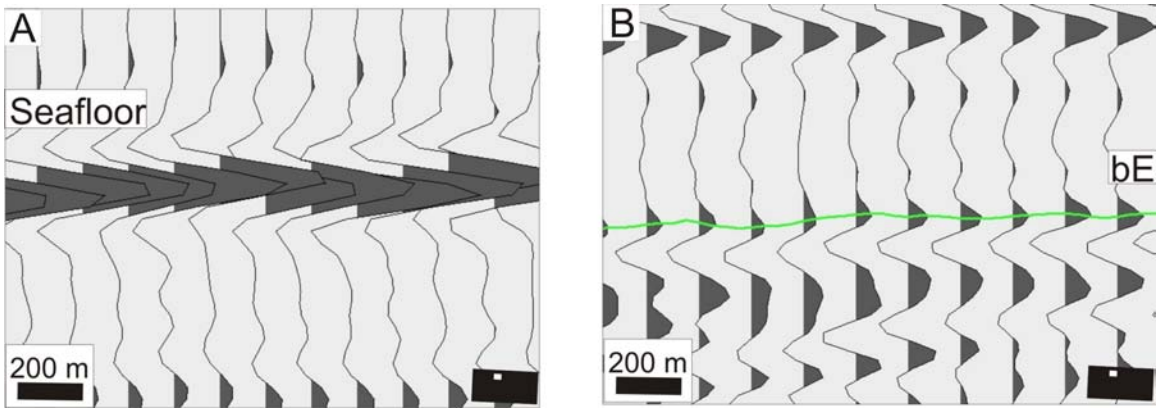

Figure 2.11: A. Wiggle trace of the seafloor. **B.** Wiggle trace of reflector bE. The small black box in the lower right corner shows the location of the profile within the 3D study area.

Terracing artifacts have been described for the seafloor interpretation of the Faroe-Shetland Island Channel by Bulat & Long (2001) and Bulat (2005). Terracing artifacts coincide with the sample rate of the data and is associated with clipped 8-bit data set and they occur due to clipping of the data. Although this dataset is not 8 bit, but 16 bit, clipping is unnecessary; however the wiggle display shows small clipping of the amplitudes both at the seafloor reflection (fig.2.11A) and at deeper reflections (fig.2.11B).

3. FEATURES IN THE SEISMIC DATA

In this chapter a description of the most common features which appear on the 3D seismic data will be described. A more detailed interpretation of the different seismic reflectors and units will be developed in chapter 4.

3.1. Curved furrows

3.1.1. Description

Curved furrows dominate the sea floor on the 3D seismic data set (fig. 3.1, 3.2a) and they appear also on deeper reflectors within the seismic unit GIII. They present a negative relief and have random orientations. Different furrows often cross each other. They do not reveal a single preferred orientation, but two main directions can be observed; E-SE and W-SW (fig.3.1). The curved furrows have lengths varying between 1 km and 10 km; most of them have lengths ranging from 1 to 5 km, although single furrows are longer than 10 km. The longest furrow observed on the seafloor is about 16 km; it could be longer because it seems to continue outside the data set. Widths of these furrows are in general around 150-180 m., although the widest furrow is 370 m wide. Their depth varies between 1-15 m (fig.3.1, 3.2). There does not seem to be any correlation between the length/width ratio and the depth of the furrows. On the seismic profiles, the furrows have a U- or V-cross section shape (fig.3.2), and normally levees occur on one or both sides of the scours (fig.3.2B). Width, depth, and form vary greatly from one furrow to another and also along the same furrow. Depending on their shape and length, the furrows can be divided in two groups. The first one contains the majority of the furrows, which are long (some of them up to 12 km), shallow (10 ms TWT) and continuous. The other group contains deeper furrows (ca 20 ms TWT) with a circular termination (fig.3.2C).

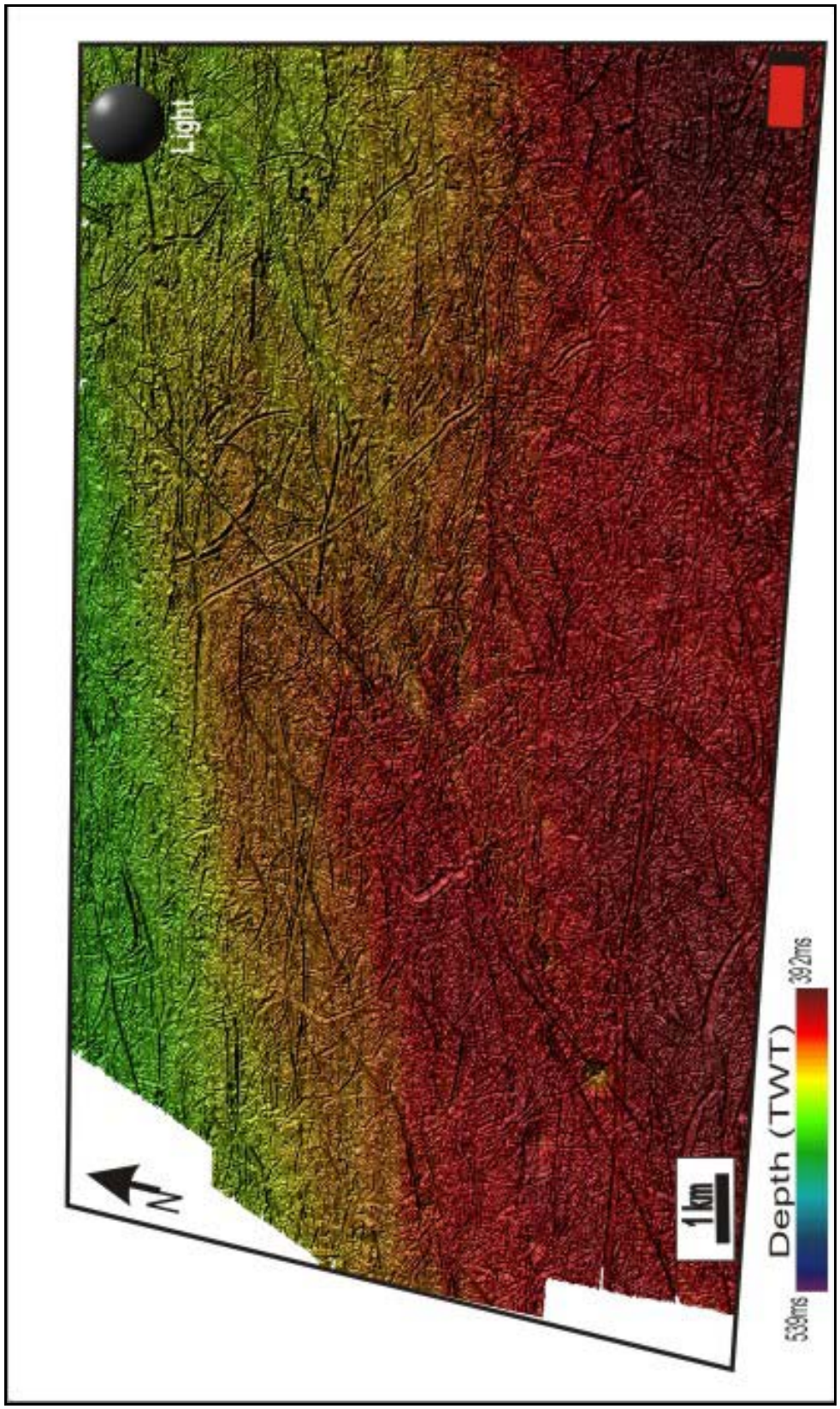

Figure 3.1: Shaded relief image of the seafloor on Veslemøy. It shows the random orientation of the iceberg ploughmarks.

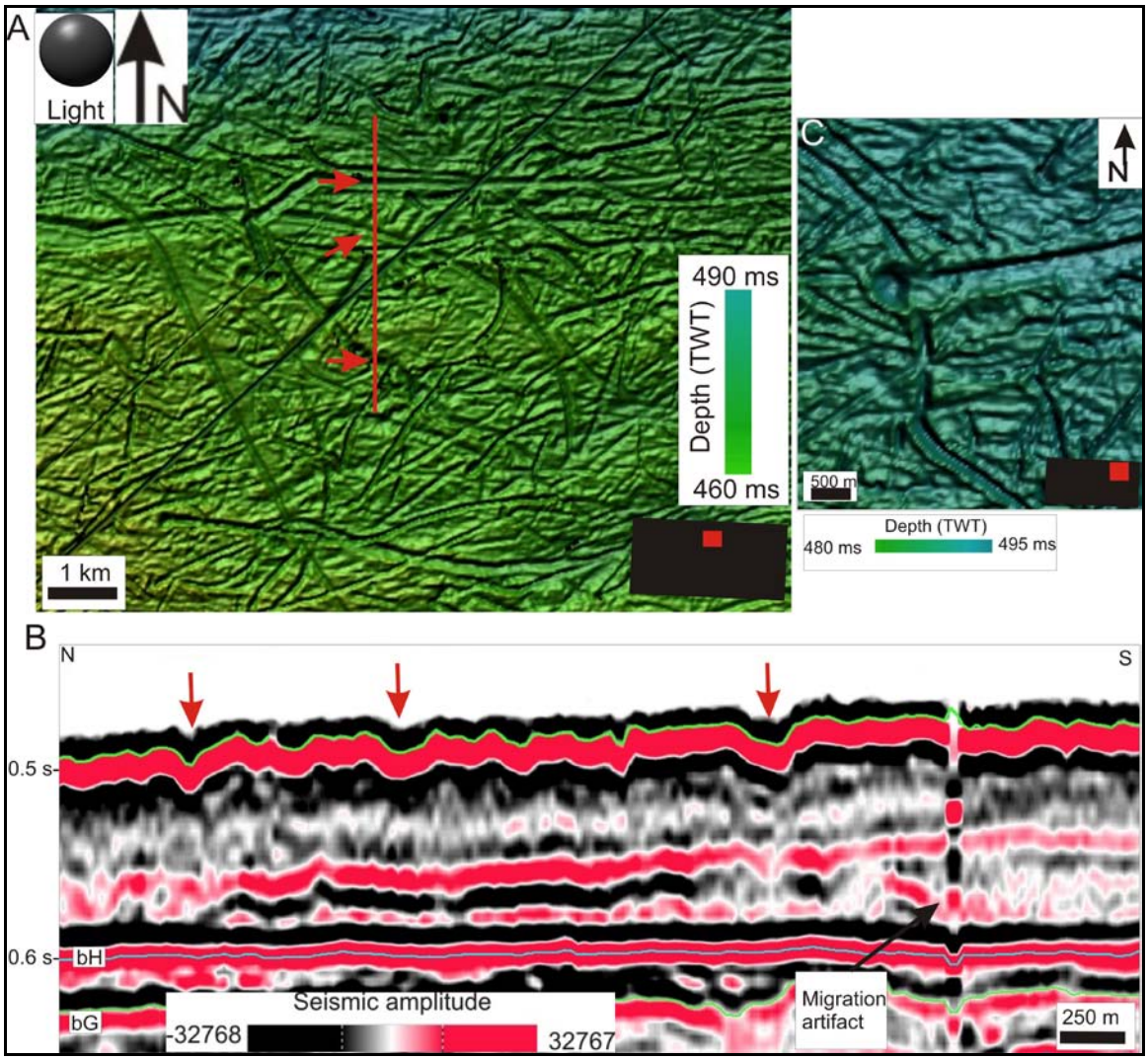

Figure 3.2: **A.** Shaded relief image of iceberg ploughmarks in the Veslemøy 3D dataset. The yellow line represents the seismic profile in B. The small red box in the lower right corner shows the location of the figure within dataset. **B.** Seismic profile across iceberg ploughmarks. The blue arrows show the location of V-shape ploughmarks and the green arrow shows a U-shape ploughmark. **C.** Shaded relief image of part of the seafloor. It focuses on a furrow with circular termination. The small red box in the lower right corner shows the location of the figure within the dataset.

3.1.2. Interpretation

The curved furrows are interpreted to be iceberg ploughmarks, indicative of a glacimarine environment (Rafaelsen et al. 2002, Andreassen et al., 2007a; 2008). Iceberg ploughmarks present a U- or V-shape cross section with a ridge on each side (Lien 1983). Calved icebergs are transported long distances before they melt and where the keel of these icebergs contacts the seafloor (fig.3.3), scouring or ploughing of the substrate takes

place (Dowdeswell et al., 1993; 2007). The scouring occurs before they come to a complete halt (Dowdeswell et al., 1993; 2007). The scours have irregular shapes and orientation because their movement is controlled by currents and wind (Lien, 1983).

The circular form at the end of some of the plough marks (fig.3.2C) has been interpreted to be due to a halt in the movement of the iceberg, where the currents, tides and waves can have moved it locally to generate the circular shape. This can be taken as an indicator or iceberg direction movements and therefore currents (Syvitski, 2001).

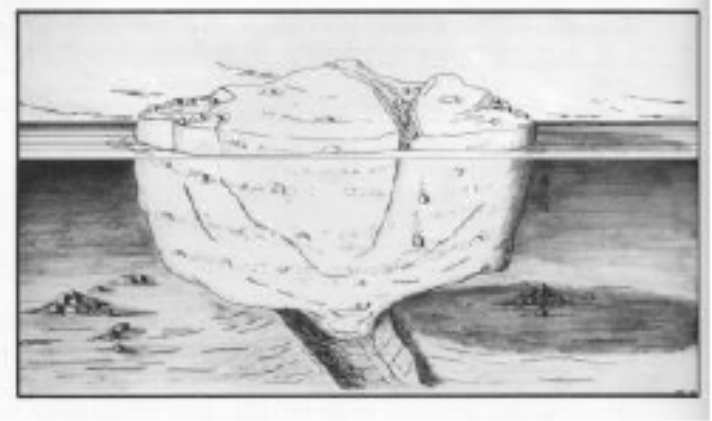

Figure 3.3: Illustration of how iceberg ploughmark are formed. From Lien (1983).

3.2. Parallel furrows

3.2.1. Description

Several of the interpreted horizons in unit GIII and reflector bC show sets of parallel lineations with a well defined orientation. The dimensions of these lineations vary between a few km and up to 26 km long, from some few meters up to some hundred meters wide and between 2 and 12 ms (TWT) in depth. They could be longer because in most of the cases, they seem to continue outside the 3D study area, both towards the east and west. On buried surfaces they seem to be negative scars on the surface (fig.3.4).

3.2.2. Interpretation

The parallel lineations in the Veslemøy High 3D dataset resemble megascale glacial lineations (MSGL) described on the continental shelf of Antarctica (O' Cofragh et al., 2002; 2005), in the Barents Sea (Canals et al., 2000; Rafaelsen et al., 2002; Andreassen et al., 2004; Ottesen et al. 2005, 2008; Andreassen et al, 2007) and other glaciated continental shelves (Clark, 1993; Stokes & Clark, 1999; 2001; 2002, Clark et al., 2003). There are two main theories about their formation (Stokes & Clark, 2002), they can be formed by fast ice streams over a short period of time, or slow ice over a long period, but most likely they are formed by fast streams in short periods of time, either as ice streams or surges (Clark, 1993; Andreassen et al., 2008). Fast flow is inferred from sets of elongated streamlined lineations with abrupt lateral margins and with high length/width ratios, exceeding 10/1 (Stokes & Clark, 1999). MSGL are interpreted to be formed by subglacial sediment deformation (Tulaczyk et al., 2001; Clark et al., 2003; Andreassen et al., 2008).

The parallel lineation in Veslemøy High 3D dataset are characterized by length:width ratios 100:1 and they are therefore interpreted to be MSGL formed during fast-flowing grounded glaciers.

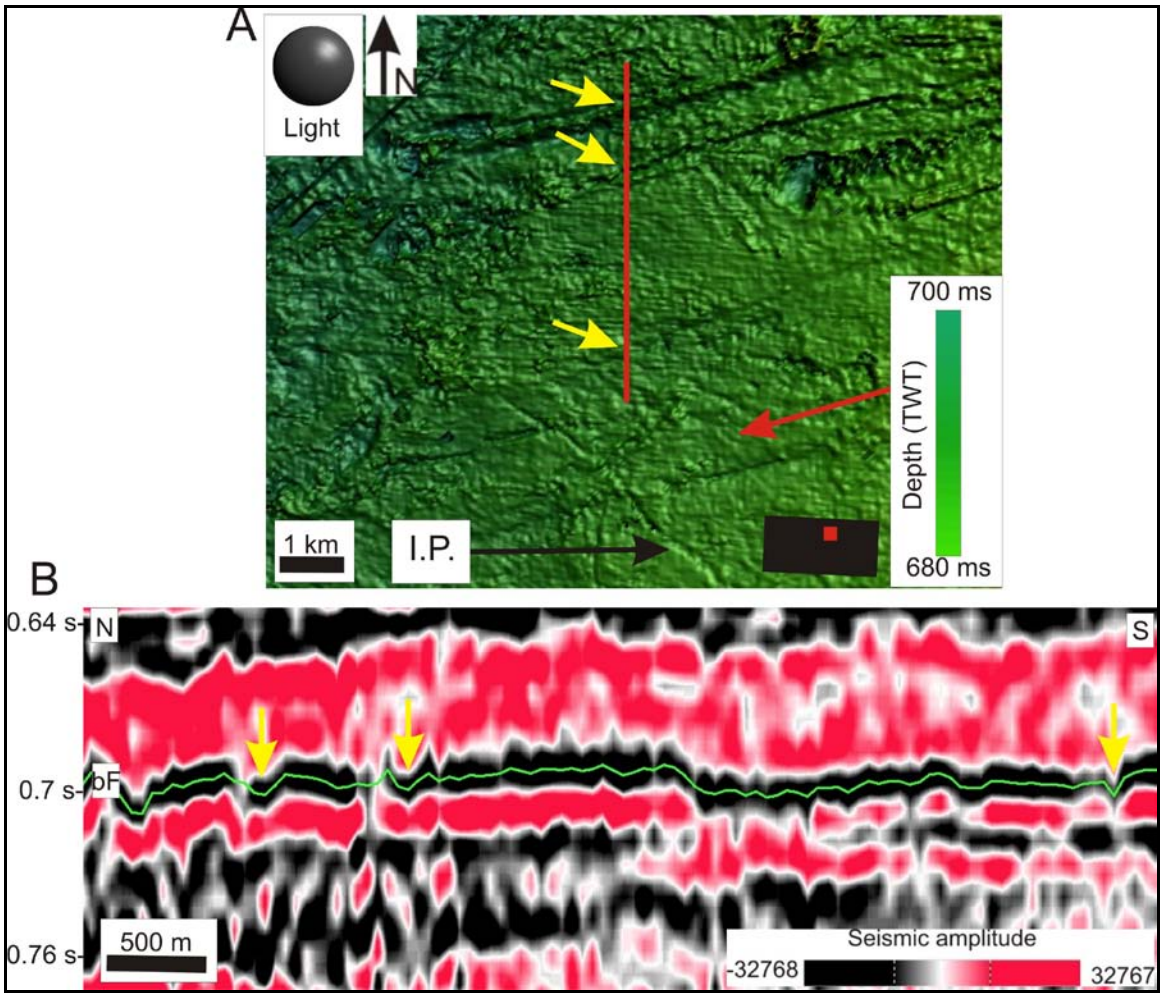

Figure 3.4: **A.** Zoomed shaded relief of a deep reflector (bF), where megascale glacial lineations going from the east to the west can be observed. The red line represents the seismic profile shown in B and the red box in the lower right corner shows the location of the area within the 3D dataset. **B.** Seismic profile across the MSGL. The yellow arrows show the location of the furrows on the shaded relief map and the seismic profile.

4 SEISMIC REFLECTORS AND SEISMIC UNITS

4.1. Introduction

In the southwestern Barents Sea continental margin, the sediment packages GI-GIII (Faleide et al., 1996; Butt et al., 2000; Andreassen et al., 2004) comprise seven regional reflectors, R1-R7 (Faleide et al., 1996). In this work, three of these regional reflectors have been studied (R1, R5 and R7), in addition to four internal reflectors within unit GIII (table 4.1; fig.4.1). The nomenclature used in this work (units A to H) corresponds to that of Nielssen (2000) and Ødegaard (2005). Reflectors bB and bD will not be studied because they are not present in the Veslemøy High 3D data set.

The seismic survey NH9702 has been used to correlate these reflectors with work previously done on the Sørvestnaget area. The seismic reflectors in the southwestern Barents Sea are characterized by westward progradation of clinoforms (fig.4.1). In the Veslemøy 3D area, reflectors within the unit GI represent only the paleo-slope, while reflectors bC and above represent only the paleo-shelf (fig.4.1). Table 4.1 gives a summary of the relationships between the nomenclature used in this work and nomenclature used for the same reflectors at a regional scale (Faleide et al., 1996). The part of the signal that has been followed during the interpretation and some key notes for the location of the reflectors is also shown.

Table 4.1: Interpreted seismic reflectors and parts of the seismic signal used to map these.

Reflector	Faleide et al. 1996	Seismic signal	Notes
baseA (bA)	R7	Minimum amplitude	Base Unit A / GI
baseC (bC)	R5	Maximum amplitude	Base Unit C / GII
baseE (bE)	R1	Maximum amplitude	Base Unit E / GIII
baseF (bF)	--	Minimum amplitude	Internal GIII reflector
intraF	--	Maximum amplitude	Internal GIII reflector
baseG (bG)	--	Maximum amplitude	Internal GIII reflector
baseH (bH)	--	Upper zero crossing	Internal GIII reflector
Seafloor		Upper zero crossing	

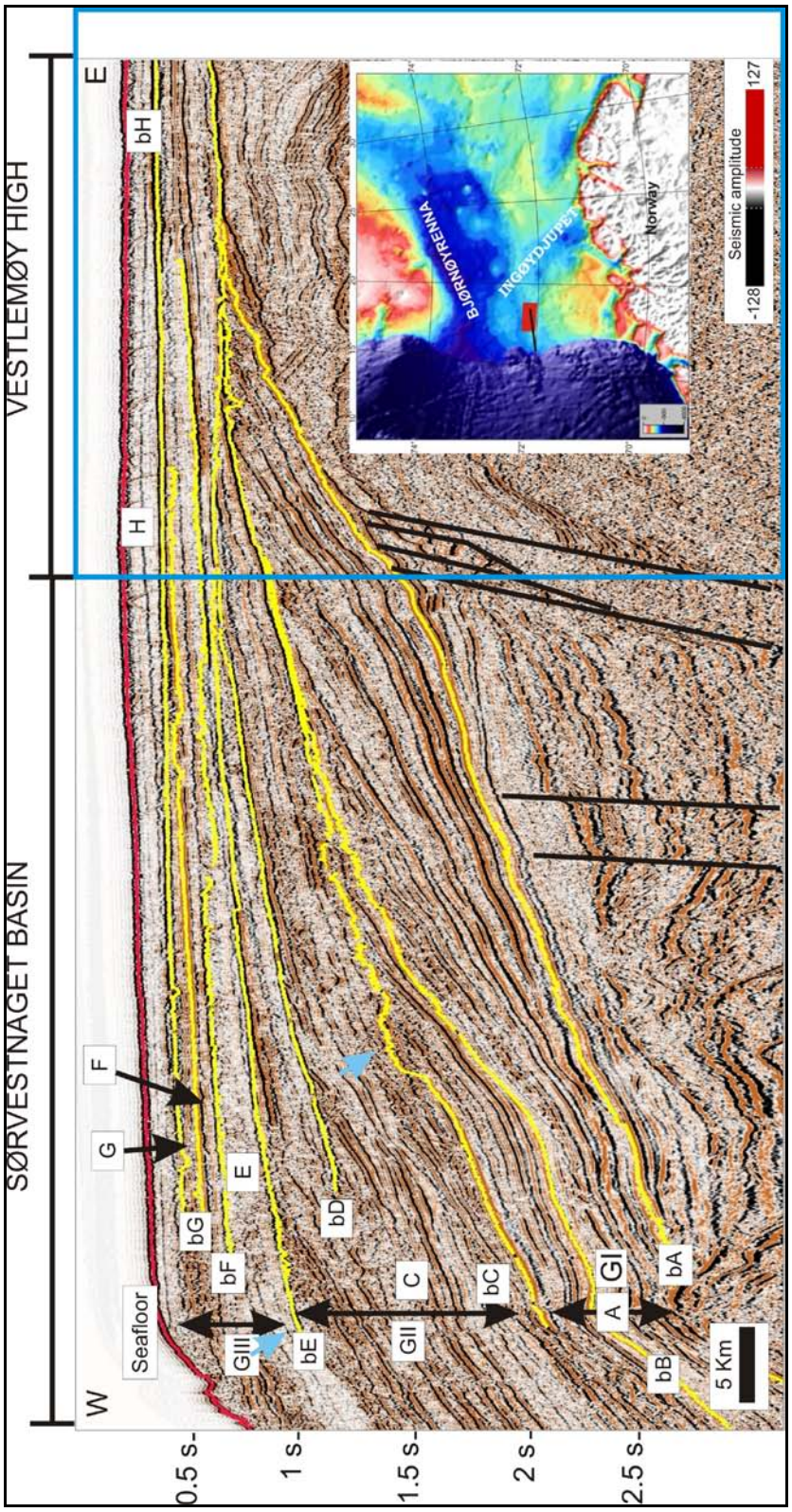

Figure 4.1: Seismic stratigraphy in the SW Barents Sea. Seismic units GI-GIII are the main glacial seismic packages (Faleide et al., 1996), while the seismic reflectors bA-bH are the interpreted seismic unconformities. Blue arrows indicate the location of the paleo-break. The 3D study area is enframed with a blue box.

4.2. Reflector bA

Reflector bA marks the base of unit A and it is present in most of the study area (fig.4.1 and fig.4.2). Towards the east, the reflector is truncated by the overlying reflector bE. In the Veslemøy area, bA is located at depths between 742 ms and 1710 ms (TWT). The reflector defines a westward dipping slope (figs.4.3 and 4.4). The reflector is affected by faulting that has resulted in local variations in gradient of the slope (fig.4.4). On a shaded relief map of the bA paleo-surface two types of morphological features are recognized: i) Straight, elongated furrows perpendicular to the slope and ii) Furrows parallel to the slope (fig.4.2).

Straight, elongated furrows perpendicular to the slope

The eastern part of the study area is characterized by several straight and elongated furrows (I-VIII in fig.4.2). Some of these can be followed towards the western limit of the study area (furrow III). These furrows are mainly straight to slightly meandering (fig.4.2). Their orientation is ENE to WSW, only the northernmost channel (fig.4.2) has a different orientation (ESE to WNW). The longest furrow can be followed for about 15 km and the shortest for around 2 km. Their widths vary in general from 150 m to 200 m except one furrow in the southwesternmost part of the study area, which is 800 m wide (furrow IV in fig.4.2). The depths of the furrows vary between 6 and 16 ms (TWT). Some of them (i.e. furrow IV in fig.4.2) show a bifurcation downslope (fig.4.5). On seismic profiles the furrows reveal a U-shaped (fig.4.6c) or a V-shaped form (fig.4.5b).

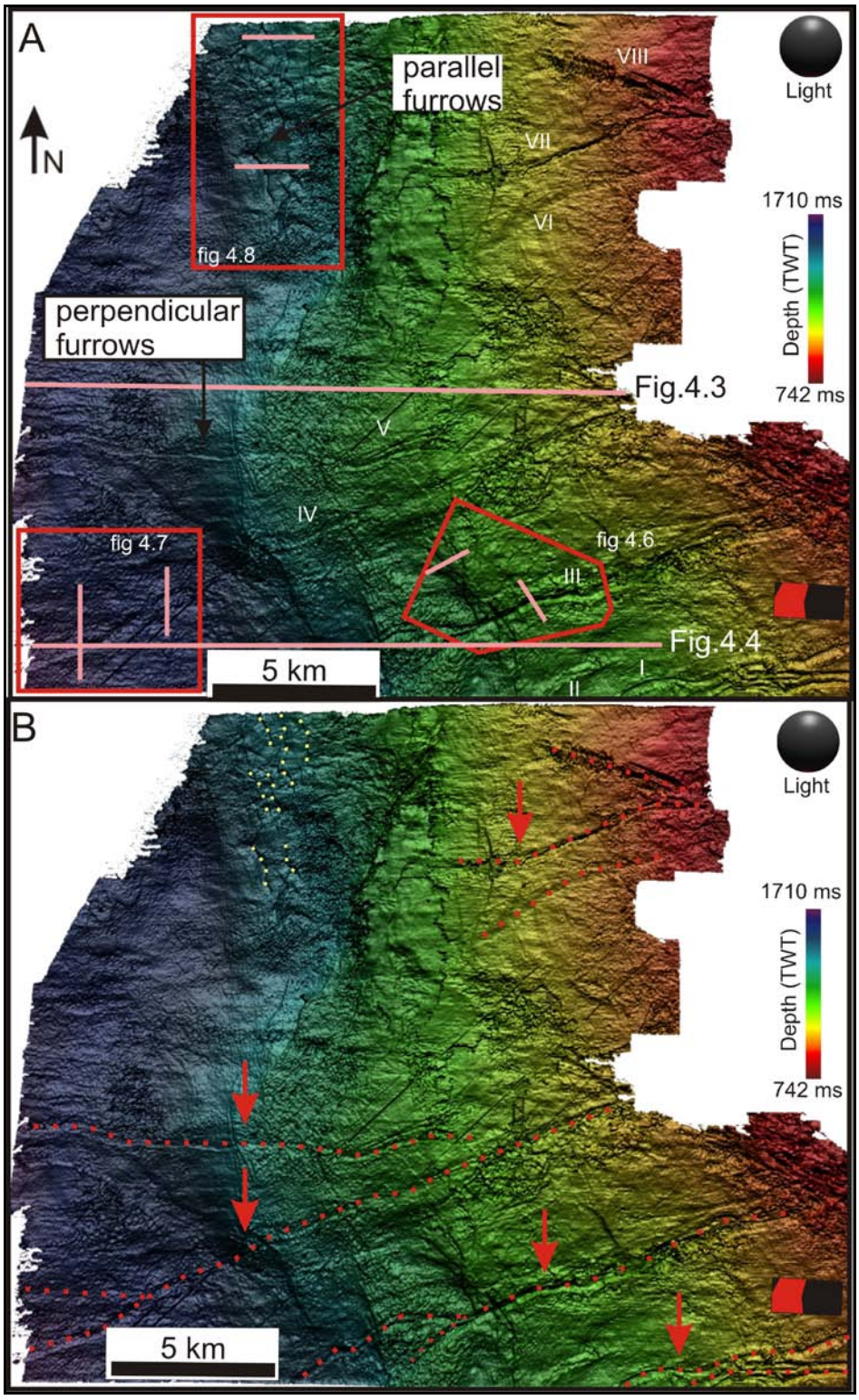

Figure 4.2: Shaded relief image of the paleo-surface bA. Paleo-channels with a WSW orientation are marked from I-VII, while the paleo-channel with a WNW orientation is marked as VIII. The red squares indicates the location of the figures 4.6-4.8, the pink lines show the location of seismic profiles shown in these figures and the yellow dotted lines indicate the features parallel to the slope. The small red boxes in the lower right corner show the location of the map within the 3D area.

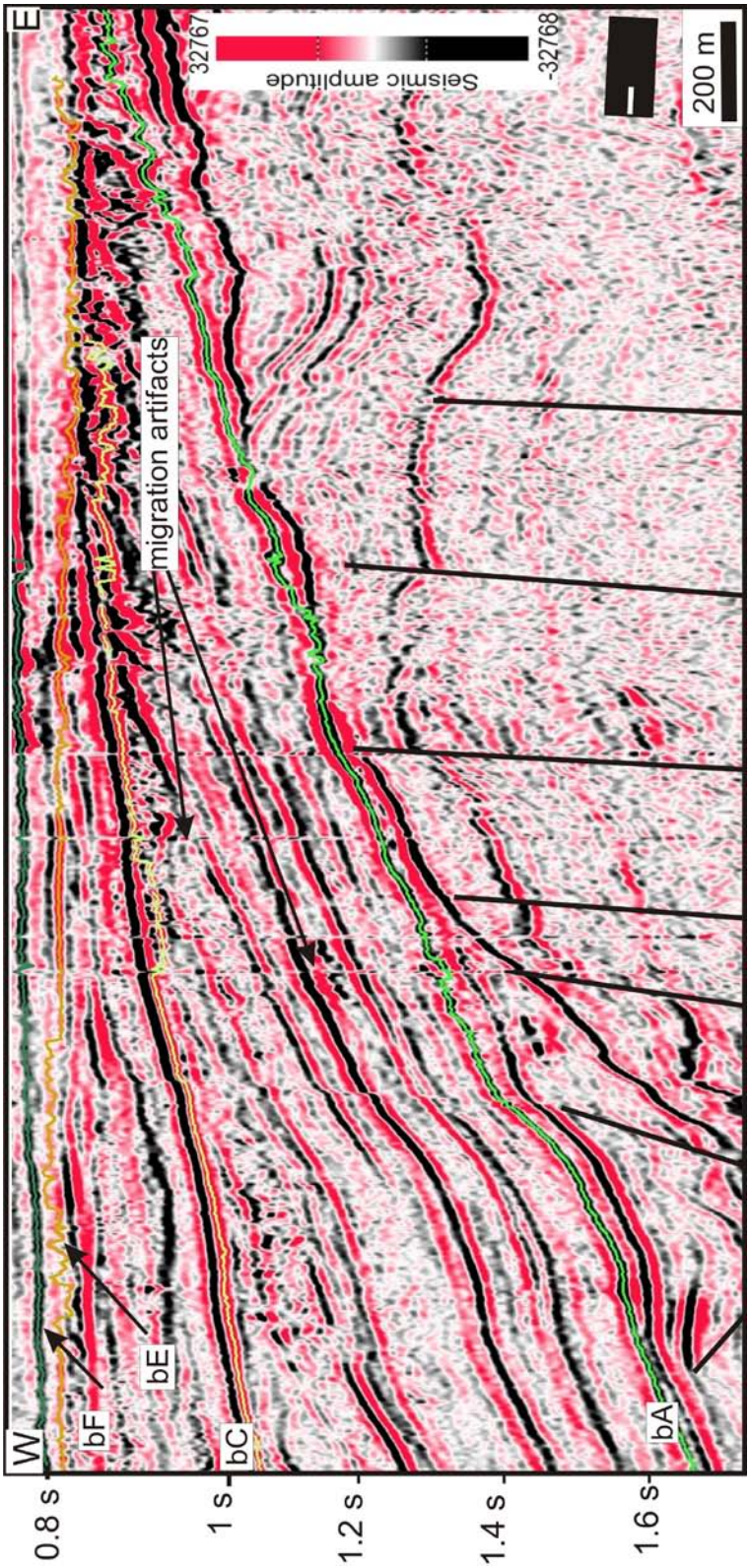

Figure 4.3: Seismic profile showing stratigraphic location of reflector bA and the location of faults below reflector bA. The small black box in the lower right corner shows the location of the seismic line within the 3D study area.

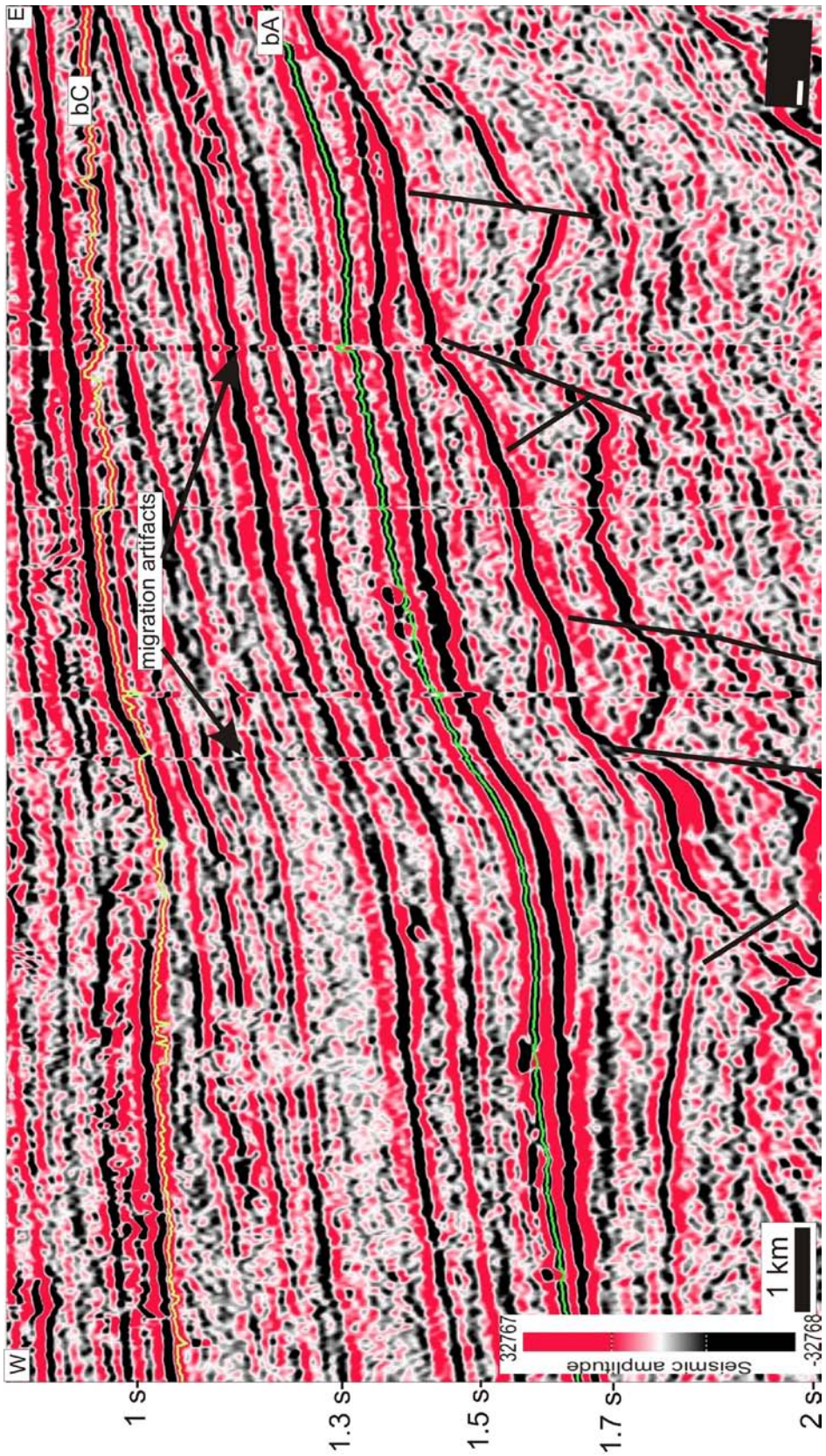

Figure 4.4: Seismic profile the location of the paleo-slope and paleo-shelf on surface bA. The small black box in the lower right corner shows the location of the seismic line within the 3D study area.

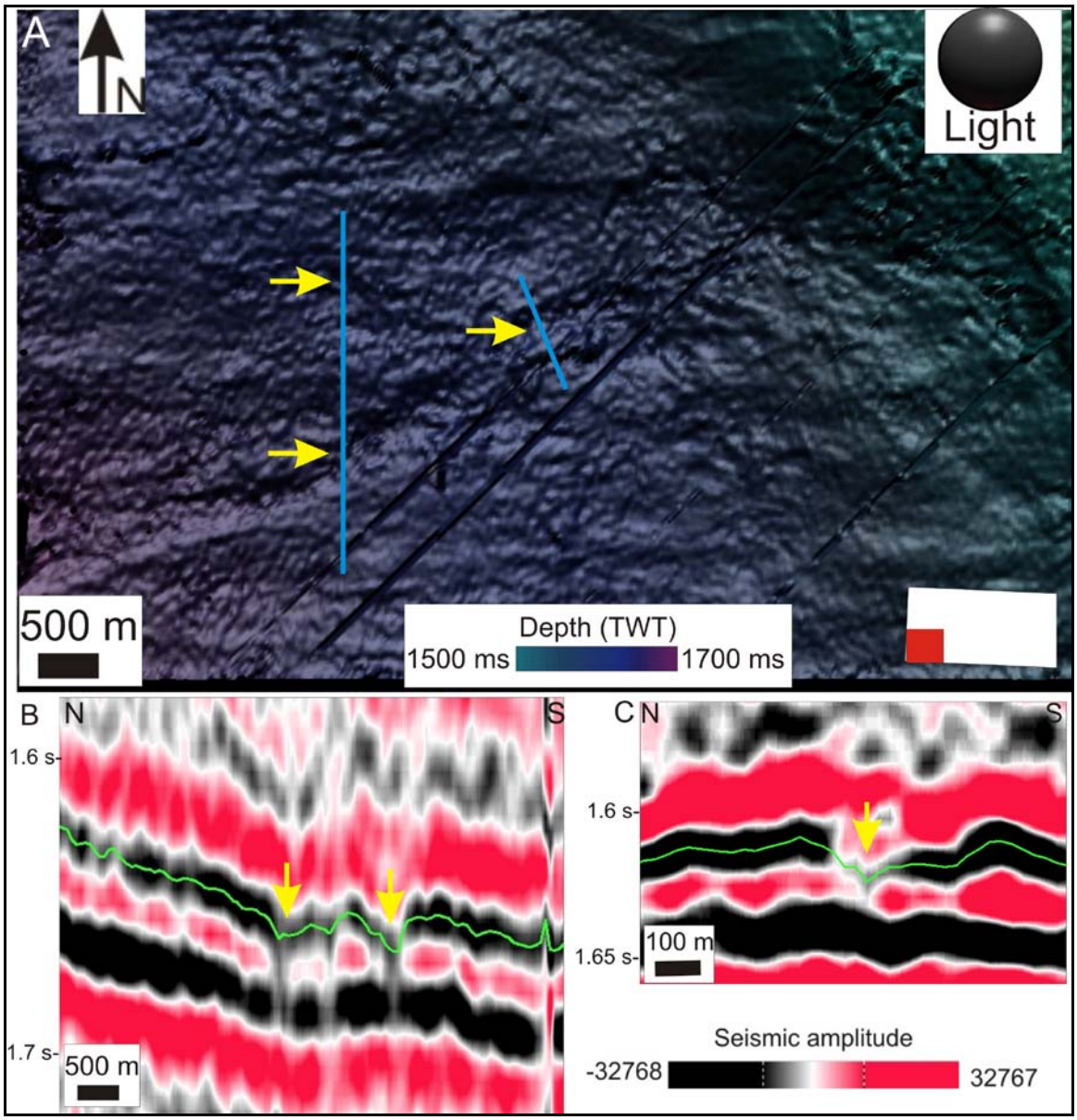

Figure 4.5: A. Shaded relief image of furrow IV and its bifurcation in the southwestern corner of the study area. The blue lines show the location of the seismic profiles shown in B and C. The small red box in the lower right corner shows the location of the image within the 3D study area. **B.** Seismic profile across the furrow which has bifurcated. **C.** Seismic profile across the furrow IV. The yellow arrows indicate the location of the furrows.

Interpretation of straight, elongated furrows perpendicular to the slope

Based on the morphology and orientation, the furrows are interpreted to be channels (fig.4.2 and 4.5) located on the paleo-slope. Straight and deep channels indicate high flow currents, while more meandering and shallower channels indicate low flow currents. There is no evidence of grounded ice in the Veslemøy High 3D area on this reflector and

therefore the channels are not interpreted as subglacial meltwater channels. On the other hand, reflector bA has been interpreted to represent the onset of ice rafting in the Norwegian-Greenland Sea (Vorren et al., 1991). For this reason, the channels on bA are interpreted to be formed by turbidity currents originating from glacial meltwater. The same interpretation has been made for channels located at the base of unit GIII in the Sørvestnaget Basin 3D area (Laberg et al., submitted) and Svalbard (Butt et al., 2000). A possible origin of these channels is inferred to be restricted ice areas in Scandinavia, where mainly alpine cirque glaciers existed at this time (Kleman & Stroeven, 1997).

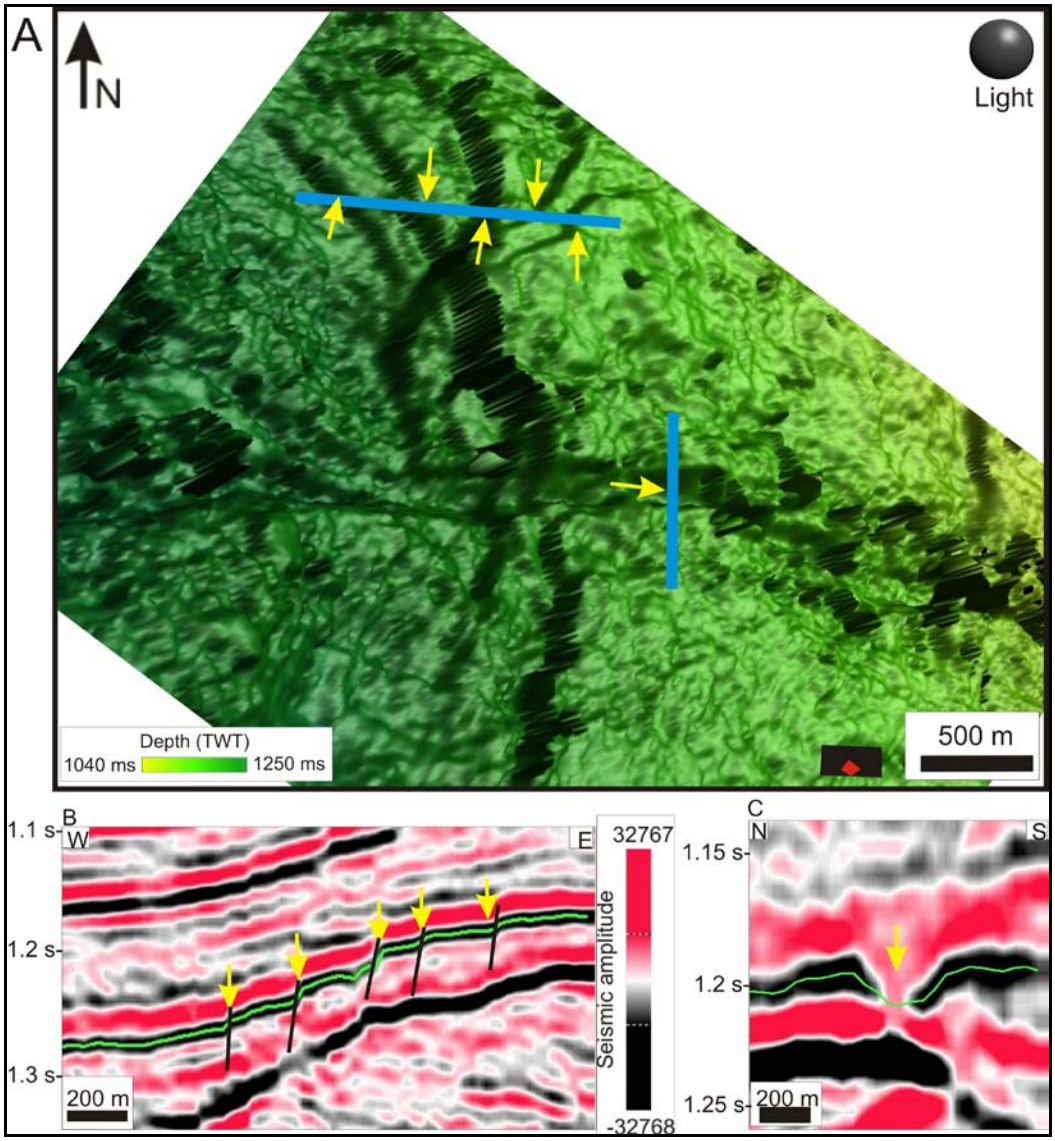

Figure 4.6: A. Shaded relief image of reflector bA showing the location of the step-like escarpments and channel III. The small red box in the lower right corner shows the location of the image within the 3D data set. **B.** Seismic profile across the escarpments. **C** Seismic profile across the channel.

Description of furrows parallel to the slope

A distinctive group of furrows is located in the northwestern part of the study area (fig.4.2). They have a NNW-SSE orientation, lengths of 1 to 2 km and widths of 170 to 300 m and most of them are less than 10 ms (TWT) deep although they can reach 20 ms (TWT). These features are parallel to the strike of the slope and parallel to the general trend of faulting in the study area (fig. 4.7; orange arrows) Fault planes can be followed upwards and downwards in the stratigraphy from these depressions (fig. 4.7).

Interpretation of furrows parallel to the slope

The orientation of these features, parallel to the strike of the slope makes it highly improbable that the features are channels. In glacimarine environments, iceberg ploughmarks are a quite common feature, but in present seafloor images they appear as curved features, with random orientation and usually present a circular termination at one end. The features on this surface present a rather defined orientation and do not resemble to iceberg ploughmarks.

The features have a NNW-SSE orientation and on seismic profiles, they are associated with fault planes (fig.4.7). In addition, previous work shows that main faults in the southwestern Barents Sea show a preferred NNW-SSE orientation and are related to the opening of the Norwegian-Greenland Sea (Faleide et al., 2008). For this reason, these features are interpreted to be faults.

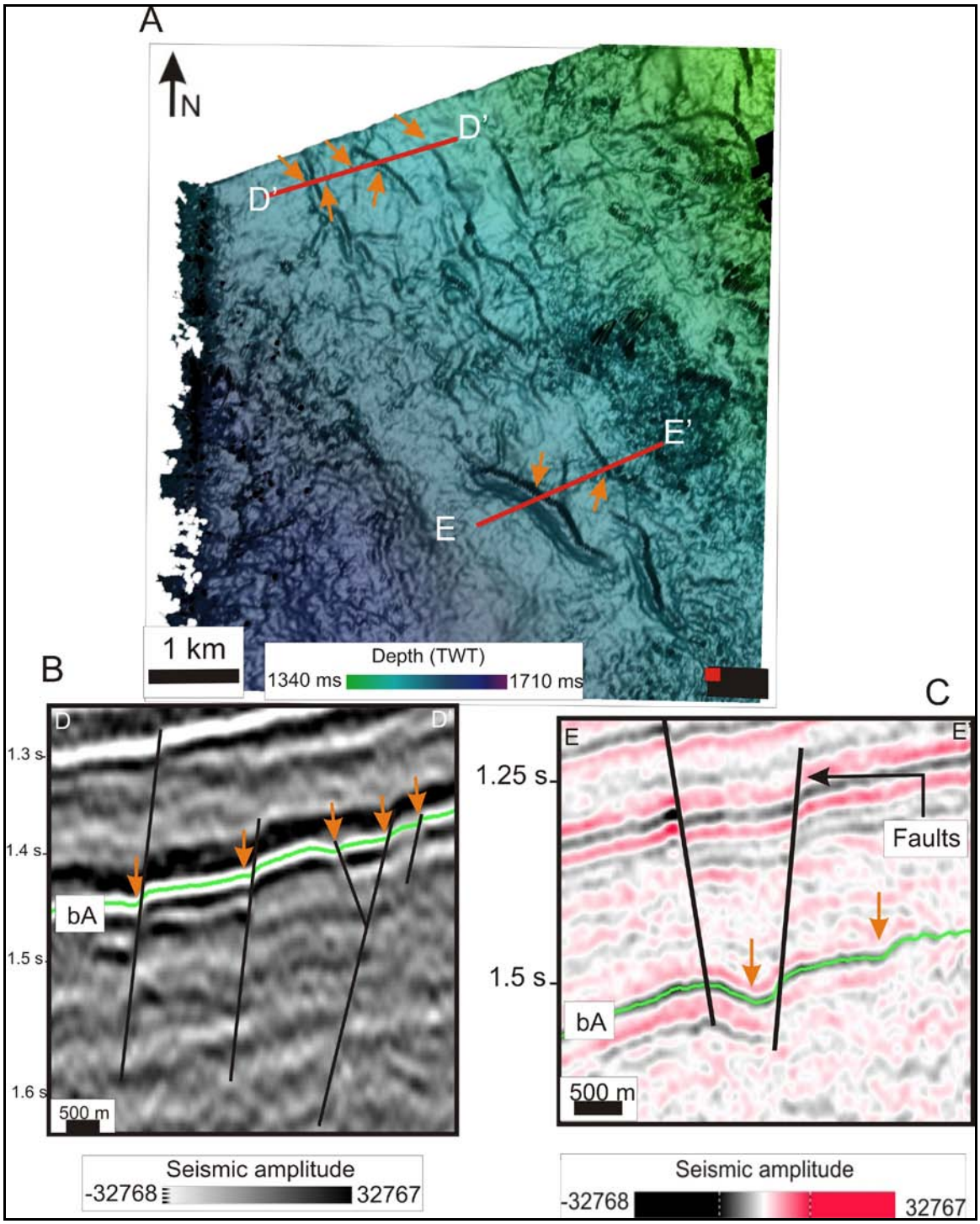

Figure 4.7: A. Shaded relief image of the furrows parallel to the slope of bA. The red lines indicate the location of the seismic profiles in B and C**.** The orange arrows indicate the location of the furrows. The small red box in the lower right corner shows the location of the image within the 3D data set**. B.** Seismic profile across the furrows as seen in figure A. **C.** Seismic profile across the furrows as seen in A.

4.3. Seismic unit A

Seismic unit A is bounded by reflectors bA and bC (fig.4.8). The top of seismic unit A in the study area is truncated by reflector bC (fig.4.8 and fig.4.9). In the Veslemøy High 3D area, the internal reflectors on the lower part of the unit are parallel to the reflector bA (fig.4.1). The internal configuration reveals a prograding oblique internal signature towards the southwest. The reflections have medium to good continuity and medium to high amplitude. In the lower part of unit A, these high amplitude reflections are separated by areas with low amplitude and transparent areas. On along-slope orientated seismic profiles, the high amplitude reflections are disrupted drastically (fig.4.8). On seismic profiles from north to south, the internal reflections also show a pattern parallel to the base and truncated by reflector bC in the north (fig.4.9). The internal reflections are dominated by different high amplitude anomalies and acoustic masking (fig.4.8 and 4.9).

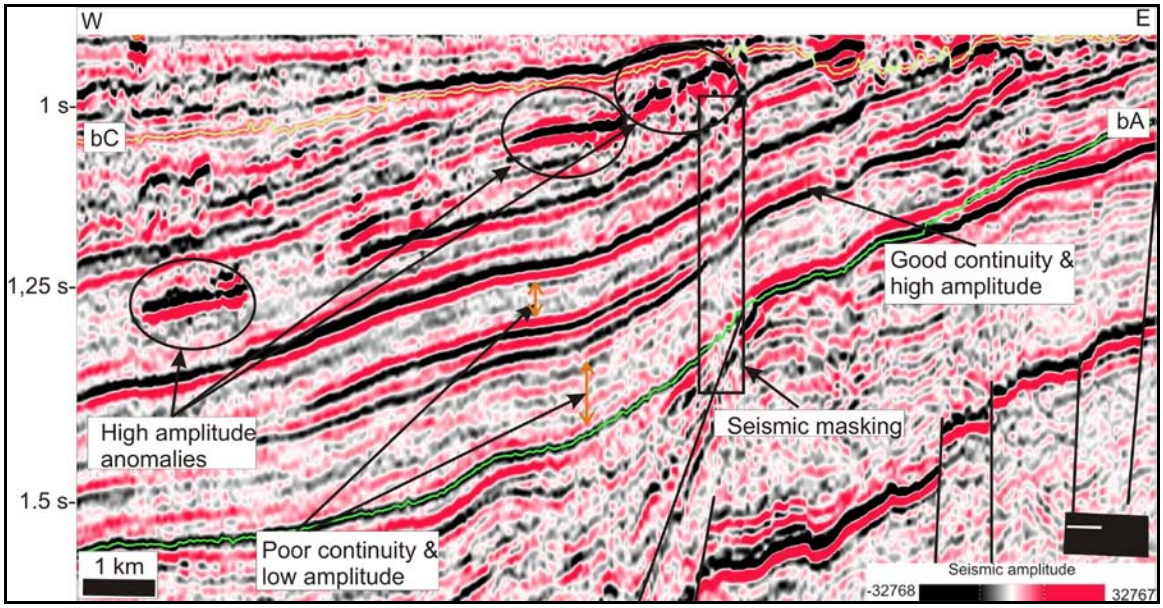

Figure 4.8: Seismic profile showing the oblique, prograding seismic signature of the seismic unit A from east to west of the study area. The black small rectangle on the lower right corner shows the location of the seismic lines within the study area.

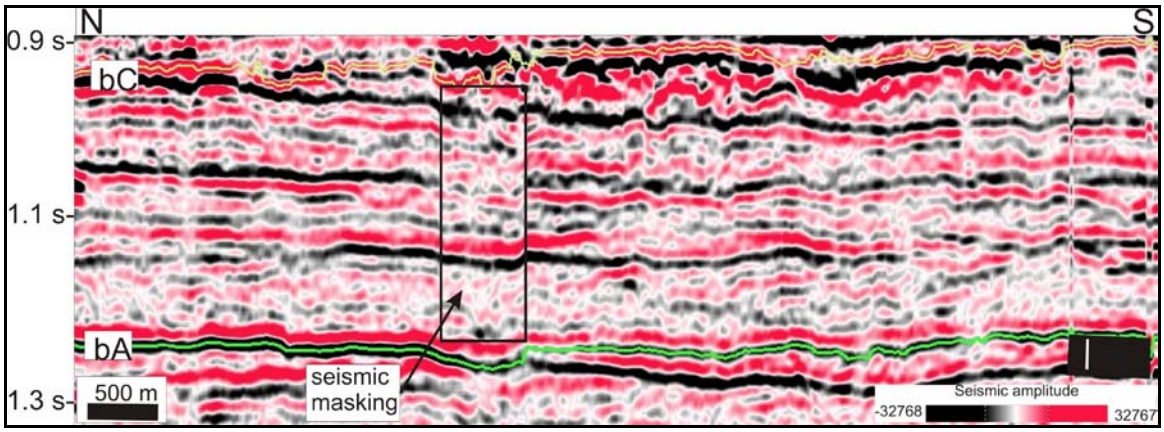

Figure 4.9: Seismic profile showing the straight-oblique, prograding seismic signature of the seismic unit A from north to south of the study area. The black small rectangle on the lower right corner shows the location of the seismic lines within the study area.

Interpretation of unit A

The seismic unit A represents paleo-slope in the southwestern Barents Sea and it is characterized by a progradational pattern of clinoforms dipping towards the southwest and seismic reflections of varying continuity interpreted to represent shelf margin deltaic facies (Andreassen et al., 2007b). Prograding oblique clinoforms are formed due to a deterioration in climate and onset of a glaciation instigated by the later Neogene uplift phase affecting the circum north Atlantic margins (Vorren et al., 1991; Doré et al., 1999; Stoker, 2002; Stoker et al., 2005; Dahlgren et al., 2005) and related to the different advances of glaciers to the slope. The sediments are eroded and transported by the glacier and deposited as gravity flows along the slope. There is no evidence of grounded ice and the channels interpreted in reflector bA may indicate a glacifluvial environment.

4.4. Reflector bC

Reflector bC is the base of unit C and it is located at depths between 663 and 1178 ms (TWT) (fig.4.10). The reflector truncates unit A and it is truncated by reflector bE in the east (fig.4.1). It can only be followed in the western half of the study area (fig.4.11). The deepest areas are located in the south of the study area. On this surface there are three main geomorphic features that will be described and interpreted. These features are i) parallel lineations; ii) east to west orientated depressions and iii) dipping layers associated with one of the depressions.

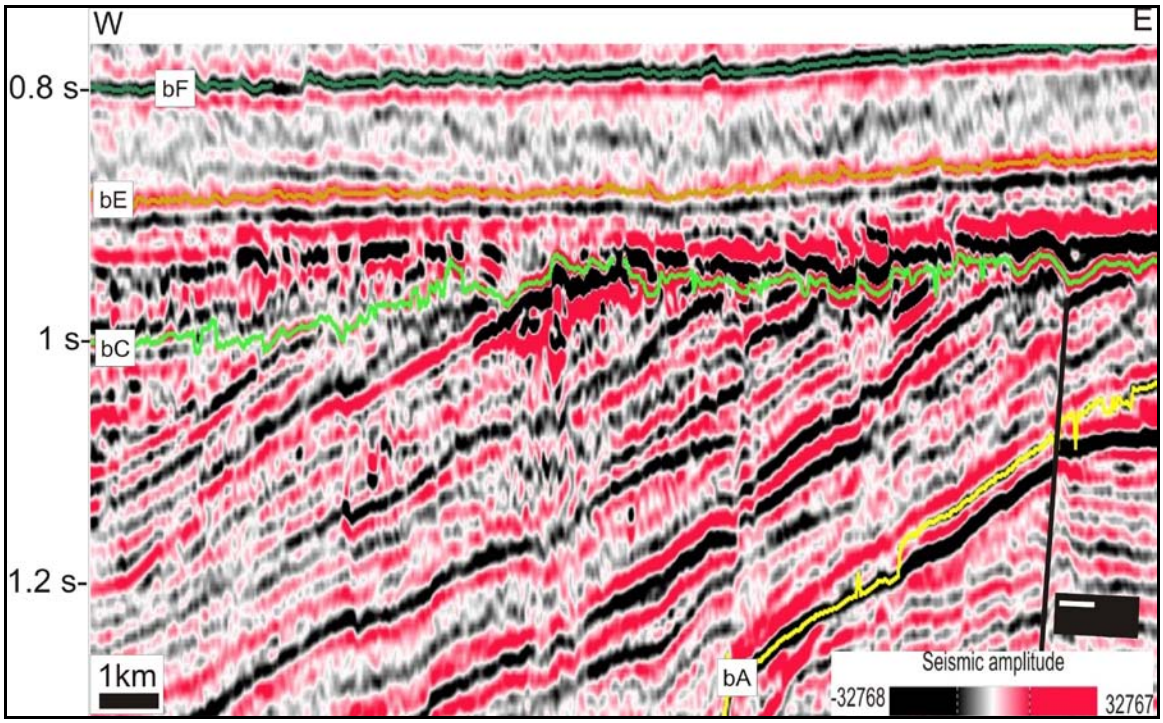

Figure 4.10: Seismic profile showing the stratigraphic location of reflector bC in relationship to the other interpreted reflectors. The small black box in the lower right corner shows the location of the seismic line within the 3D study area.

Parallel lineations on reflector bC

The seismic horizon bC reveals in the westernmost part of the study area a series of parallel lineations with an ENE to WSW orientation. These lineations are visible on the shaded relief map (fig.4.11 and 4.12A), but are difficult to recognize on any of the surface based attribute maps (i.e fig.4.12A). The lineations have an ENE-WSW orientation, indicated by red arrows in fig.4.12A. Seismic profiles across the lineations show that it is difficult to decide whether they are furrows or ridges; however, on zero-crossing they appear to be furrows rather than ridges (i.e. fig.4.12C). The lineations are between 5 and 10 km long and around 70 m wide, and they have maximum depths of 10 ms (TWT), although there are several of these lineations which are shallower than 5 ms (TWT).

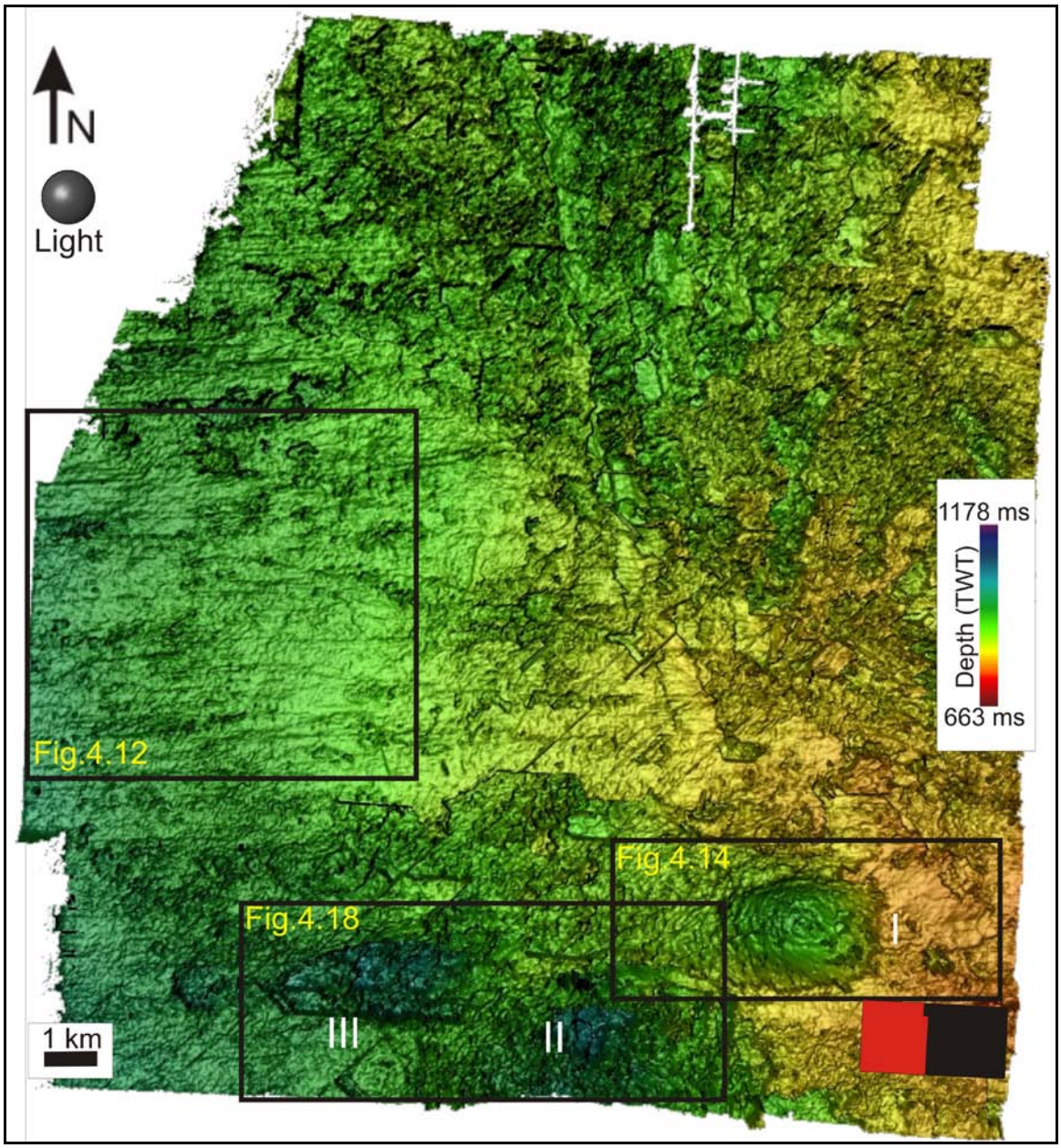

Figure 4.11: Shaded relief image of the reflector bC. Depressions are indicated with numbers (I-III). The small red box in the lower right corner shows the location of the map within the 3D study area**.**

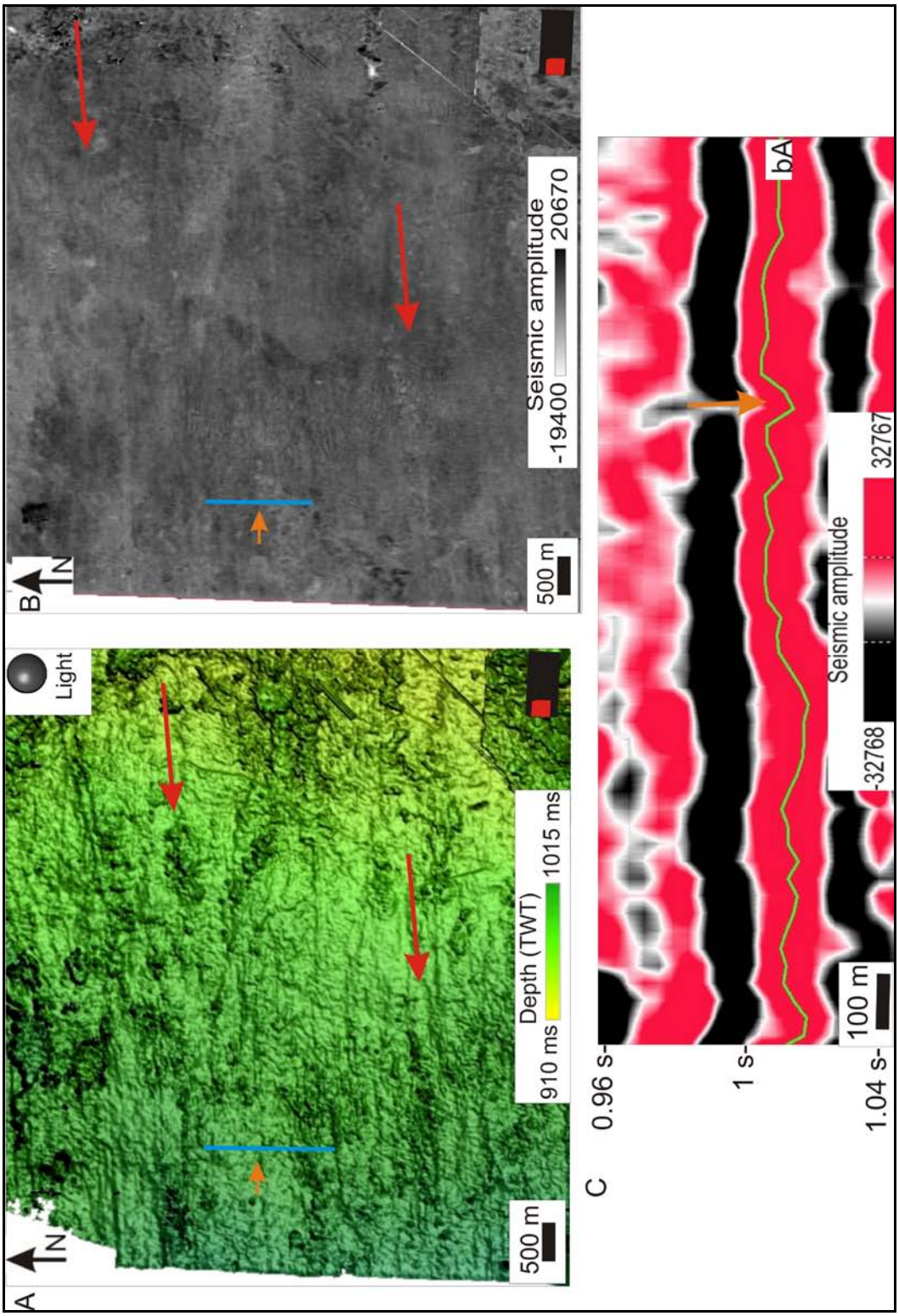

Figure 4.12: **A**. Shaded relief image of reflector bC with focus on parallel lineations. The blue line indicates the location of the seismic profile in C. The red arrows indicate the orientation of the lineations. The small red box in the lower right corner shows the location of the map within the 3D study area. **B**. Surface based amplitude map of A**. C**. Seismic profile across the lineations. The orange arrow indicates the furrow.

Interpretation of parallel lineations of reflector bC

The east to west orientated straight lineations on reflector bC have length:width ratios higher than 10:1 and are interpreted as megascale glacial lineations (MSGL). The MSGL are inferred to have been eroded by ice streams with an E-W orientation (fig.4.13).

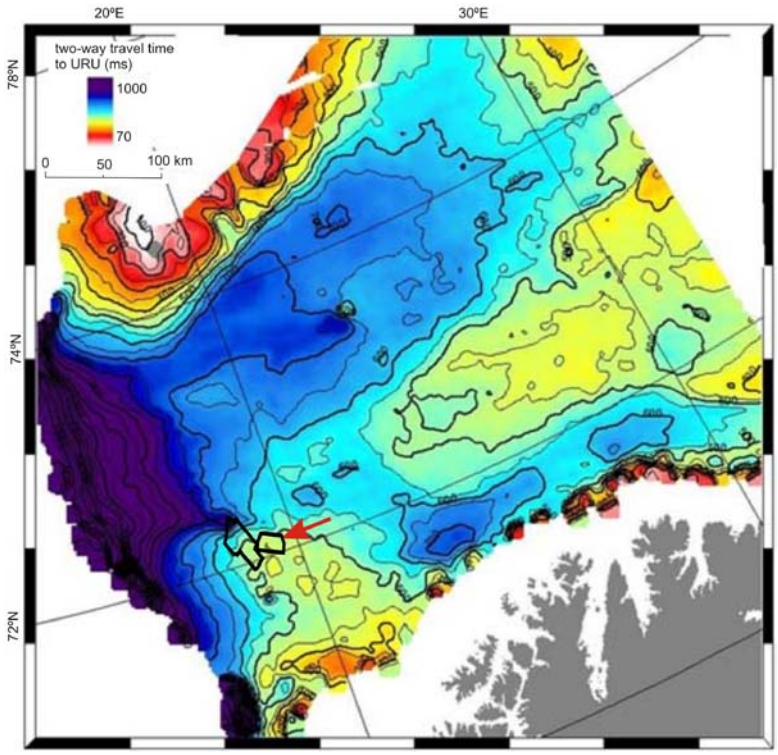

Figure 4.13: Orientation of inferred ice stream on reflector bC in the study area on a time-depth map of URU (modified from Andreassen et al., in prep.).

Large circular and elliptic depressions on reflector bC

The most characteristic features located on the horizon bC are three large depressions (from I-III in fig.4.11). The three depressions are located in the south of the 3D dataset. The depressions measure between 3 and 5 km from east to west, and between 2 and 3 km from north to south. The most impressive depression is numbered as I (fig.4.11). It is semi-circular, where the deepest part is in the center of the feature. The depression is 4 km long in the EW axis, and the flank in the west has a gentler slope than in the east. It is 3 km in the NS axis and it has a depth of 190 m (fig.4.14). The diameter/depth ratio is 22:1 and a volume of 19 km^3. On a seismic profile, the base of the depression seems to consist of small spoon-shaped segments rather than being a continuous surface (fig.4.19).

The sediment infill of depression I is characterized by a chaotic seismic reflection with low amplitude (i.e. fig.4.14). An overall impression of the depression is given by the seismic profiles on figures 4.14 to 4.17. In those, it is clear that the depression is eroded into the underlying reflections.

Other similar depressions are located to the west and to the southwest of depression I (II and III in fig.4.11). Depression II is about 4 km from east to west and 2 km from south to north and 190 m deep. Depression III is measured to be 2 km from east to west and at least 2 km from north to south, although it seems to continue to the south of the study area (fig.4.18). These depressions show a much more irregular base than depression I and the shapes are elliptic (fig.4.18). The sediment infill of depressions II and III is characterized by chaotic seismic reflection configuration and internal high-amplitude reflection segments which are between 200 and 400 m wide (i.e. fig.4.18).

Interpretation of large circular and elliptic depressions on reflector bC

There are several geological processes that create circular to semicircular depressions in seismic profiles, including fluid migration and meteorite impacts. The seismic 3D survey is located on an area where glacial erosion and gas migration have been identified. Pockmarks craters should be accompanied by other indications of gas migration, such as pull-down and seismic masking, which does not occur on seismic profiles from these depressions (fig.4.14 to 4.18). The size of the depressions, the shape, and the diameter/depth ratios (20:1) are comparable to those of ice-melt collapses related to the volcanic eruption in 1991 of the Volcán Hudson, Chile (Branney & Gilbert, 1995; Branney, 1995), but the seismic profiles (fig.4.14-4.18) show erosion along the borders of the depressions rather than sedimentation, which would be expected in ice-melt collapses. For the same reason, a meteorite impact is rather unlikely.

The depressions have the same orientation as the megascale glacial lineations that are located on reflector bC (fig.4.11 and 4.12) and it is likely that they are formed by glacial erosion. The most likely hypothesis I can see, is that the depressions are part of gigantic

glacitectonic hill-hole pairs. They are most likely eroded by ice flowing west because of their open-like shape towards the west (fig. 4.14 - 4.18). The chaotic seismic signature that characterizes the infill of the depressions is interpreted to be caused by a combination of basal shear stress caused by associated crevasse zone (Vorneberger & Whillians, 1986) and complex variations in the thermal conditions (Røthlisberger & Iken, 1981). These conditions may result in chaotic spatial variations in consolidation (Sættem, 1990), and hence acoustic impedance of the substratum. The formation of hill-hole pairs will be further discussed in chapter 5.

High amplitude anomalies west of depression I on reflector bC

An amplitude map of reflector bC shows a series of segments of anomalous high amplitude reflections located to the west of depression I (fig.4.19). These segments have different amplitude than the surrounding, but the same amplitude than reflections inside depression I (fig.4.19A). The anomalies cover an area of 18 km^2 and are up to 5 km long. A seismic profile along the reflections shows that the anomalies have an imbricate pattern toward the west (fig.4.19B).

Interpretation of high amplitude anomalies west of depression I

The high amplitude anomalies are interpreted to be sediment blocks consisting of a different type of sediment (different acoustic impedance) than the surrounding and that have been eroded from depression I during glacier advance. They are probably remnants of a hill associated with depression I. The displacement of sediments during hill-hole pair formation has been interpreted to be due to basal freezing and thrust faulting of consolidated sediments at the base (Sættem et al., 1990). The imbricate layers are interpreted to be thrust faults formed during the displacement of sediments. A sketch of how sediments can be deposited as imbricate layers in a subglacial environment is shown in figure 4.20.

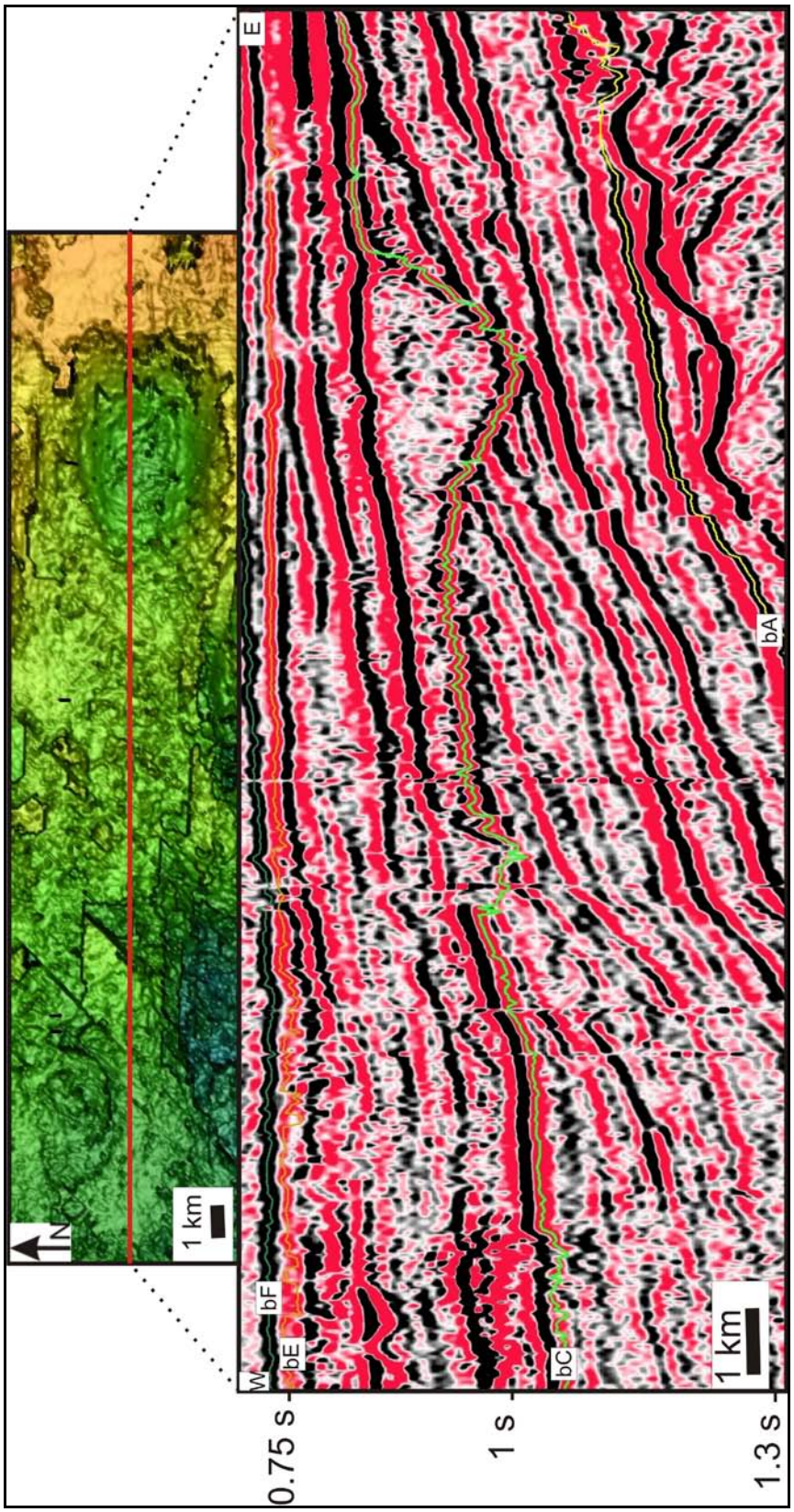

Figure 4.14: Shaded relief image and E-W seismic profile of depression I. See Fig.4.11 for location within the 3D area.

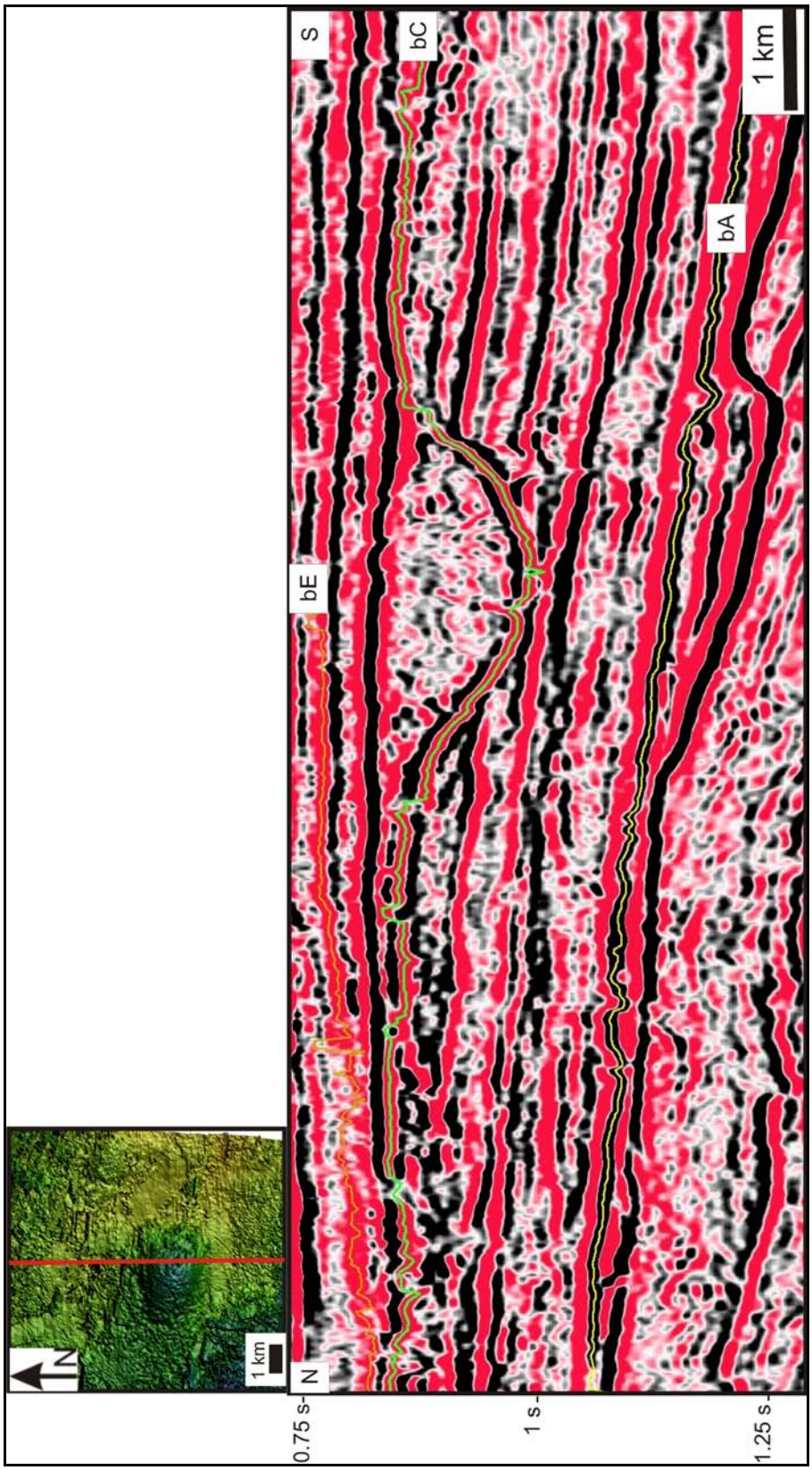

Figure 4.15: Shaded relief image and N-S seismic profile of depression I. See Fig.4.11 for location within the 3D area.

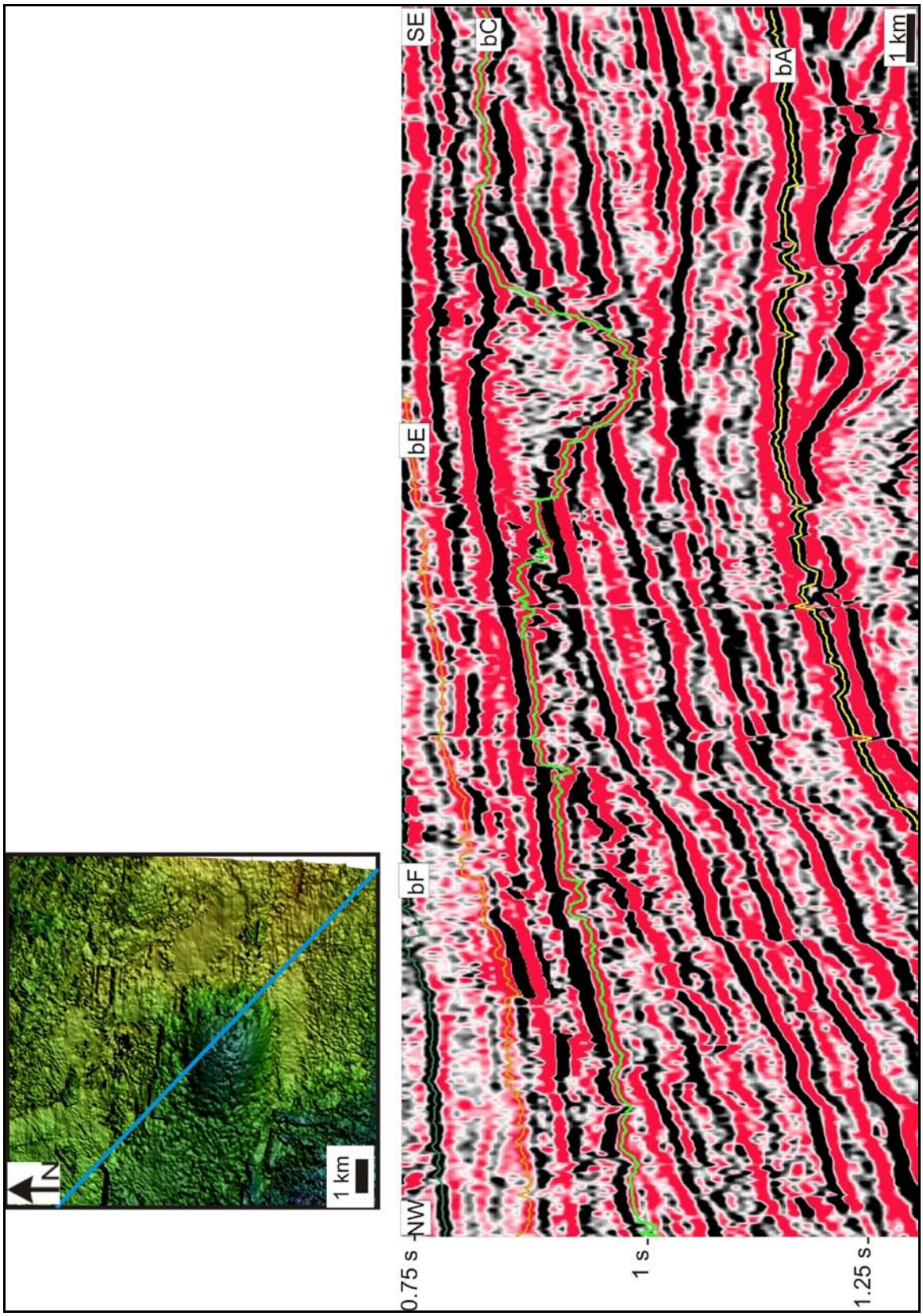

Figure 4.16: Shaded relief image and NW-SE seismic profile of depression I. See Fig.4.11 for location within the 3D area.

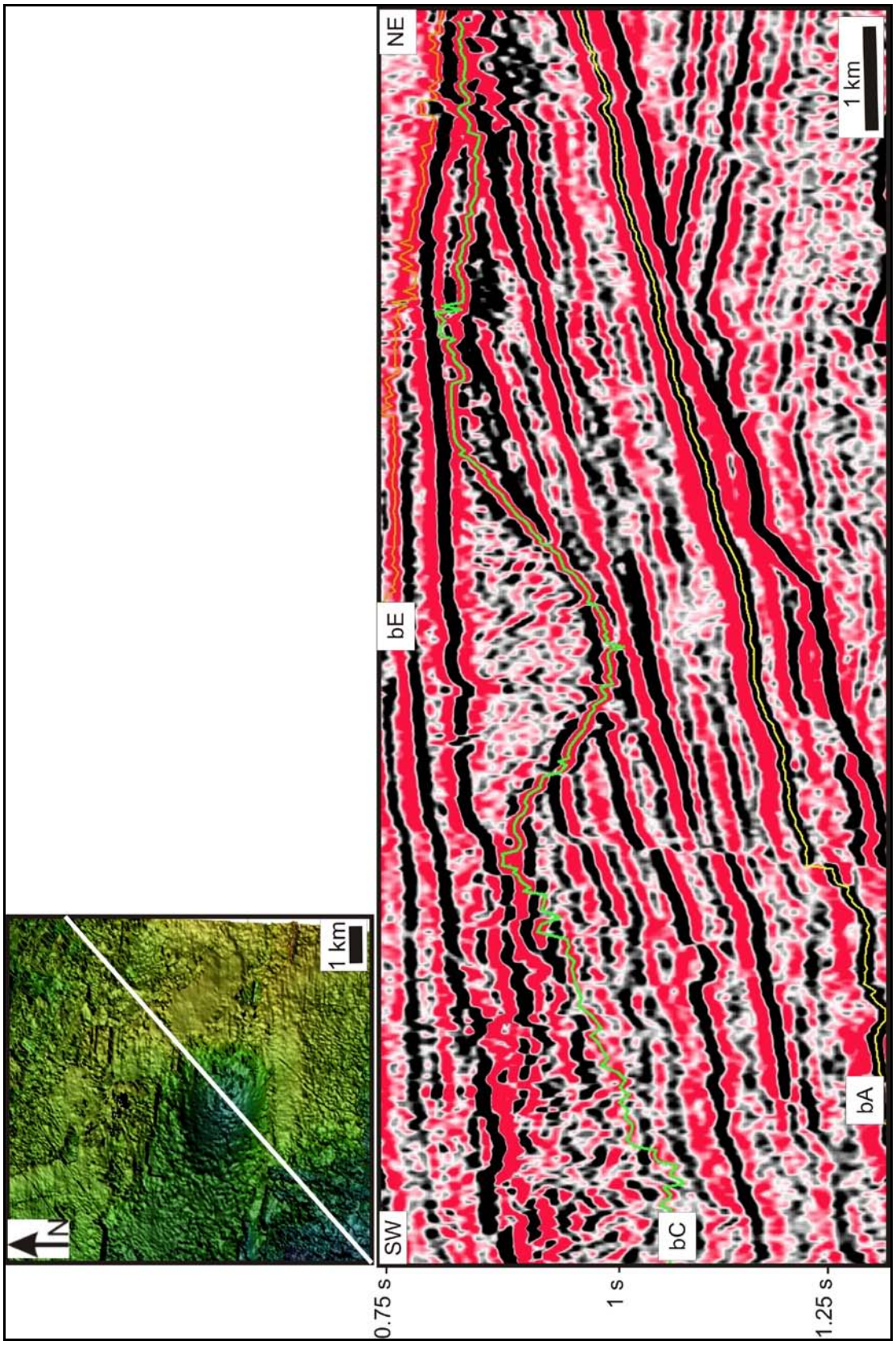

Figure 4.17: Shaded relief image and NE-SW seismic profile of depression I. See Fig.4.11 for location within the 3D area.

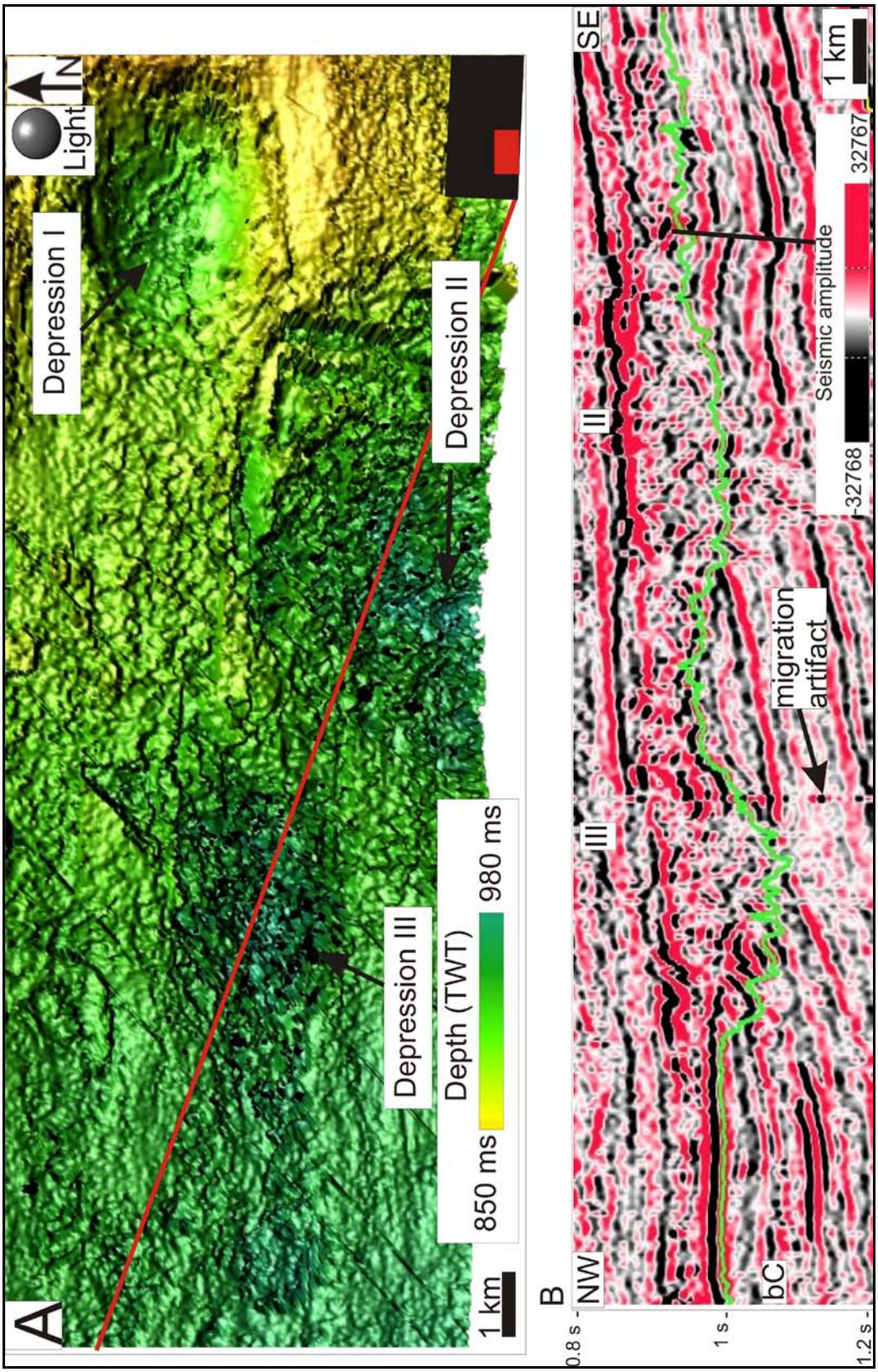

Figure 4.18: **A**. Shaded relief image of depressions II and III. The red line shows the location of the seismic profile shown in B. The small black rectangle on the lower right corner shows the location of the map within the study area. **B.** Seismic profile across the depressions.

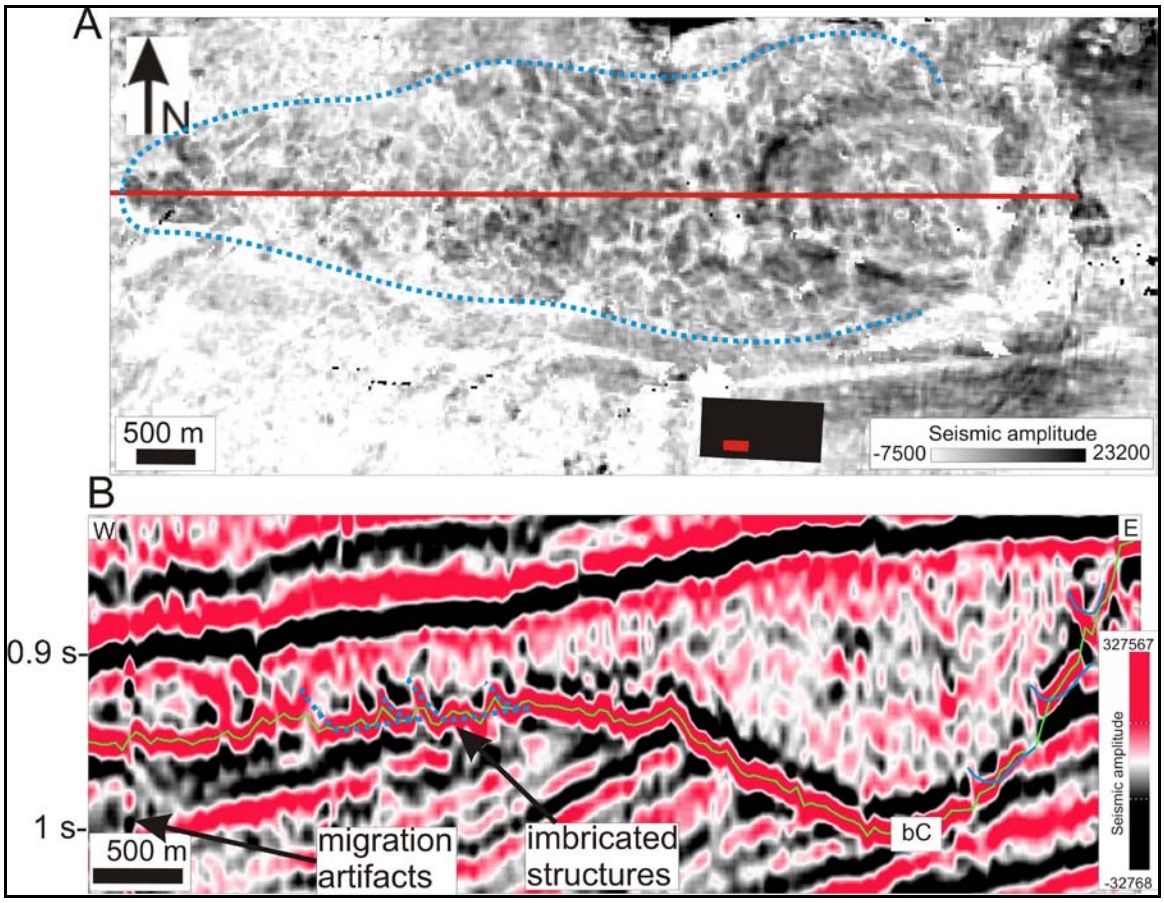

Figure 4.19: **A.** Surface based amplitude map of the depression I. The red line represents the seismic profile in B. High amplitude anomalies located within the blue dotter line. The red box in the in the lower right corner shows the location of the map within the 3D data set. **B.** Seismic profile where imbricate reflections and discontinuous reflections constitute the seismic reflector bC. The blue curved lines represent the extension of the imbricate layers.

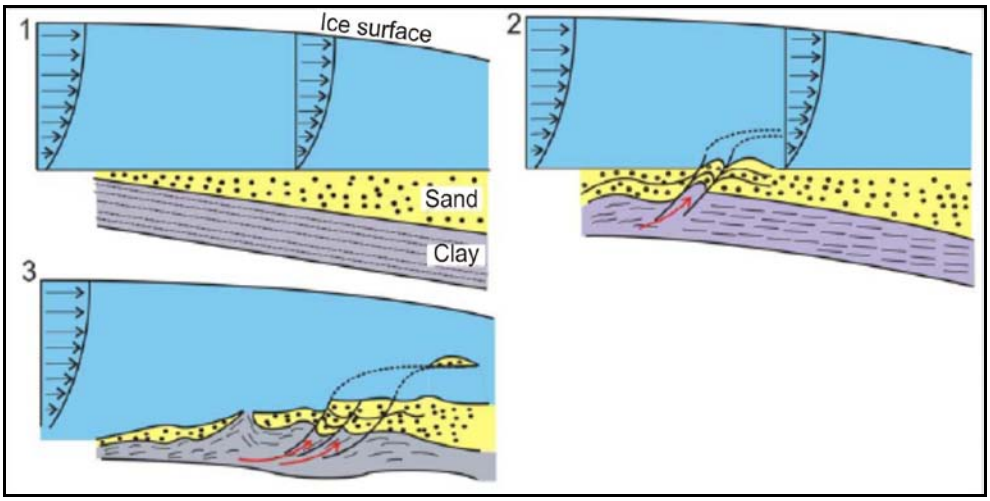

Figure 4.20: Sketch of how sediments are deposited as imbricate structures in a subglacial environment. From Astakhov et al. (1987).

4.5. Seismic unit C

Seismic unit C is bounded by reflectors bC and bE. The top of seismic unit C reflectors are truncated by reflector bE while the reflectors in the lower part of the seismic unit are parallel to seismic reflector bC (fig.4.21). Seismic unit C represents part of the paleo-shelf with a low gradient slope towards the southwest. The internal reflections have medium to high amplitude and are of medium to good continuity and there is presence of high amplitude anomalies within the unit. There are high amplitude anomalies within the unit in the westernmost part of the study area.

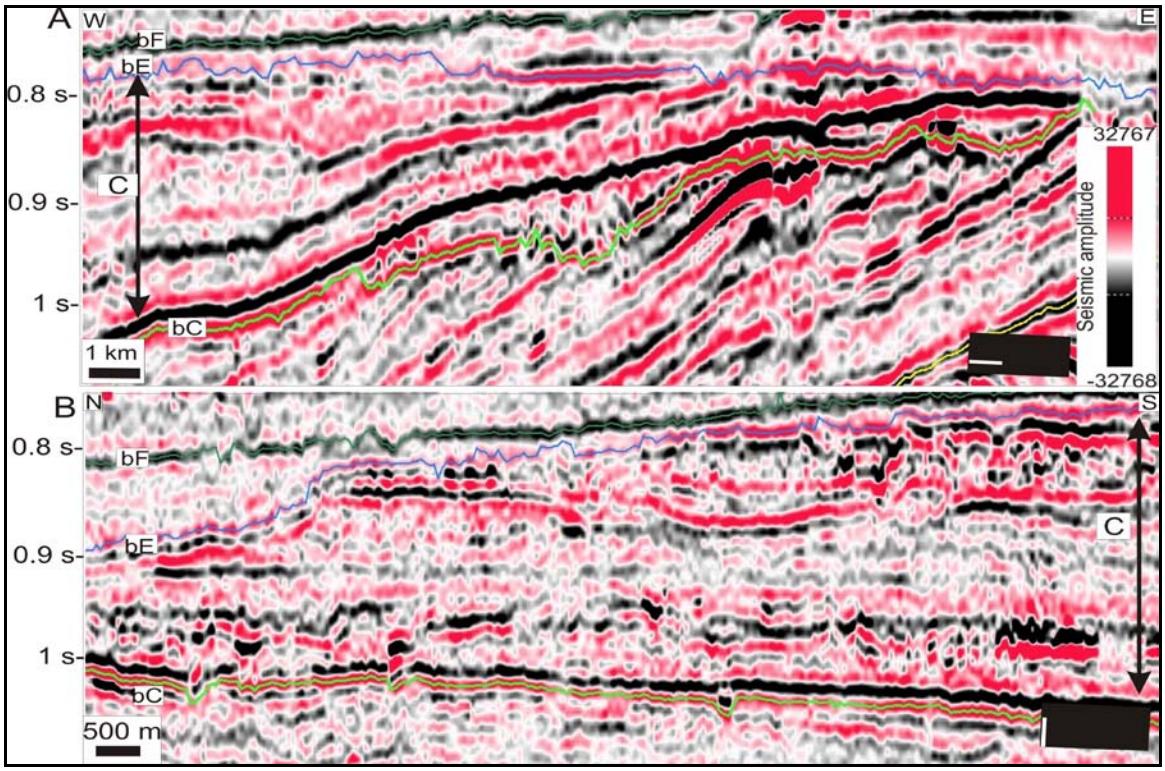

Figure 4.21: A. East to west seismic profile showing dipping reflections in unit C parallel to the base of the unit and truncated by bE. **B.** South to north seismic profile of unit C showing a rather parallel to the base disposition. Both profiles show the presence of high amplitude anomalies. The small black boxes in the lower right corner show the location of the seismic line within the 3D area.

Description of high amplitude anomalies in unit C

The western part of unit C is characterized by a series of reflection segments of high anomalous amplitudes (fig.4.22). The high amplitude reflections have diameter between 150 and 500 m. They are randomly distributed, however, they have a preferred NE-SW

orientation in groups up to 7 km long (fig.4.22A). On seismic profile, these groups appear as a series of high amplitude anomalies with distance between segments of a few m. to up to 1.5 km (fig.4.22C).

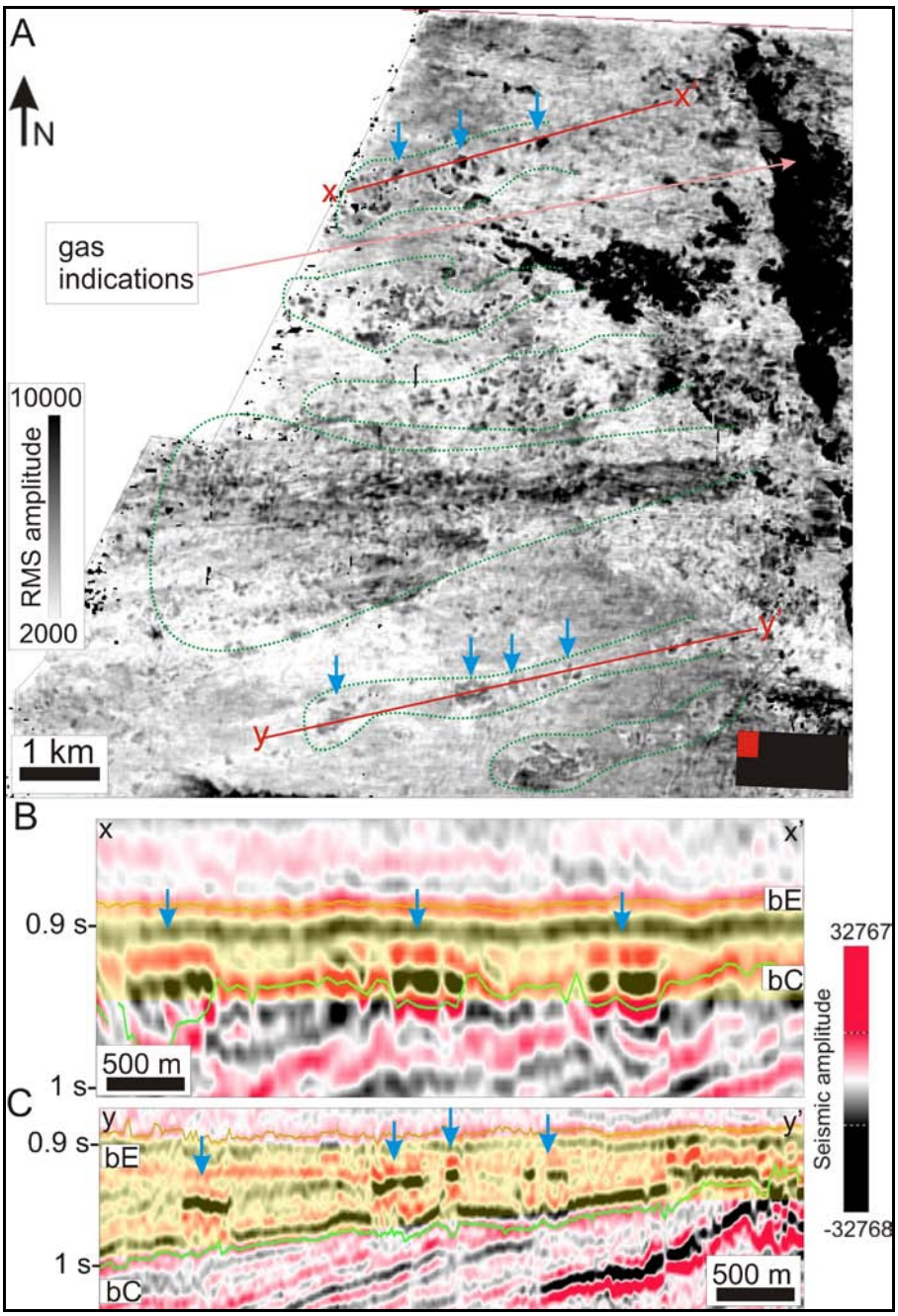

Figure 4.22: **A.** RMS amplitude volume map of seismic unit C where groups of sediments spread towards the west (green dotted areas). The red lines represent the seismic profile in B and C. **B.** Seismic profile across sediment blocks in the north. **C.** Seismic profile across sediment blocks in the middle of the 3D study area. The RMS volume is highlighted in yellow. The small red box in the lower right corner shows the location of the image within the 3D study area.

In the southwestern part of the study area, accumulations of high amplitude anomalies occur to the west of depressions I, II and III (fig.4.23). The sediment infill of depressions II and III has also accumulations of high amplitude anomalies (fig.4.23A). The high amplitude anomalies located to the west have the same characteristics as the anomalies located within depression III (fig.4.23C).

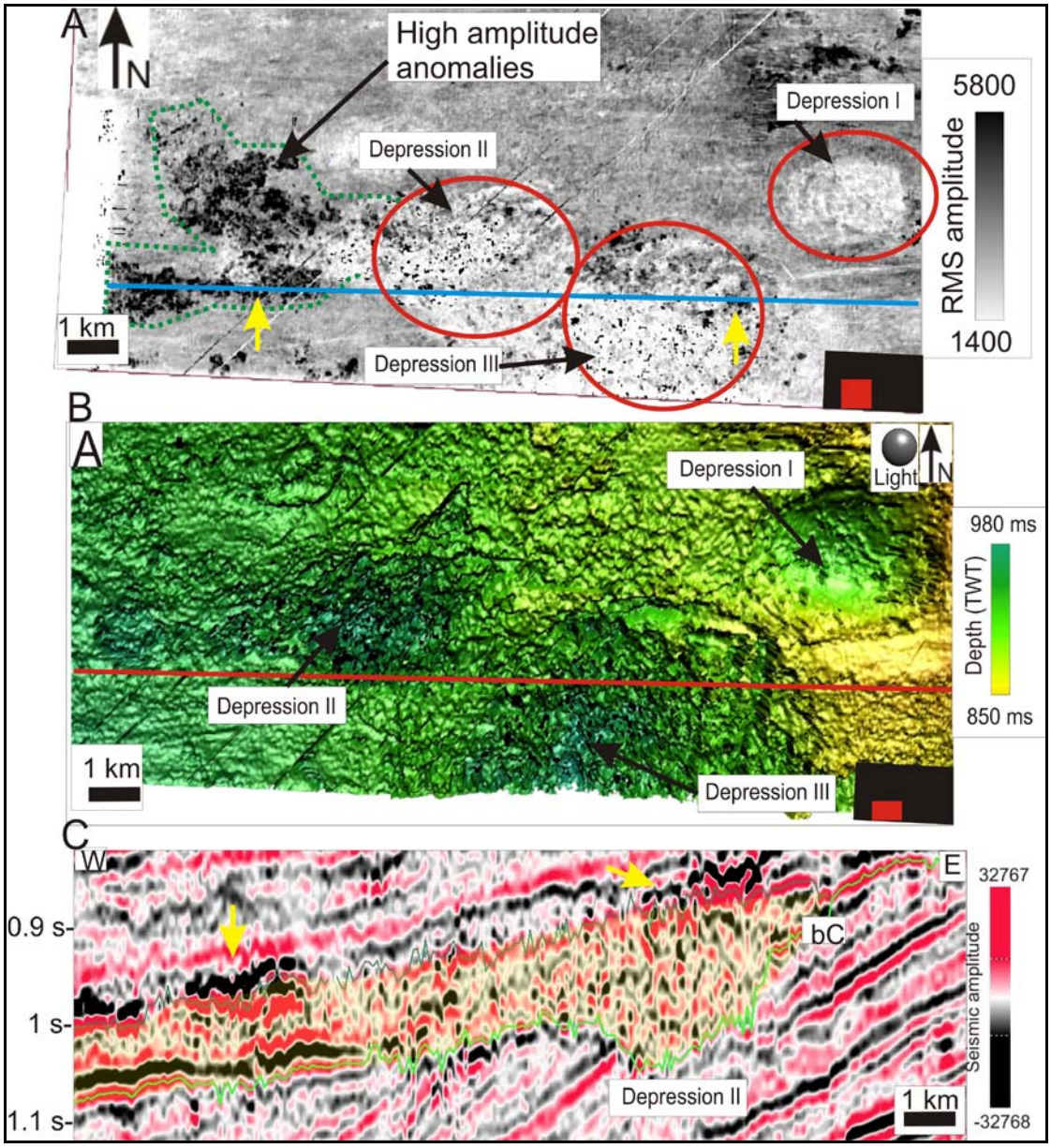

Figure 4.23: A. RMS amplitude image of the lower part of unit C. High amplitude anomalies are located to the west of the depressions on reflector bC. The volume for the RMS volume is shown in C. The red box in the lower right corner shows the location of the image within the 3D dataset. The blue lines shows the location of the seismic profile in C. **B.** Shaded relief image of reflector bC showing the location of the depressions I, II, III. The small red box in the lower right corner shows the location of the image within the 3D dataset. **C.** Seismic profile across the high amplitude anomalies in the south. The yellow shadowed area show the volume used for the RMS map shown in A.

Interpretation of high amplitude anomalies in unit C

The high amplitude anomalies described above in unit C are interpreted to be sediment blocks, consisting of a different type of sediment (higher acoustic impedance) than the surrounding sediments of unit C.

In the west part of the study area, some of the sediment blocks appear grouped with a WSE orientation (fig.4.22). These groups reveal the same orientation as the MSGL described on reflector bC (fig.4.12A) and for this reason they are interpreted to be sediment blocks eroded and transported by paleo-ice streams in the area.

In the southern part of the study area, the sediment blocks appear in large accumulations just west and downstream of the depressions (fig.4.23). These sediment accumulations are interpreted to represent the hill part of the depression holes, being hill-hole pairs, based on the location and orientation of the groups of sediments, west of the depressions. However, this sediment accumulation does not show evidence of thrust faulting as occurred with the sediments associated with depression I (fig.4.19).

4.6. Reflector bE

Reflector bE is the base of unit E and it has been interpreted following the maximum amplitude of the seismic signal (fig.4.24) and can be followed through most of the study area. In the Veslemøy High 3D area, this reflector is parallel to the seafloor and it is located at depths between 627 ms and 932 ms (TWT), dipping towards the northwest. Its surface is quite irregular and it has the shape of a large trough (fig. 4.25).

The trough has a SE-NW orientation and it is flanked by two higher areas in the southwest and the northeast (fig.4.25). The trough is around 20 km wide in the southeastern part and it widen towards the northwestern part (fig.4.25). The floor of the trough is rather flat; however it is highly influenced by the terracing effect (chapter 2.5.4) that can mask features of smaller scale.

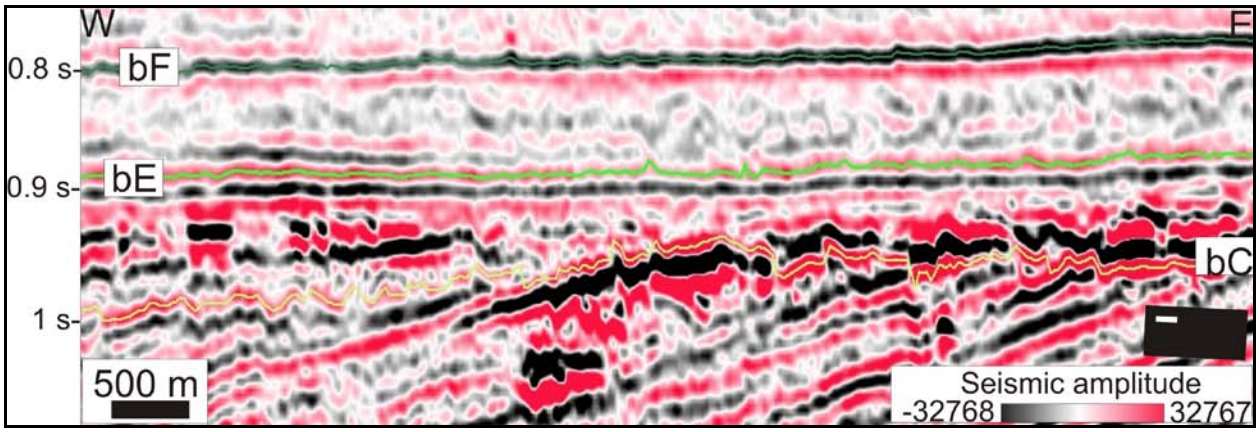

Figure 4.24: Seismic profile showing stratigraphic location of reflector bE.

Interpretation of shape of reflector bE

URU is interpreted to have formed as a fluvial surface, which was modified by glaciers during the Plio-Pleistocene and two big rivers have been reconstructed to have an E-W orientation in the Barents Sea based on its morphology (Vorren et al., 1988). The dataset is located at the edge of a trough with a S-N orientation, which connects Scandinavia with the Bjørnøyrenna (fig.4.26). Several tributaries discharge from Scandinavia in a larger river running from east to west (fig.4.27). It is therefore interpreted that the surface of bE in the Veslemøy High 3D area is the result of glacial erosion in a fluvial valley.

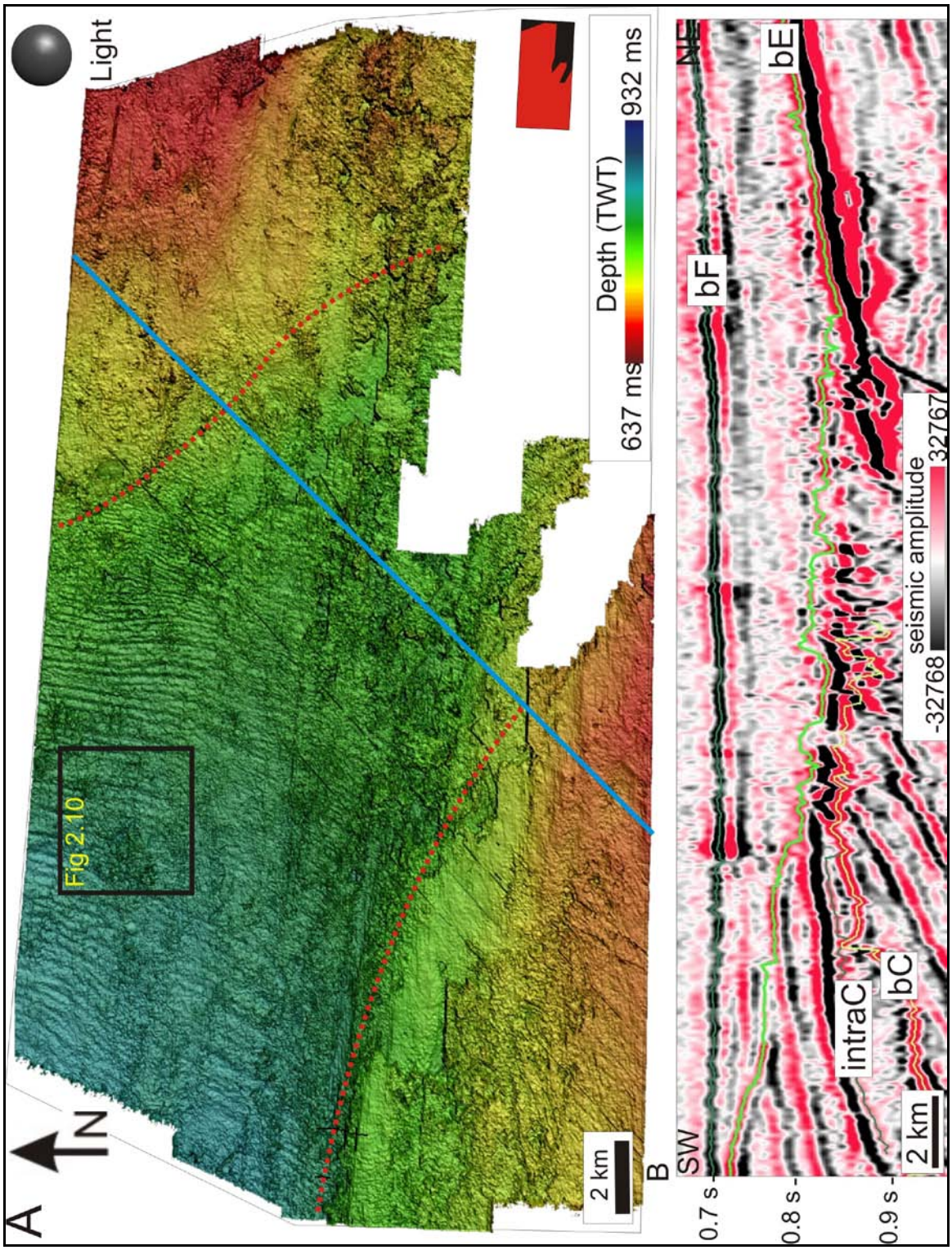

Figure 4.25: **A.** Shaded relief image of the surface bE showing the shape of an anticline. The blue line shows the location of the seismic profile in B. The squares show the location of figures 4.28 and 4.29. **B.** Seismic profile across the anticline.

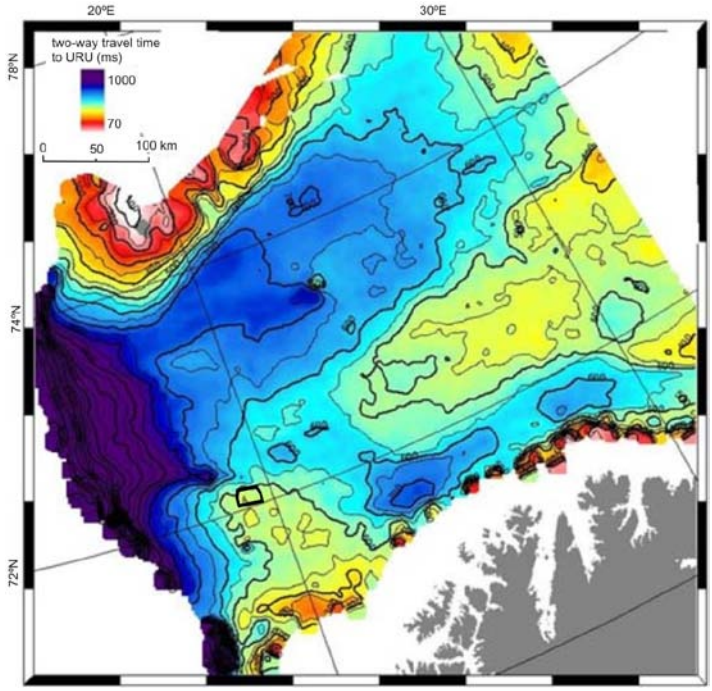

Figure 4.26: Time-depth map of URU in the SW Barents Sea (modified from Andreassen et al., in prep.). The rectangle shows the location of the study area.

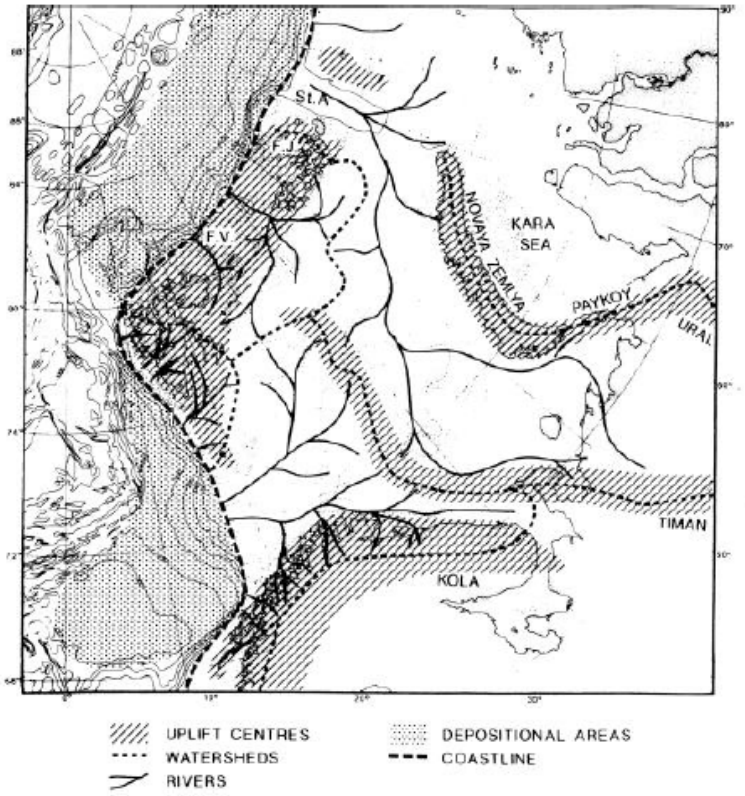

Figure 4.27: Reconstruction of Late Neogene-Early Pleistocene draining system in the Barents Sea. Today's bathymetry and geography is used as base map. St.A = St. Anna trough, F.V. = Franz Victoria-trough, F.J. = Franz Josefs land. From Vorren et al. (1991).

4.7. Reflector bF

Reflector bF has been interpreted following the minimum amplitude of the seismic signal (fig.4.28) and it has been interpreted in almost all the 3D seismic area. The depth of this reflector goes from 562 ms to 831 ms (TWT) in the Veslemøy 3D dataset (fig.4.33). It is shallower in the southeast and becomes deeper towards the northwest although it presents a rather gentle slope of less than 1º from the SE to the NW (fig.4.28 and 4.29). On reflector bF, megascale glacial lineations and iceberg ploughmarks are observed (fig.4.29).

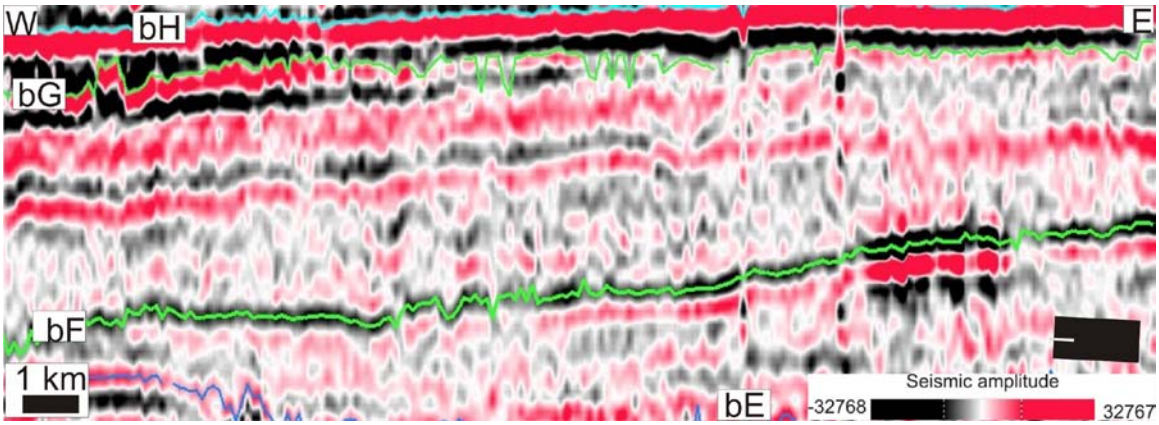

Figure 4.28: Seismic profile showing stratigraphic location of reflector bF.

Iceberg ploughmarks on reflector bF

Iceberg ploughmarks with varying orientation are observed on reflector bF. Some ploughmarks are visible in the southwest part (fig.4.29 and 4.30) and in the north (fig.4.29), and in the southeastern corner of the 3D area (fig.4.29). They have random orientations although many of the furrows tend to have a S-N or W-E orientation (fig.4.29). The ploughmarks are between 1 and 5 km long, between 100 and 110 m wide and most of them around 5 ms (TWT) deep. They appear as individual furrows (fig.4.29) or in some cases as pairs of two parallel furrows (fig.4.30).

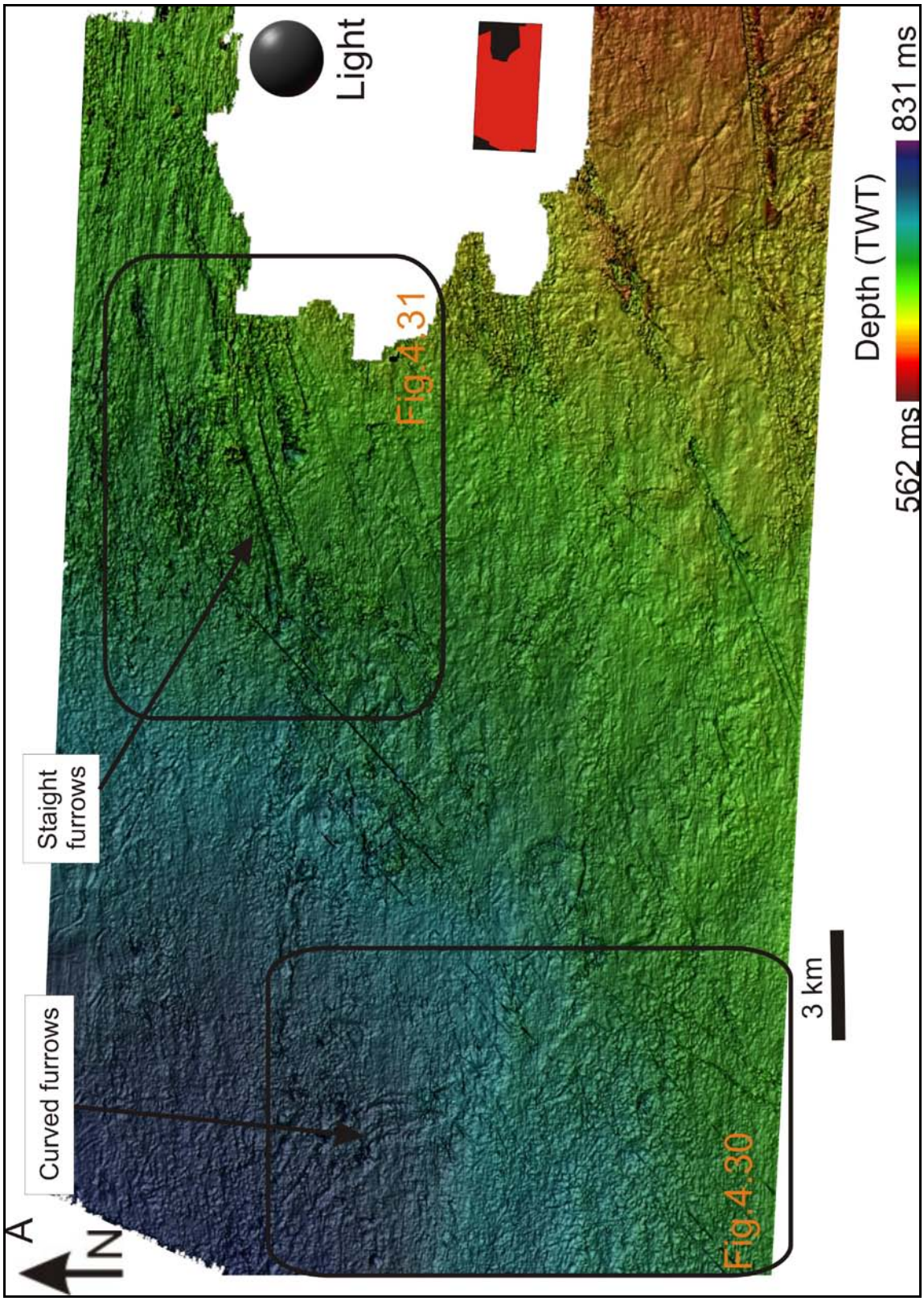

Figure 4.29: **A.** Shaded relief image of the horizon bF. The black rectangles show the areas shown in figures 4.30, 4.31.The small red box in the lower right corner show the location of the map within the 3D dataset.

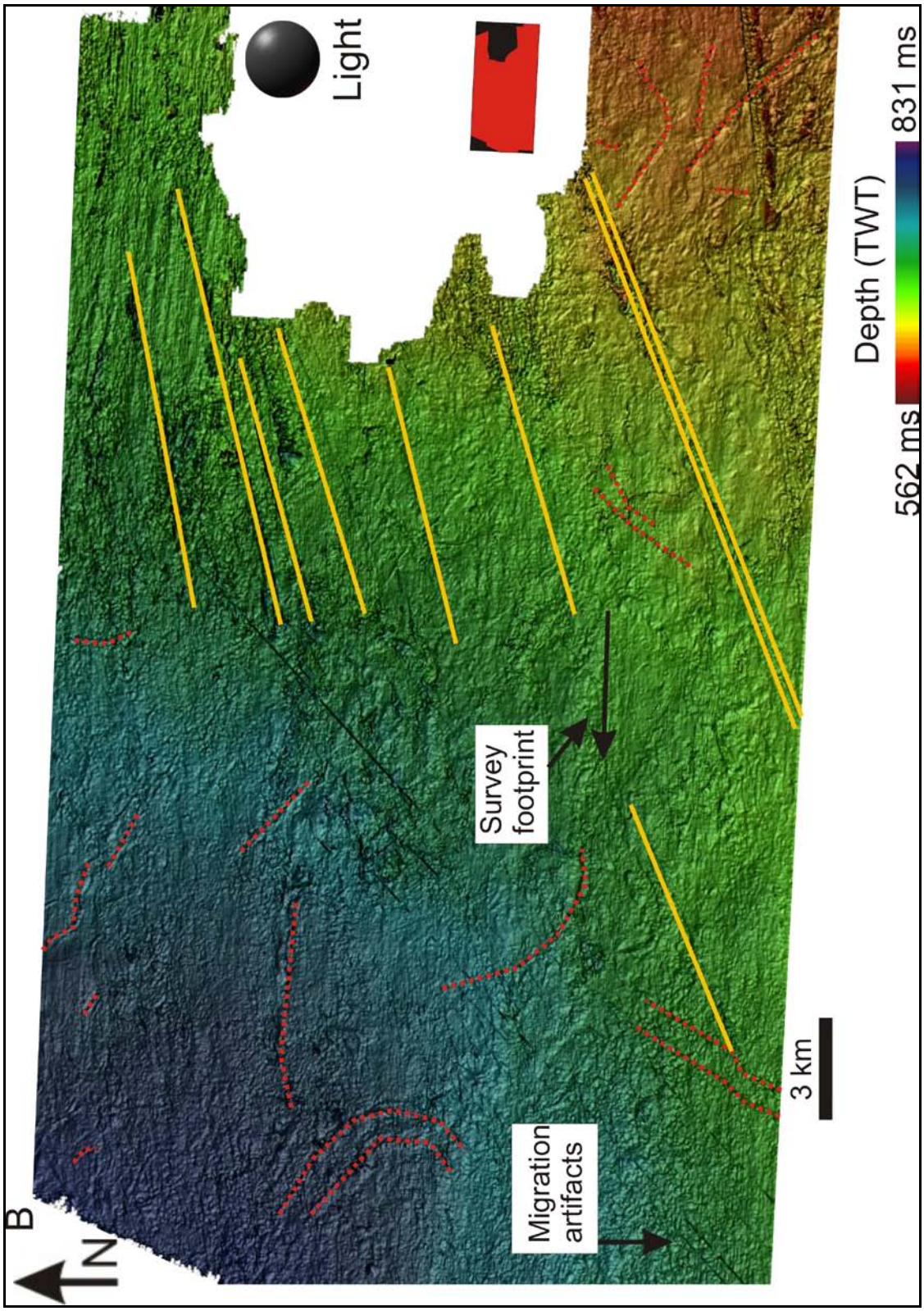

Figure 4.29: B. Shaded relief image of the horizon bF with interpreted features. Red dotted lines are iceberg ploughmarks, yellow lines are MSGL, and yellow dotted lines are iceberg ploughmarks. The small red box in the lower right corner shows the location of the map within the 3D dataset.

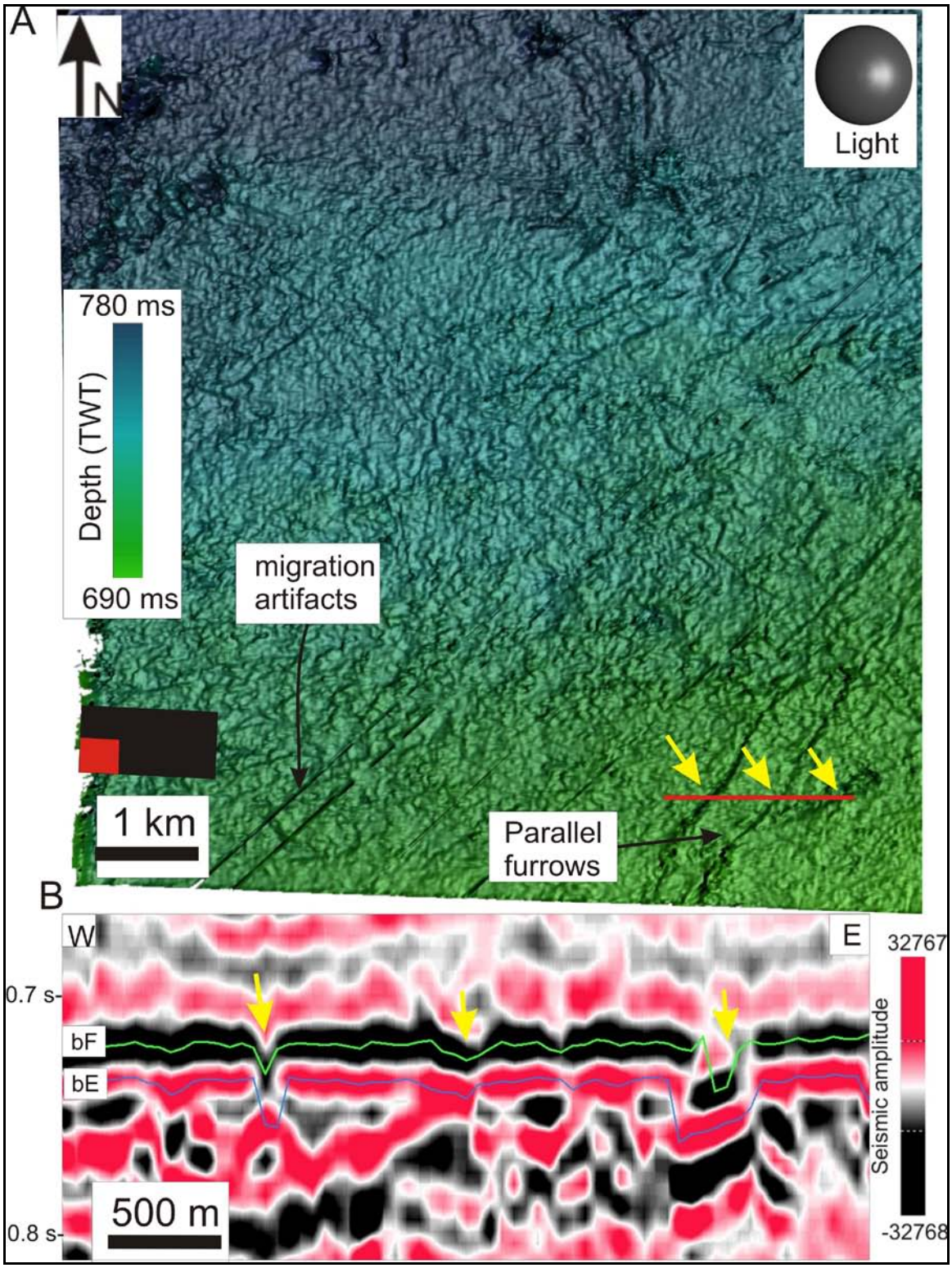

Figure 4.30: **A.** Shaded relief image of reflector bF showing a pair of iceberg ploughmarks. The red line shows the location of the seismic profile in B. The red box in the lower left corner shows the location of the map within the 3D data set. **B**. Seismic profile across a pair of iceberg ploughmarks. The yellow arrows show the location of the furrows.

Megascale glacial lineations on reflector bF

Long and straight parallel lineations appear with a NE-SW orientation (fig.4.29 and 4.31). They are measured to be between 6 and 12 km and probably longer because they seem to continue outside the interpreted area in the east. They are between 120 and 150 m wide and not higher than 10 ms (TWT) deep and they are interpreted as MSGL eroded in the surface by a NE-SW orientated ice flow (fig.32).

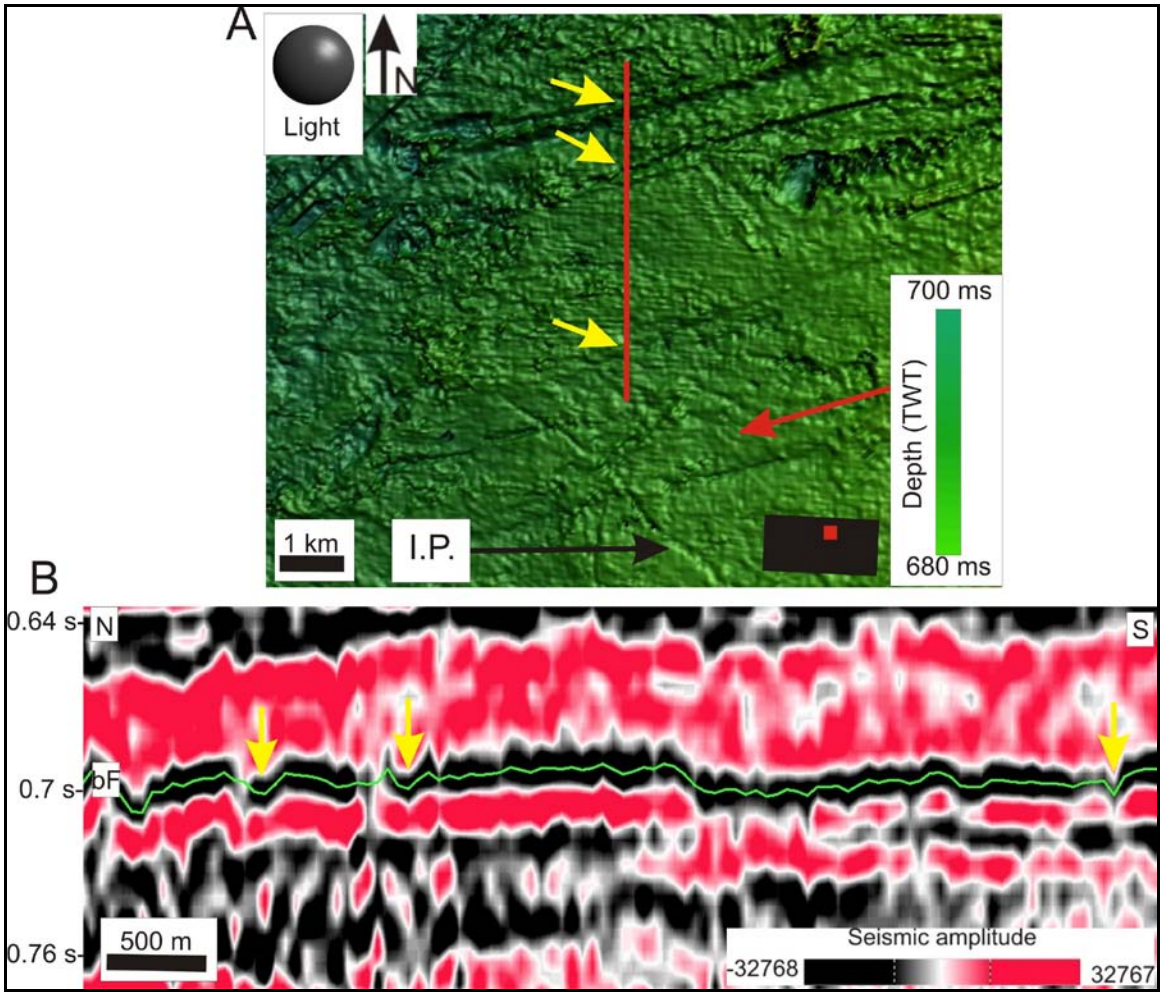

Figure 4.31: A. Shaded relief image of reflector bF showing MSGL with a SW orientation. Red line shows the location of seismic profile in B. Yellow arrows indicate the location of the furrows. Red arrow indicated the orientation of the MSGL. The small red box shows the location of the map within the 3D dataset. I.P= Iceberg ploughmark. **B.** Seismic profile across the MSGL. Yellow arrows indicate the location of the lineations.

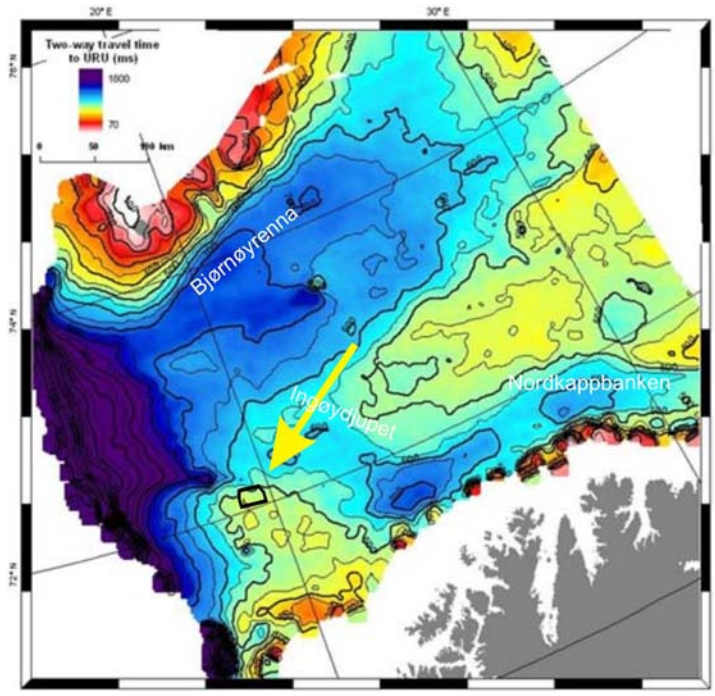

Figure 4.32: Orientation of inferred ice stream on reflector bF in the study area on a time-depth map of URU (modified from Andreassen et al., in prep.).

4.8. Seismic unit F

Seismic unit F is bounded by reflectors bF and bG and in the Veslemøy area the internal reflections are truncated by reflector bH (fig.4.33). The unit is divided in two subunits by reflector intra-bF (fig.4.33). The lower part of the unit is chaotic with discontinuous internal reflections, while the upper part is dominated by parallel, west dipping reflections of low to moderate amplitude and good continuity (fig.4.33).

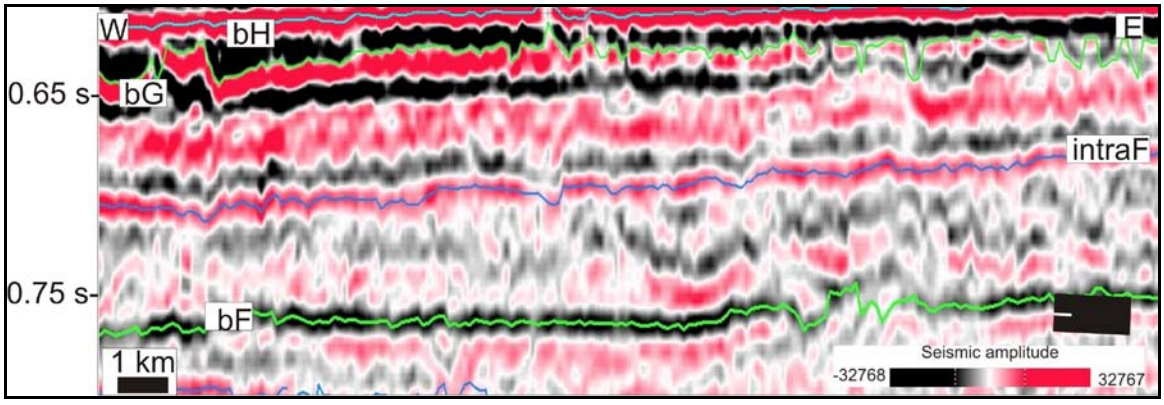

Figure 4.33: Seismic profile showing the internal configuration of unit F.

4.8.1. Reflector intraF

Reflector intraF has been interpreted following the reflection which divides unit F into two subunits (fig.4.33). Reflector intraF has depths between 615 ms and 745 ms (TWT) and dips towards the west (fig.4.34). This reflector is dominated by two sets of MSGL (sets I and II in fig.4.34). Set I is only found in the south and the southeastern part of the interpreted area and it has a NNE to SSW orientation (fig.4.34). The furrows are between 6 and 15 km long, around 250 m wide and up to 12 ms (TWT) deep (fig.4.34 and 4.35B). On the other hand, set II has an ENE-WSW orientation (fig.4.34) and they are best seen in the north and the west of the interpreted area. The lineations of set II are between 30 and 40 km long, around 150 m wide and < 10 ms (TWT) deep (fig.4.34 and 4.35B). These two sets of MSGL are interpreted to be indicative of two different fast ice flows draining out the Veslemøy High 3D area. The MSGLs are interpreted to appear to result from soft-sediment deformation at the base of fast-flowing ice streams that are draining large ice sheets (Tulaczyk et al., 2004).

Relative age of two sets of lineations on reflector intraF

The ice flow which formed lineations I is interpreted to be older than the ice flow which formed lineations II (fig.4.35D). This interpretation is based on two criteria. 1) A criterion to elucidate which lineation is younger is to study a cross-point between the lineations. Ay the cross point, younger lineations will overlie older lineations. In this horizon, it seems like lineation I crosses over lineation II in the southeastern corner (fig.4.34A). 2) A second criterion is that set II is widespread all over the surface, while set I is only located on the southeastern flank of the reflector. It is expected that younger lineations overprint the older ones and therefore set II is interpreted to be younger than set I (fig.4.35D).

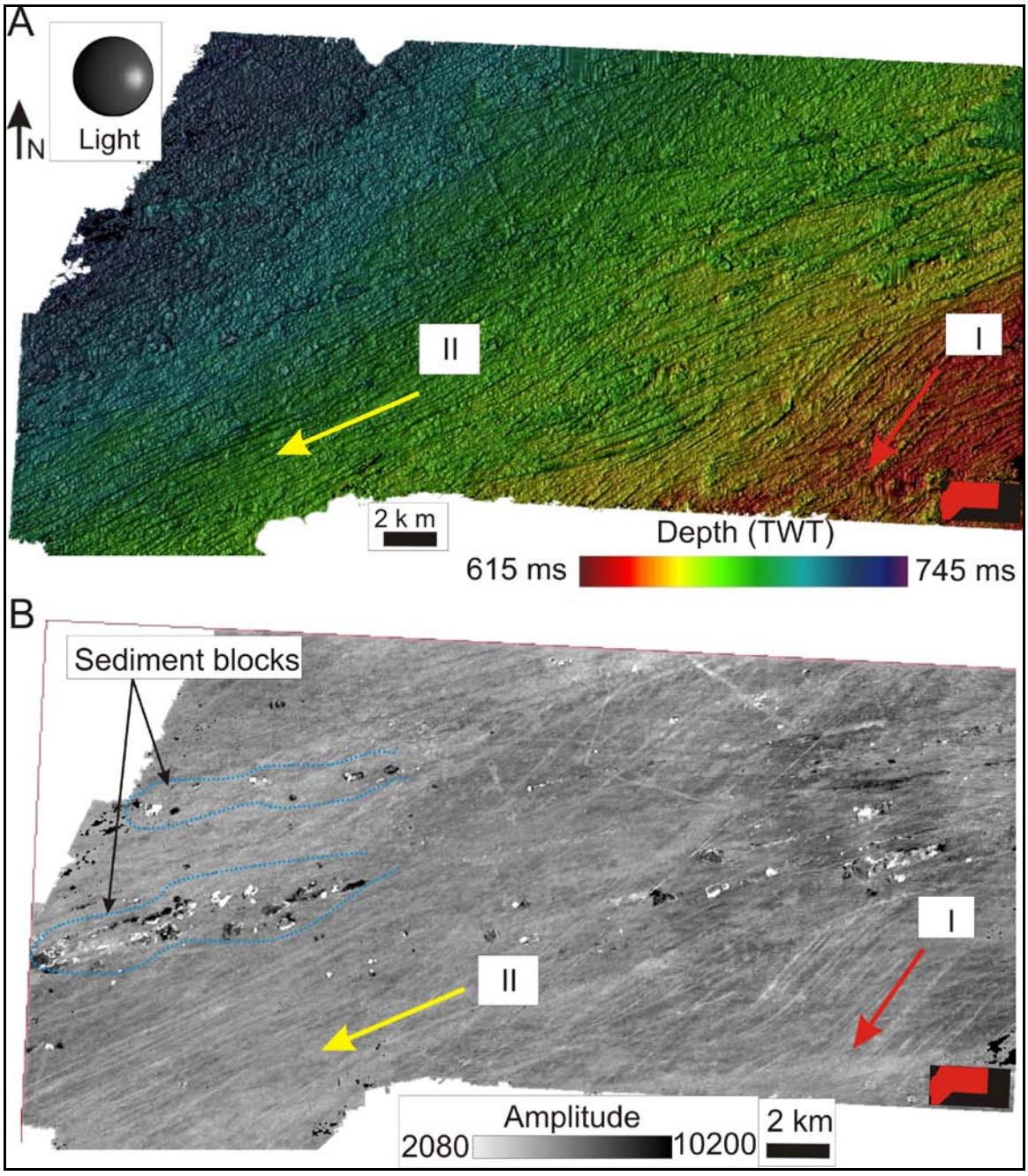

Figure 4.34: A. Shaded relief image of horizon intraF. Two sets of megascale glacial lineations can be inferred (red and yellow arrows). **B.** Surface based amplitude map of the horizon intraF. The small red box in the lower right corner shows the location of the map within the 3D dataset. Sediment blocks have been interpreted in fig. 4.38.

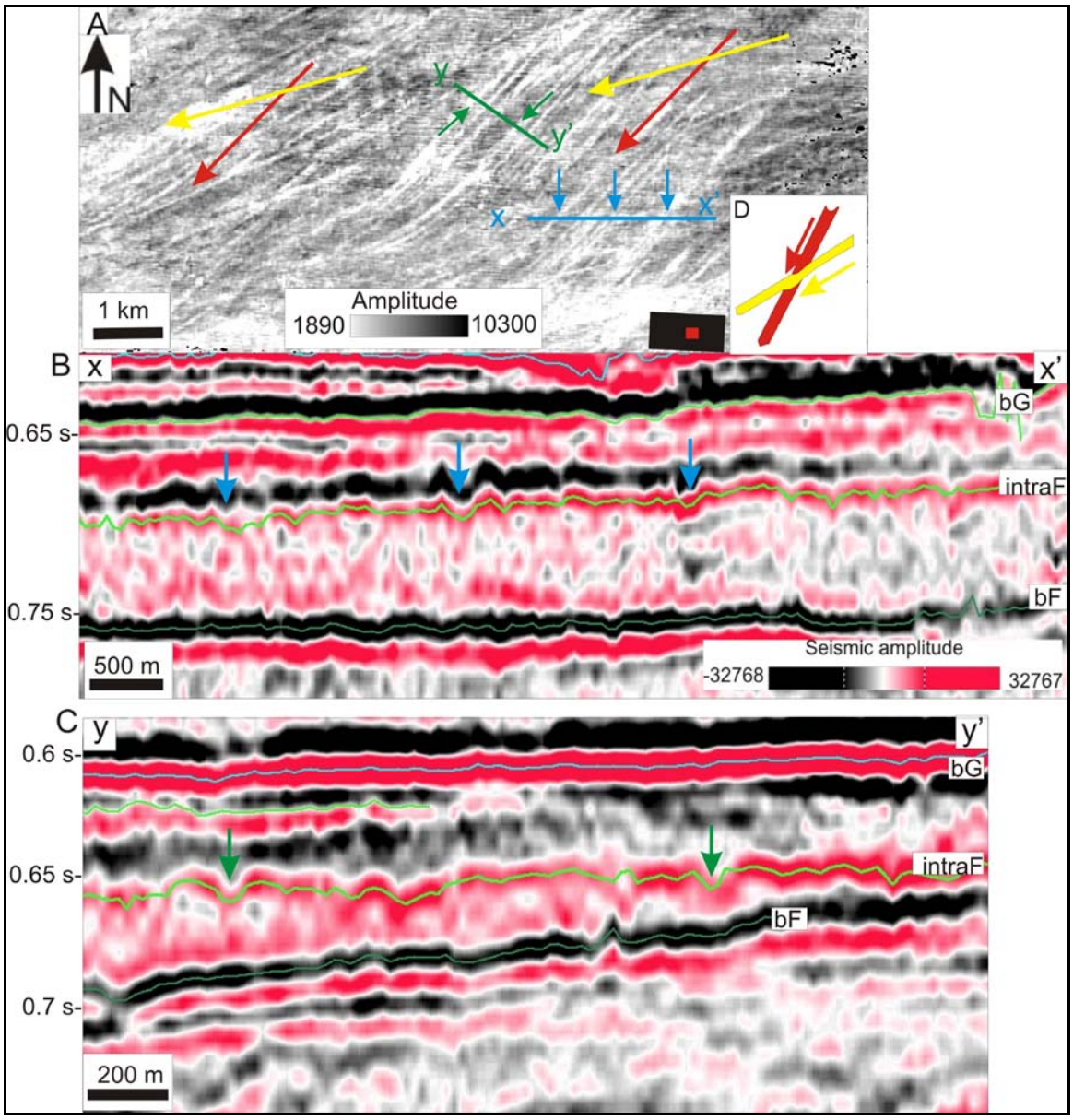

Figure 4.35: A. Surface based amplitude map of reflector intraF. The red and yellow arrows indicate the orientation of MSGL. The blue and green lines indicate the profiles in B and C. The small red box in the lower right corner shows the location of the map within the 3D dataset. **B.** Seismic profile across N to S lineations. Blue arrows indicate the location of the furrows. **C.** Seismic profile across MSGL from the NE. Green arrows indicates the location of the furrows. **D.** Schematic illustration of relative age of the MSGL.

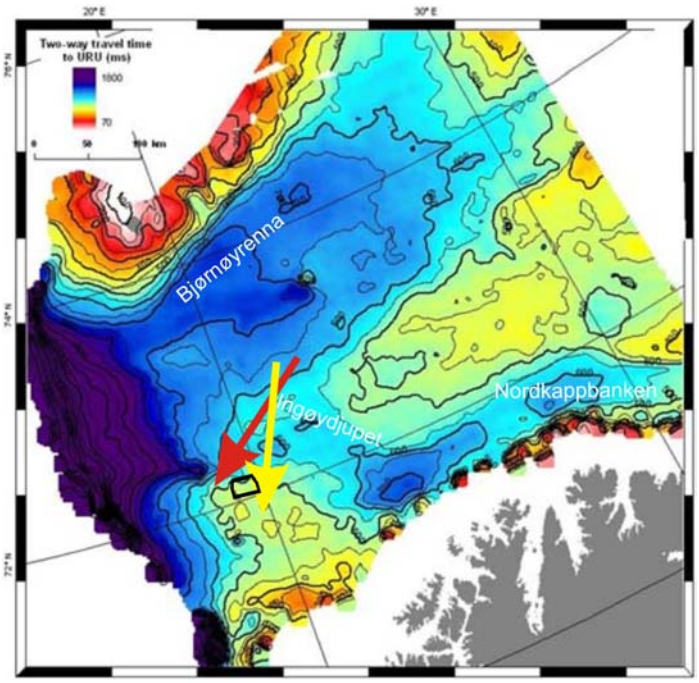

Figure 4.36: Orientation of inferred ice stream on reflector intraF in the study area on a time-depth map of URU (modified from Andreassen et al., in prep.).

High amplitude segments in seismic unit F

The lower part of seismic unit F is characterized by series of reflections of anomalously high amplitude values (fig.4.37B). These reflections have anomalously high amplitudes compared to the surroundings and in RMS amplitude map generated for the base of the unit, these anomalies are seen as black areas and the lower amplitude areas with a light gray (fig.4.37A). These anomalies have diameter between 500 and 700 m, although there are several which are smaller than 100 m. and a few larger than 1 km, and they are semicircular or oval (fig.4.37A). These anomalies are randomly distributed within the unit; however in the middle of the unit, there is a series of anomalies which are aligned in chains with a southwestern orientation. These series of anomalies are up to 12 km long (fig.4.37).

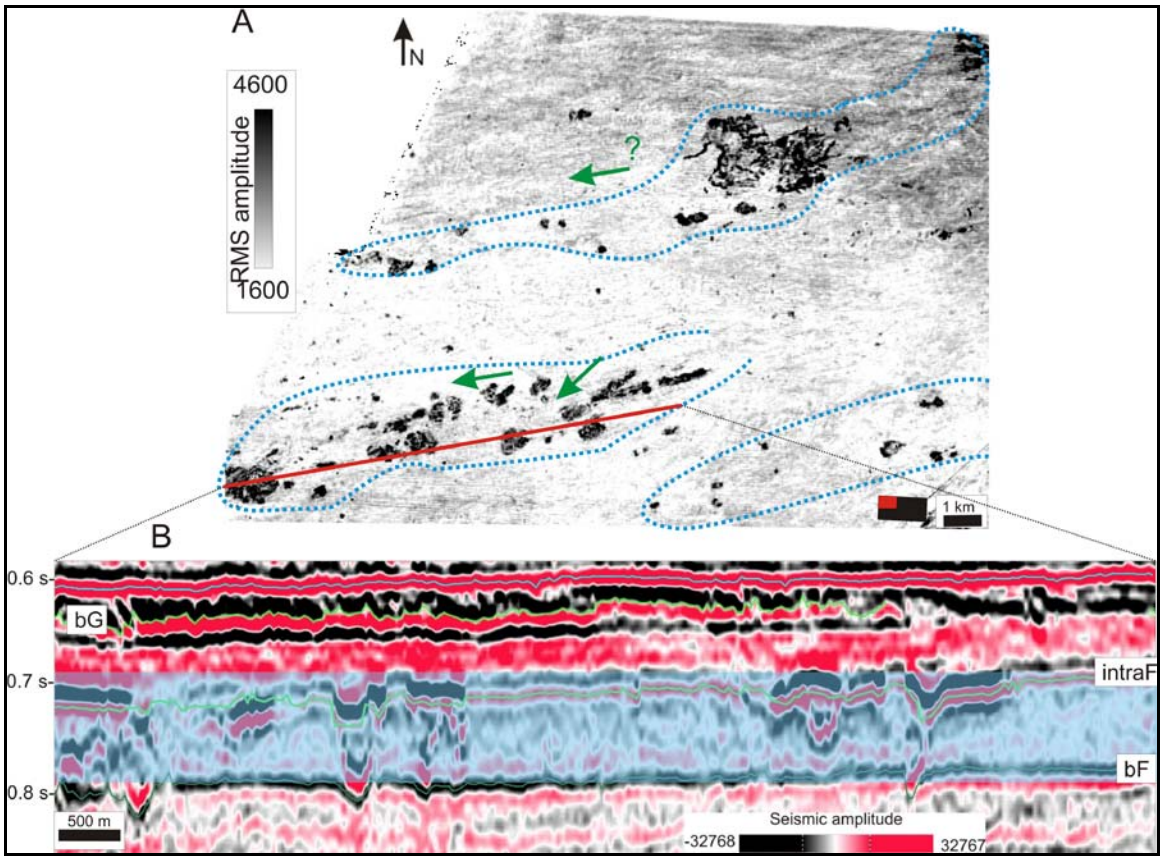

Figure 4.37: **A.** RMS amplitude map of western part of seismic unit F. Red line indicates seismic profile in B. Blue dotted line shows the High amplitude anomalies. The small red box in the lower right corner shows location of the map within the 3D dataset. **B.** Seismic profile along some anomalies. The yellow dotter areas indicate the high amplitude anomalies. The RMS volume is highlighted in blue.

Interpretation of high amplitude anomalies in unit F

The high amplitude anomalies are interpreted to be blocks of different sediment type (higher acoustic impedance) than the surroundings (fig.4.37). It is suggested that they have been subglacially transported by basal freezing (Aber et al., 1989, Andreassen et al., 2004). An RMS amplitude map for the lower part of seismic unit F shows chains of sediments that have a NE-SW orientation (fig.4.37). The RMS volume has its top in reflector intraF (fig.4.37B). On this reflector, two possible chains of sediment blocks have the same orientation as MSGL interpreted in reflector intraF (fig.4.34A) and it is therefore conclude that ice streams at the base of reflector intraF have transported sediments and deposited those in chains.

4.9. Reflector bG

Reflector bG has been interpreted following the positive part of the seismic signal (fig.4.38). It has been interpreted across almost the entire study area (fig.4.39). Reflector bG is almost parallel to the seafloor and has a gentle slope towards the west (fig.4.39). In the 3D study area, the reflector bG has depths between 589 ms to 650 ms (TWT). There are two main features to be interpreted on this surface: megascale glacial lineations and iceberg ploughmarks.

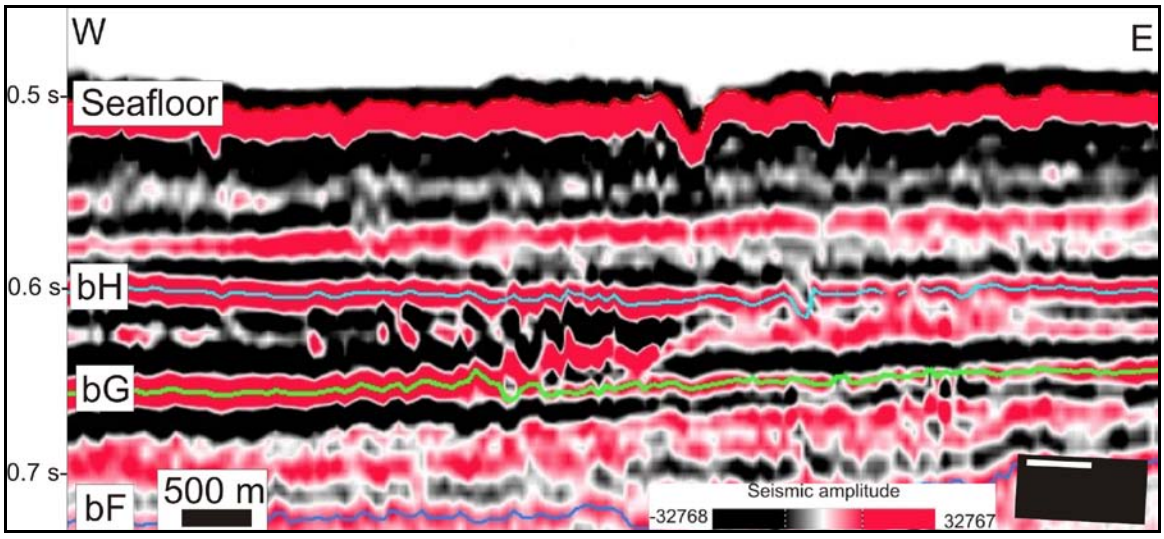

Figure 4.38: Seismic profile showing stratigraphic location of reflector bG.

Megascale glacial lineation on reflector bG

Two sets of parallel lineations (sets 1 and 2 on fig.4.39) are observed on reflector bG in the 3D study area. The set of lineations 1 has an ENE-WSW orientation and the set of lineation 2 has a NE-SW orientation. On seismic profiles both sets appear as sets of furrows with lengths of up to 20 km, width between 100 and 150 m and less than 6 ms (TWT) troughs (fig.4.40).

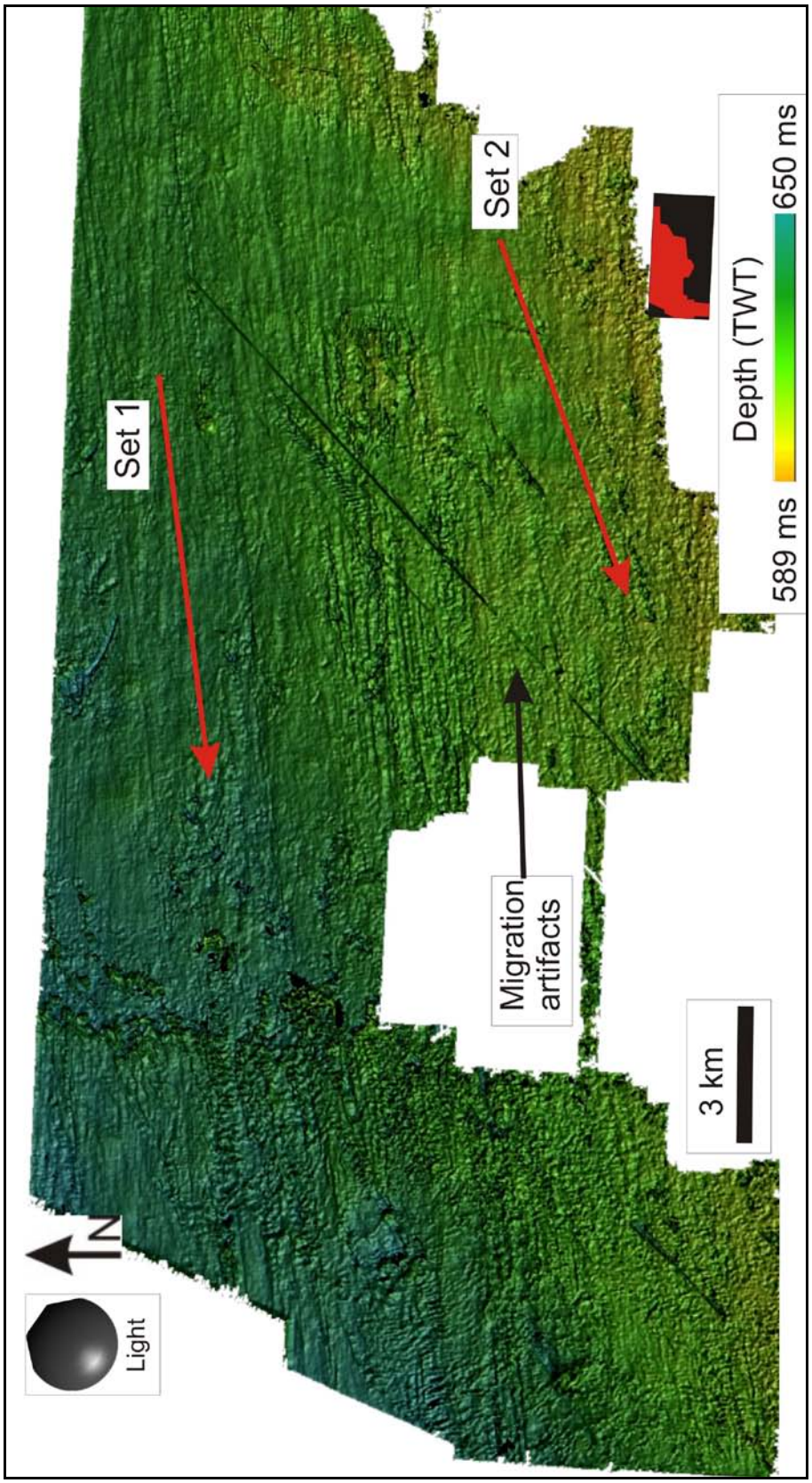

Figure 4.39: Shaded relief image of reflector bG. MSGL orientation is indicated with red arrows. The small red box in the lower right corner shows the location of the image within the 3D dataset.

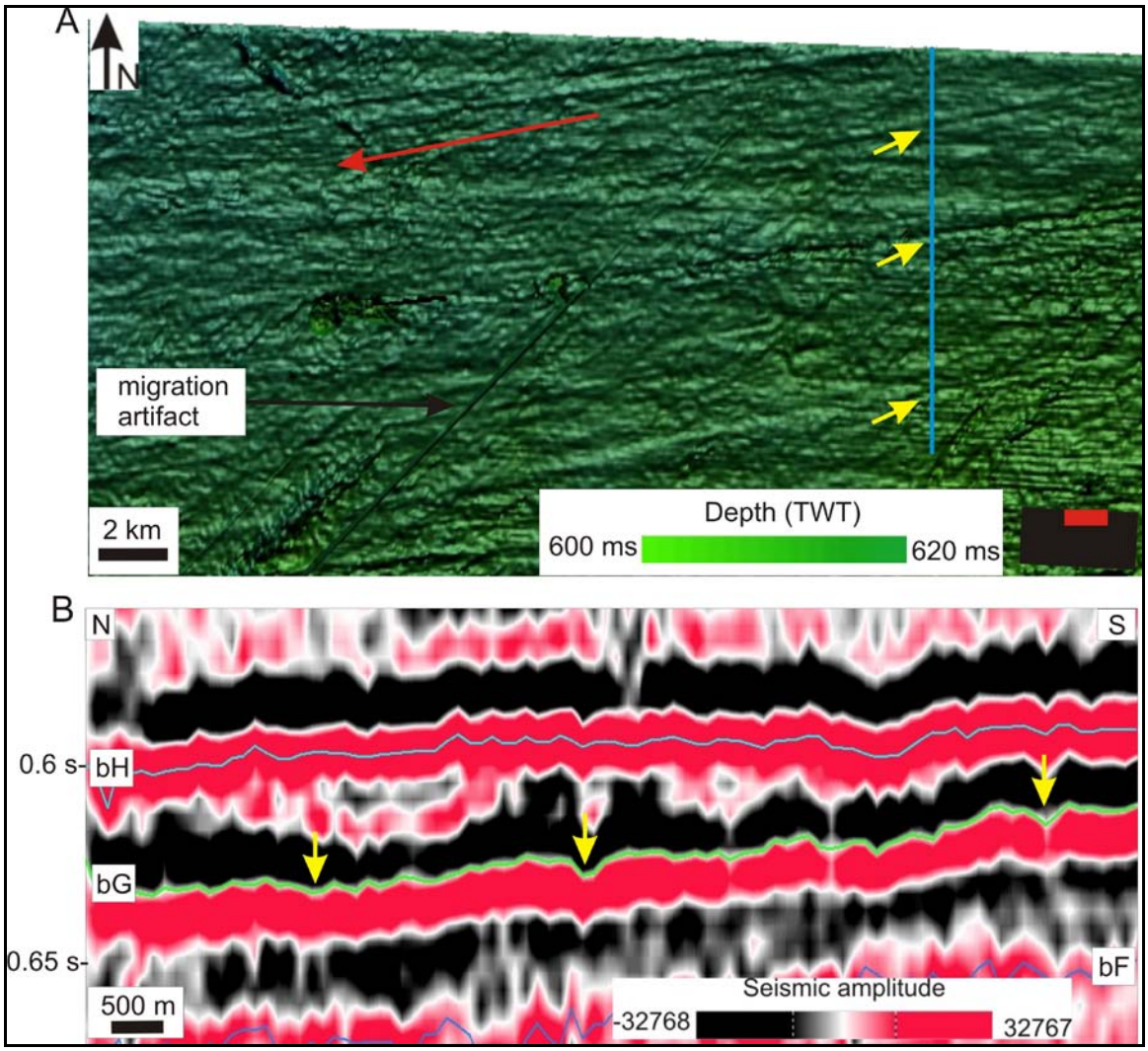

Figure 4.40: A. Shaded relief image of reflector bG. Orientation of MSGL is indicated with a red arrow. Blue line indicates the location of the seismic profile in B. The small red box in the lower right corner indicates location of the image within the 3D dataset. **B.** Seismic profile across MSGL. The yellow arrows indicate the location of the grooves eroded by ice streams.

Based on the orientation of the megascale glacial lineation, the large length:width ratios (>100:1), it is interpreted that the MSGL indicate a paleo ice-stream draining out Bjørnøyrenna (fig.4.41). Ice streams are unstable parts of a glacier. This stability can lead to a change in orientation of the ice stream (Dowdeswell & Elverhøi, 2002; Christoffersen & Tulaczyk, 2003). The two sets of lineations are interpreted to represent the same ice stream and the small difference in orientation is related to changes in ice stream orientation.

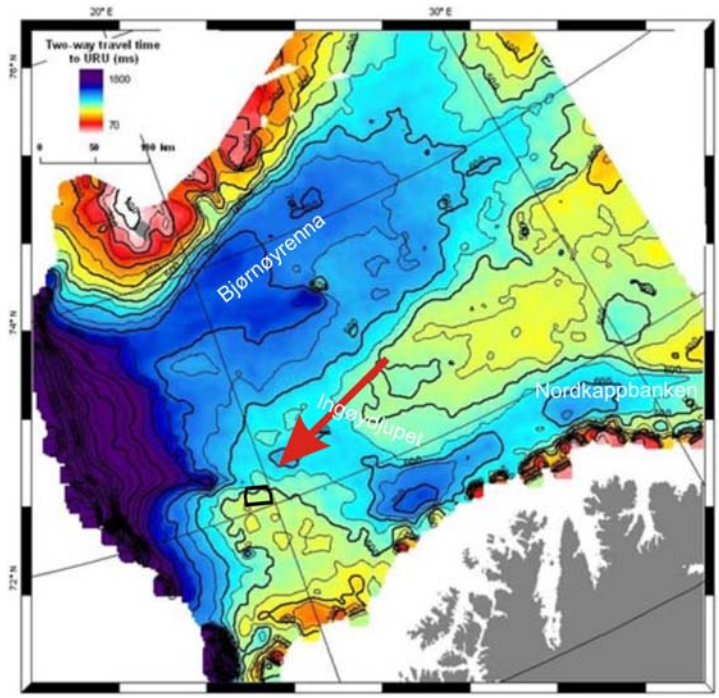

Figure 4.41: Orientation of inferred ice stream on reflector bG in the study area on a time-depth map of URU (modified from Andreassen et al., in prep.).

4.10. Seismic unit G

Seismic unit G is bounded by reflectors bG and bH (fig.4.42). Seismic unit G is transparent with small discontinuous internal reflections. In the west of the study area the base of the unit reveals a series of dipping reflections towards the west (fig.4.43A).

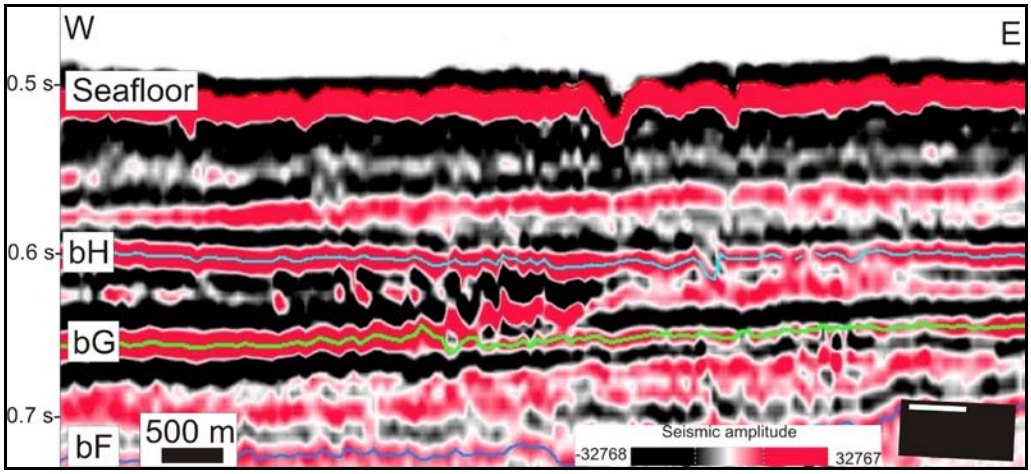

Figure 4.42: Stratigraphic location of seismic unit G.

Imbricate reflections in unit G

The northwestern part of the 3D dataset is characterized by a series of imbricate reflections on the northwestern part of the 3D dataset (fig.4.43A and C). These reflections extend over 8 km from east to west and 20 km from north to south (fig.4.44). Single seismic profiles reveal that the dipping reflections have their base at reflector bG and the top at reflector bH (fig.4.43). They occur as dipping reflectors that are stacked obliquely in an imbricate manner (fig.4.43A and C). The layers have dips of >40º towards the west. A time slice across the reflections shows a characteristic U- and V-shapes, which are stacked upon each other (fig.4.43B and D). An RMS map of the seismic unit G shows that the dipping layers have different amplitude values than the surroundings (fig.4.44). In the RMS map, a set parallel lineations, interpreted to be evidence of paleo-ice streams on reflector bH (chapter 4.11), have the same orientation as the imbricated structures (fig.4.44).

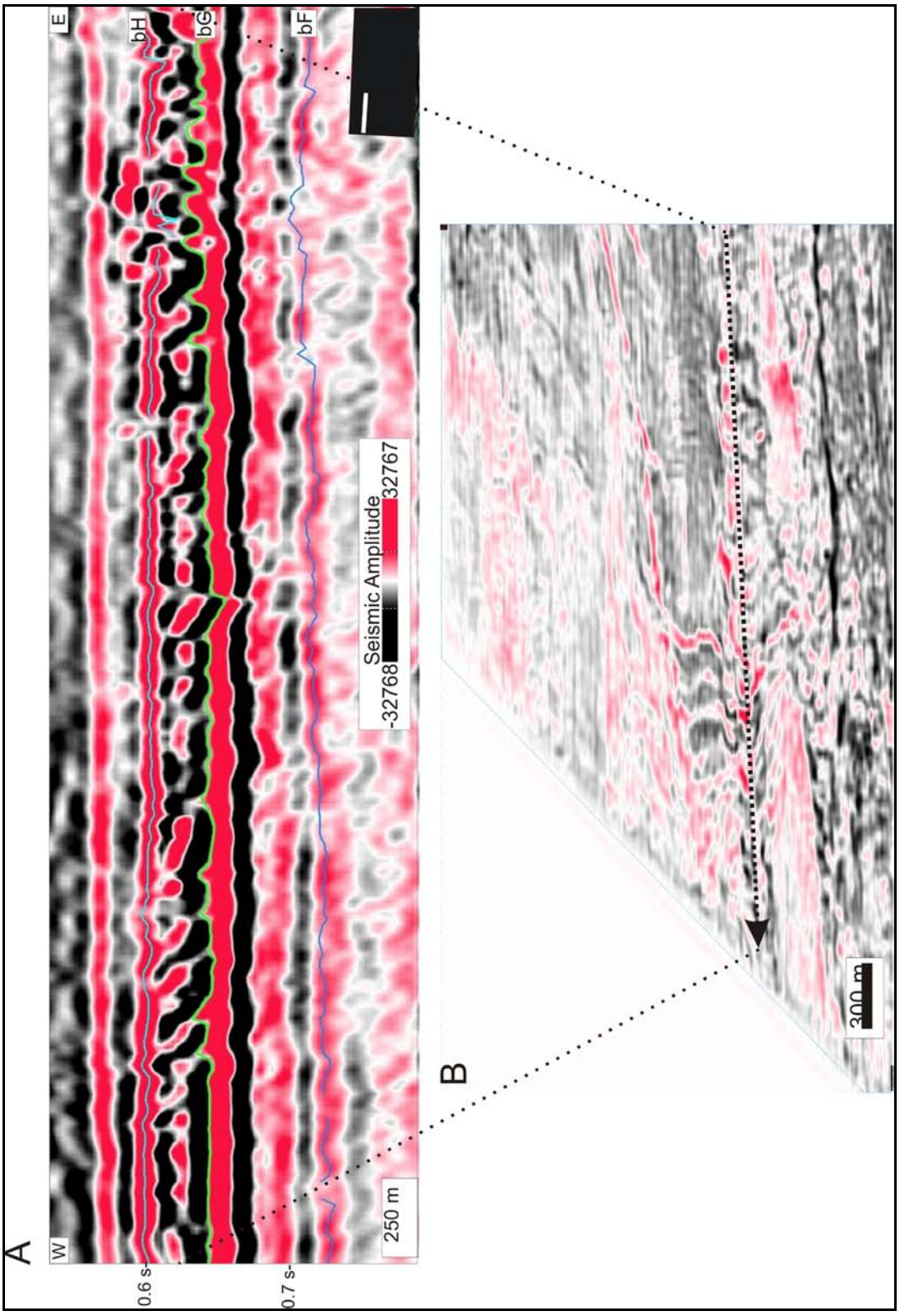
A
B
W
E
bH
bG
bF
Seismic Amplitude
32767
-32768
250 m
300 m
0.6 s
0.7 s

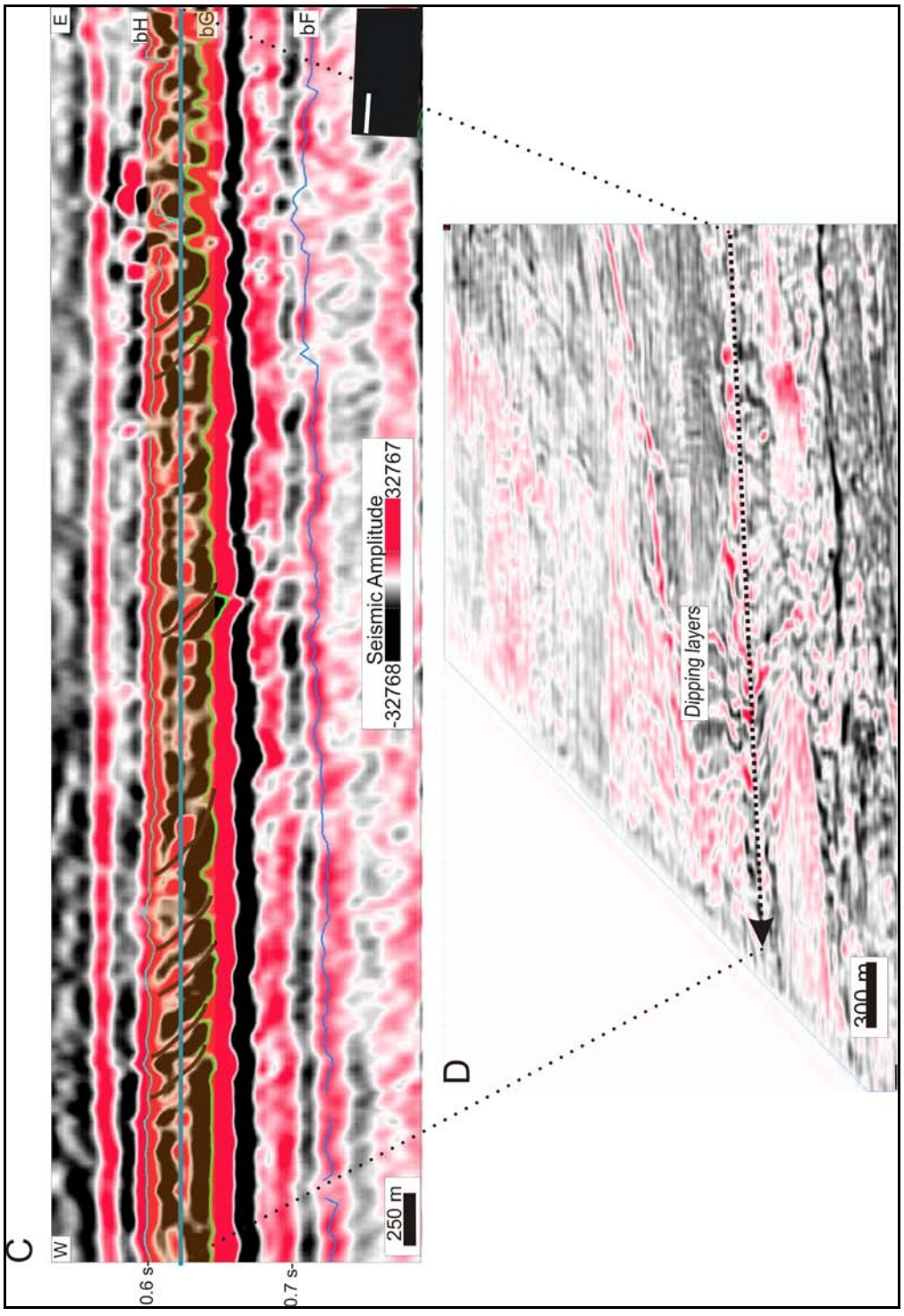

Figure 4.43: **A.** Seismic profile across dipping layers in unit G. Black box in the lower right corner shows the location of the seismic line within the 3D dataset. **B.** Time slice in the middle of unit G cutting through the dipping layers. **C.** Seismic profile across dipping layers in unit G. Volume taken for the RMS amplitude study is shadowed in orange. Black box in the lower right corner shows the location of the seismic line within the 3D dataset. The blue line represents the time slice shown in C. **D.** Time slice showing the characteristic U-shape of the dipping layers.

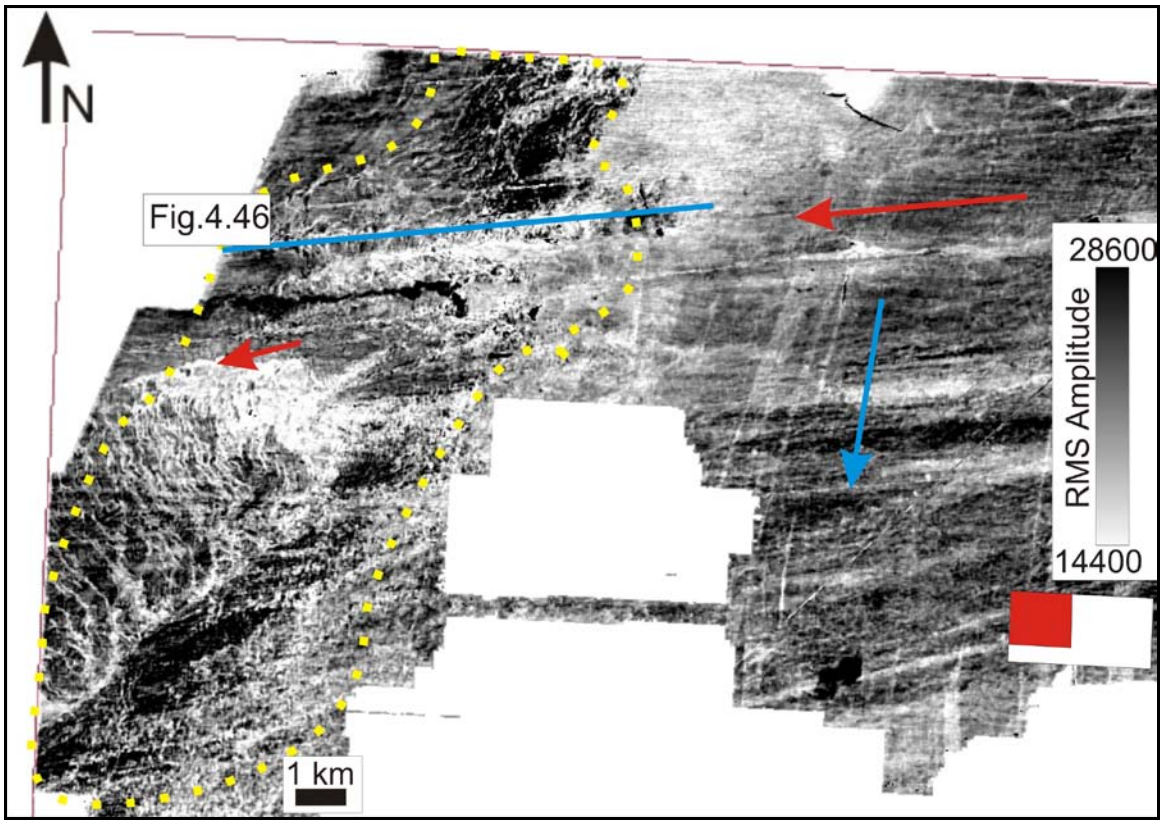

Figure 4.44: RMS amplitude map of seismic unit G. The yellow dotter area indicates the location of the dipping layers. The red and blue arrows indicate the orientation of inferred paleo-ice streams on reflectors bG (red arrow) and bH (red and blue arrow). The small red box in the lower right corner shows the location of the image within the dataset.

Interpretation of imbricate dipping layers in unit G

Sub/proglacial thrust faulting can form thrust blocks (Aber, 1988). Pedersen (2000) suggests a model where imbricated structures are formed by thrust faulting of thrust blocks in front or under a glacier. Glaciers will probably erode the upper part of blocks when they move over them resembling eroded duplex (McClay, 1992). These thrust blocks are usually detached, transported some distance, and stacked up in an imbricated structures and are therefore glaciotectonically allochthonous. The imbricate layers in unit G are therefore interpreted as indicative of sub/proglacial erosion of sediments by a glacier with a WSW orientation. The upper part of the sediments has probably been eroded during the advance of the glacier (fig.4.45).

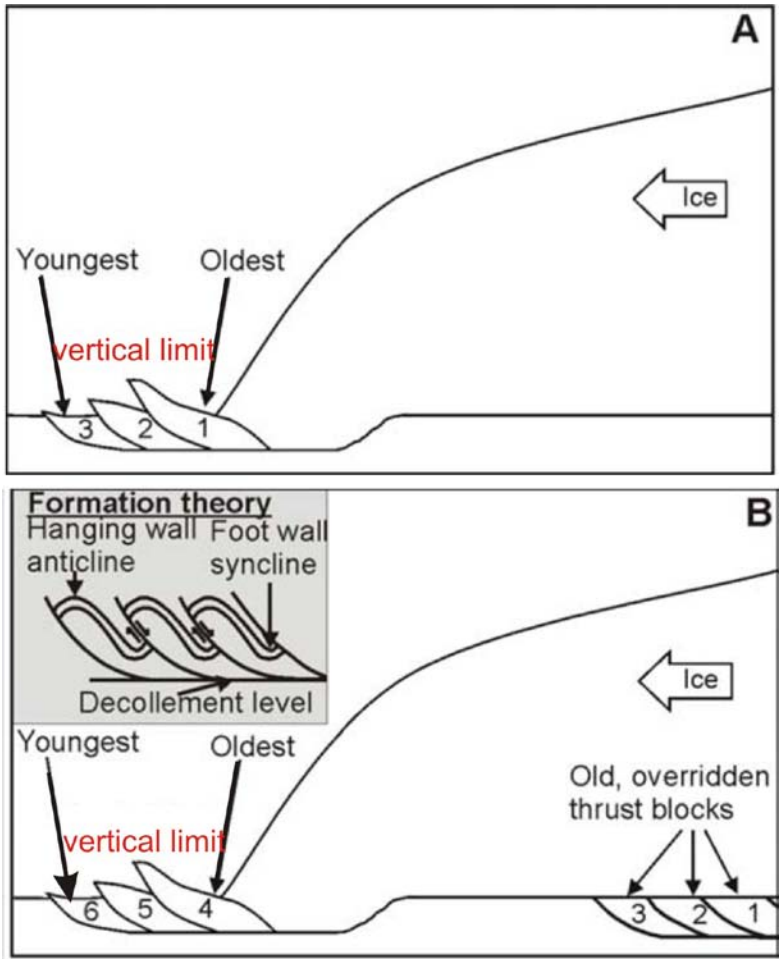

Figure 4.45: A. Schematic diagram illustrating displacement of inclined ice-marginal thrust blocks. **B.** Older blocks are probably eroded in the upper part when the glacier overrides them. Not to scale. Modified from Aber et al. (1989).

4.11. Reflector bH

Reflector bH has been interpreted following the upper cross-zero part of the seismic signal (fig.4.46). This reflector has depths between 484 ms and 618 ms (TWT). Reflector bH has a gentle slope towards the NW (fig.4.47). On the shaded relief surface, two sets of parallel lineations and iceberg ploughmarks are seen (fig.4.47).

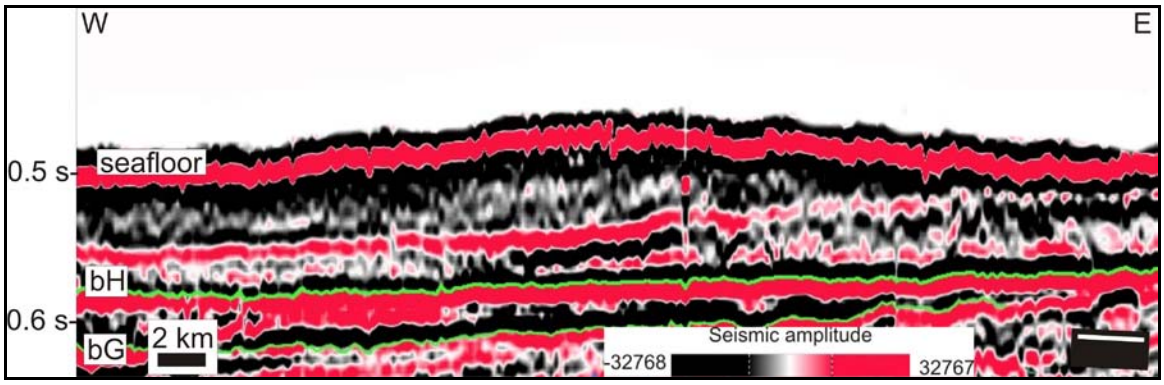

Figure 4.46. Seismic profile showing stratigraphic location of reflector bH**.**

Sets of parallel lineations on reflector bH.

Two sets of parallel lineations are seen on reflector bH (blue and red arrows in fig.4.47A and B). Set 1 has lengths between 15 and 20 km; however, the longest is measured to be up to 50 km long. They have widths up to 300 m. and depths of 6 ms (TWT) and an ENE-WSW orientation (fig.4.47C and D). In the south of the study area, the lineations have small ridges to the sides (fig.4.47A). Set 2 has north-south orientation and it is barely seen on a relief map (fig.4.47A), but best seen on amplitude maps (fig.4.47B). On surface-based amplitude maps, these lineations have similar amplitude values as lineation set 1 (fig.4.47). They are up to 25 km long, up to 450 m wide and they have varying depths within the same lineations and the lineations have a concave shape upstream. They are up to 10 ms (TWT) in the north and almost do not show relief in the south (fig.4.47A and D).

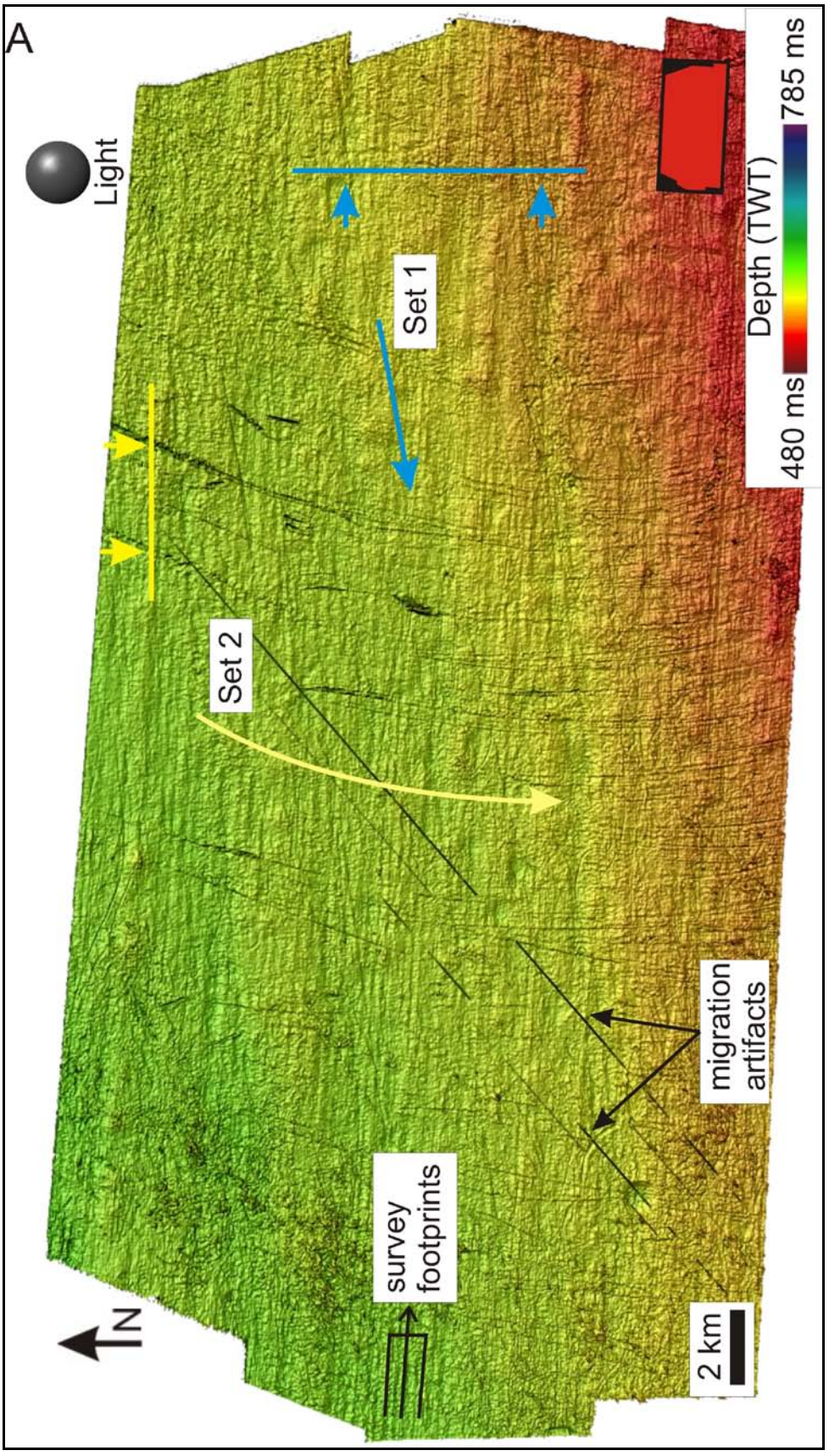
A
Light
Set 1
Set 2
Depth (TWT)
785 ms
480 ms
migration artifacts
survey footprints
N
2 km

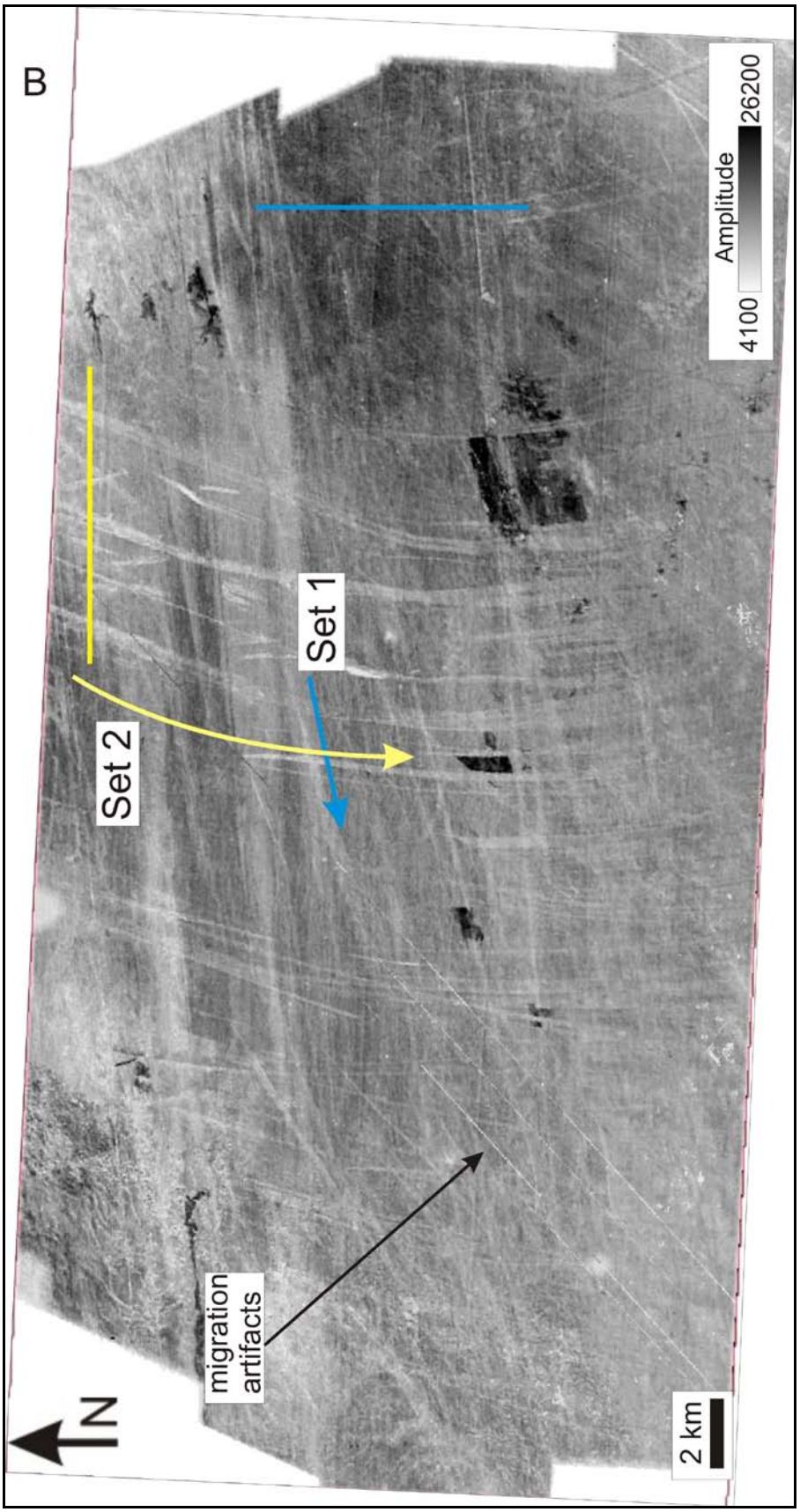
B
Amplitude
26200
4100
Set 1
Set 2
migration artifacts
N
2 km

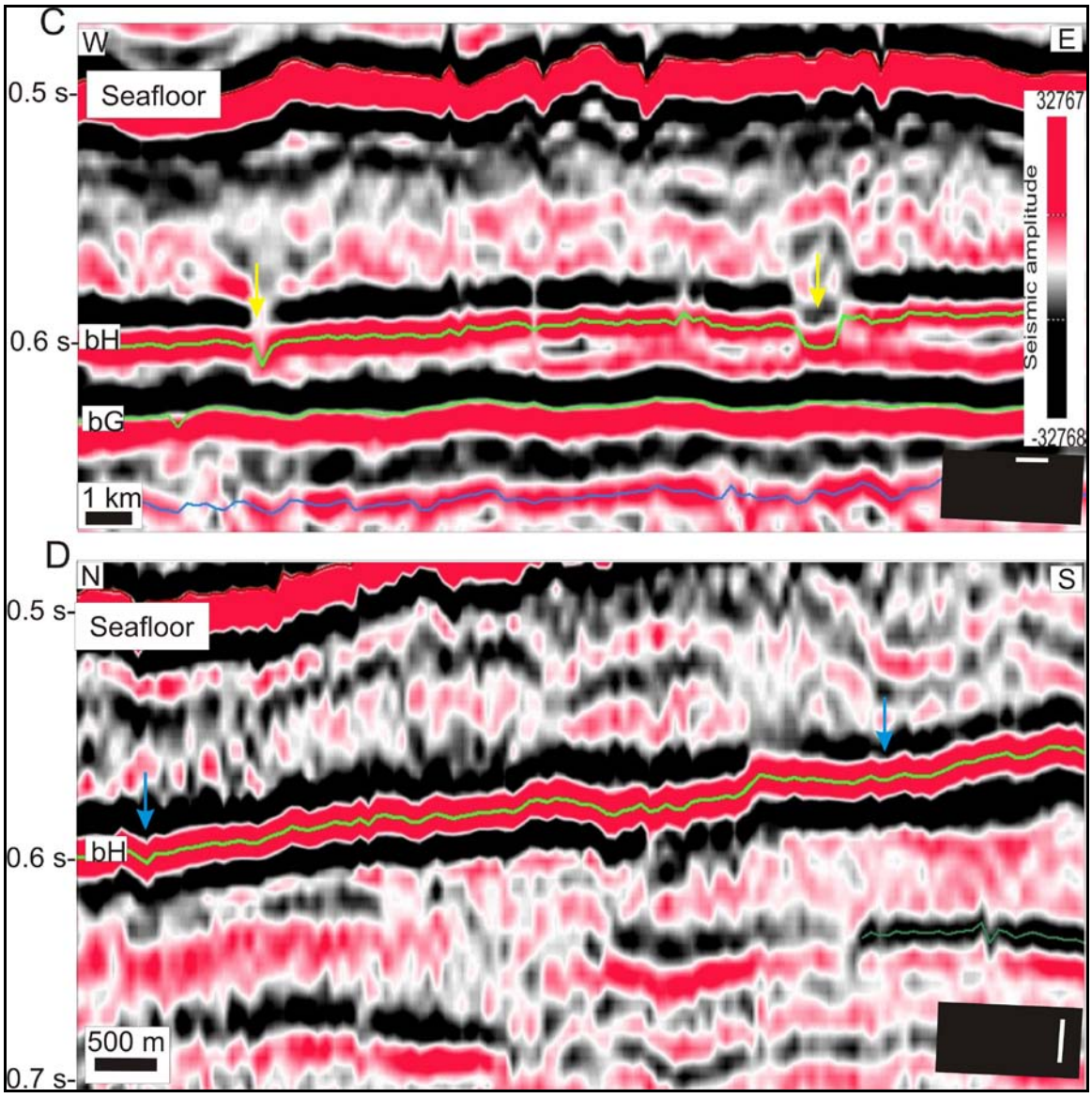

Figure 4.47: **A.** Shaded relief image of reflector bH. Blue and yellow arrows show orientation of MSGLs. The red box in the lower right corner shows the location of the image within the 3D dataset. **B.** Surface based amplitude map for reflector bH. Blue and yellow arrows show orientation of MSGLs. Yellow and blue lines show the location of the seismic profiles in C and D. **C.** Seismic profile across N-S orientated MSGLs. The yellow arrows indicate the location of the MSGLs. **D.** Seismic profile across E-W orientated MSGLs. The blue arrows indicate the location of the MSGLs.

Interpretation of MSGL on reflector bH

Two sets of MSGLs have been interpreted on the surface of reflector bH (fig.4.47). Set of lineations 1 has large length/width ratios (>100/1) and it is interpreted to be formed by fast ice flow draining out the Veslemøy High 3D area (yellow arrow in fig.4.48). On the other hand, set of lineations 2 has also large length/width ratios; however the lineations show a concave shape upstream (fig.4.47A and B). Clark et al. (2003) hypothesized that when ice keels pass downstream from grounded ice, through the grounded line to floating ice, ice keels and MSGLs could show a sharp transition in planform shape and that the exactly straight and parallel grooves may show a discordance at the grounding line, as floating ice is less laterally constrained. This would imply some sinuosity and directional shifts in groove pattern downstream from the transition. Longva & Thorsnes (1997) show MSGLs which changed downstream from straight to parallel lineations into sinuous and occasionally cross-cutting grooves. Studies carried out in the Ice Stream C in Antarctica suggested that shifts in ice stream orientation is a result of continuing thinning of the neighboring Whillians Ice Stream and recent thickening of Ice Stream C (Conway et al., 2002).

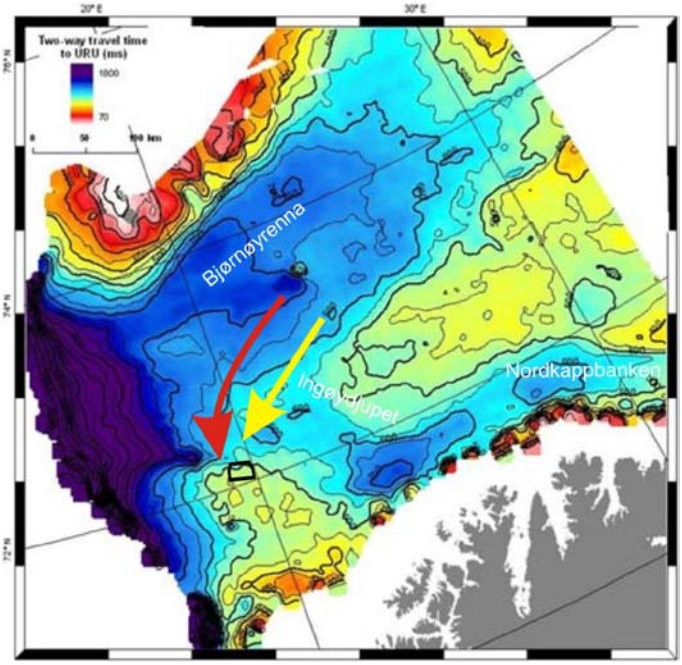

Figure 4.48: Orientation of inferred ice stream on reflector bH in the study area on a time-depth map of URU (modified from Andreassen et al., in prep.).

Set of lineations 2 is interpreted to be formed by a thin ice sheet, probably an ice lobe similar to those described on the seafloor of the Bjørnøyrenna by Andreassen et al. (2008).

4.12. Seafloor

The seafloor has been interpreted following the upper cross-zero part of the seismic signal through the whole 3D area. Depths in the area go from 392 ms to 539 ms (TWT). The seafloor dips towards the northwest (fig.4.49). This surface is dominated by iceberg ploughmarks (fig.4.49 and 4.50) and NE-SW orientated ridges and grooves (I-IV in fig.4.49).

Iceberg ploughmarks on the seafloor

The seafloor is clearly dominated by iceberg ploughmarks with varied orientations, lengths, widths and depths (fig.4.49 and 4.50). Most ploughmarks have lengths between 1 and 5 km. The longest ploughmark measured in this dataset is 16 km long (probably longer because it seems to continue outside the 3D area in the southwestern corner). Widths are between 100 to 300 m; however, single ploughmarks reach widths up to 350 m. The iceberg ploughmarks are between 1 and 15 m deep (fig. 4.50B). It seems that the dominant orientation of the ploughmarks is WNW-ESE. All the ploughmarks have random curving forms; both gradually and in almost right angles and they cross each other in a chaotic way (fig.4.49). Some of the iceberg ploughmarks have a characteristic semicircular lobe in one of the extremes (fig.4.50C). It is also observed in seismic profiles that small ridges are situated at one or two sides of the scours (fig.4.50B).

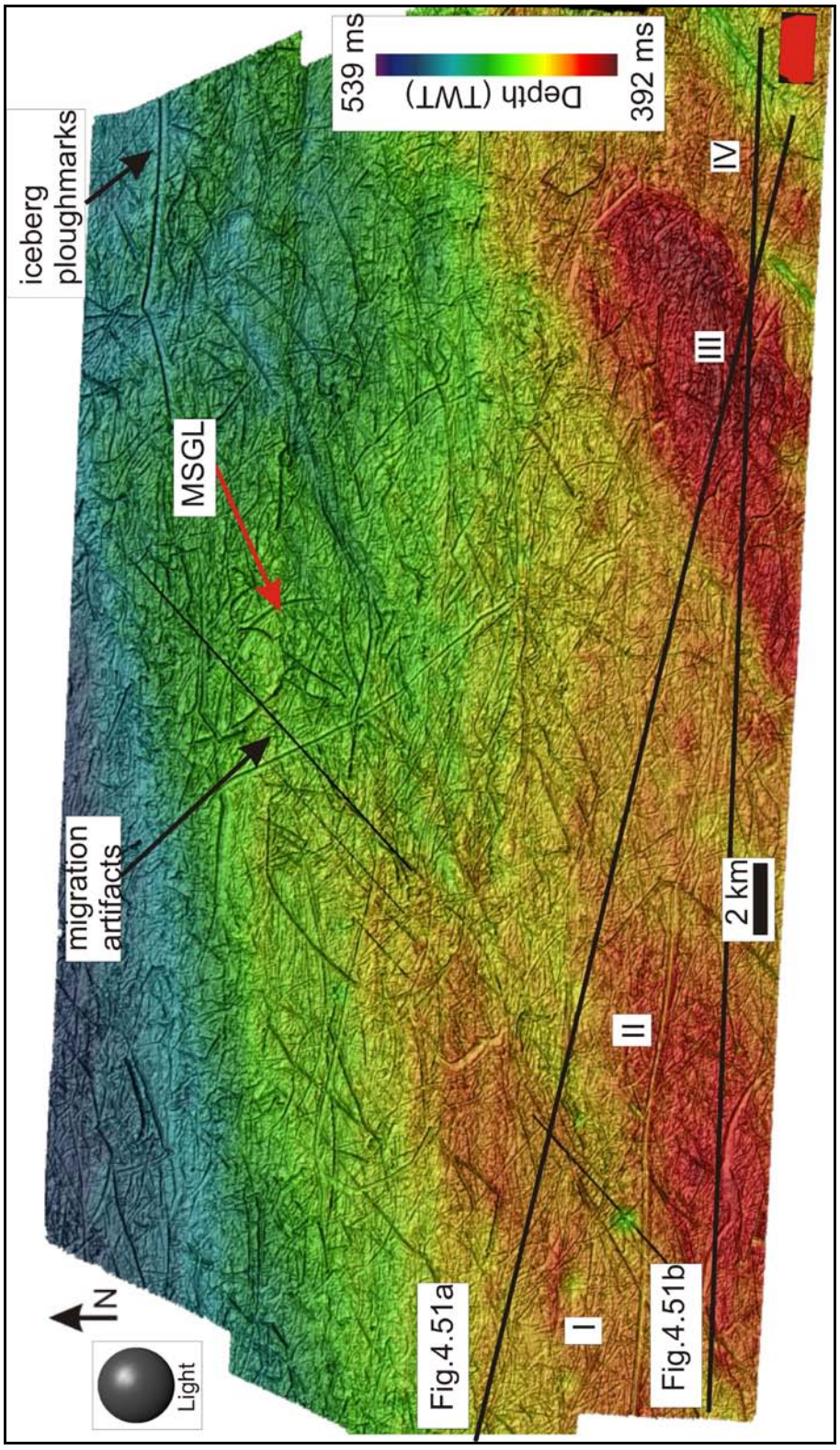

Figure 4.49: Shaded relief map of the seafloor. Red arrow indicates the orientation of MSGLs on the seafloor. The small red box in the lower right corner shows the location of the map within the 3D dataset. NE-SW orientated ridges are numbered as I-IV.

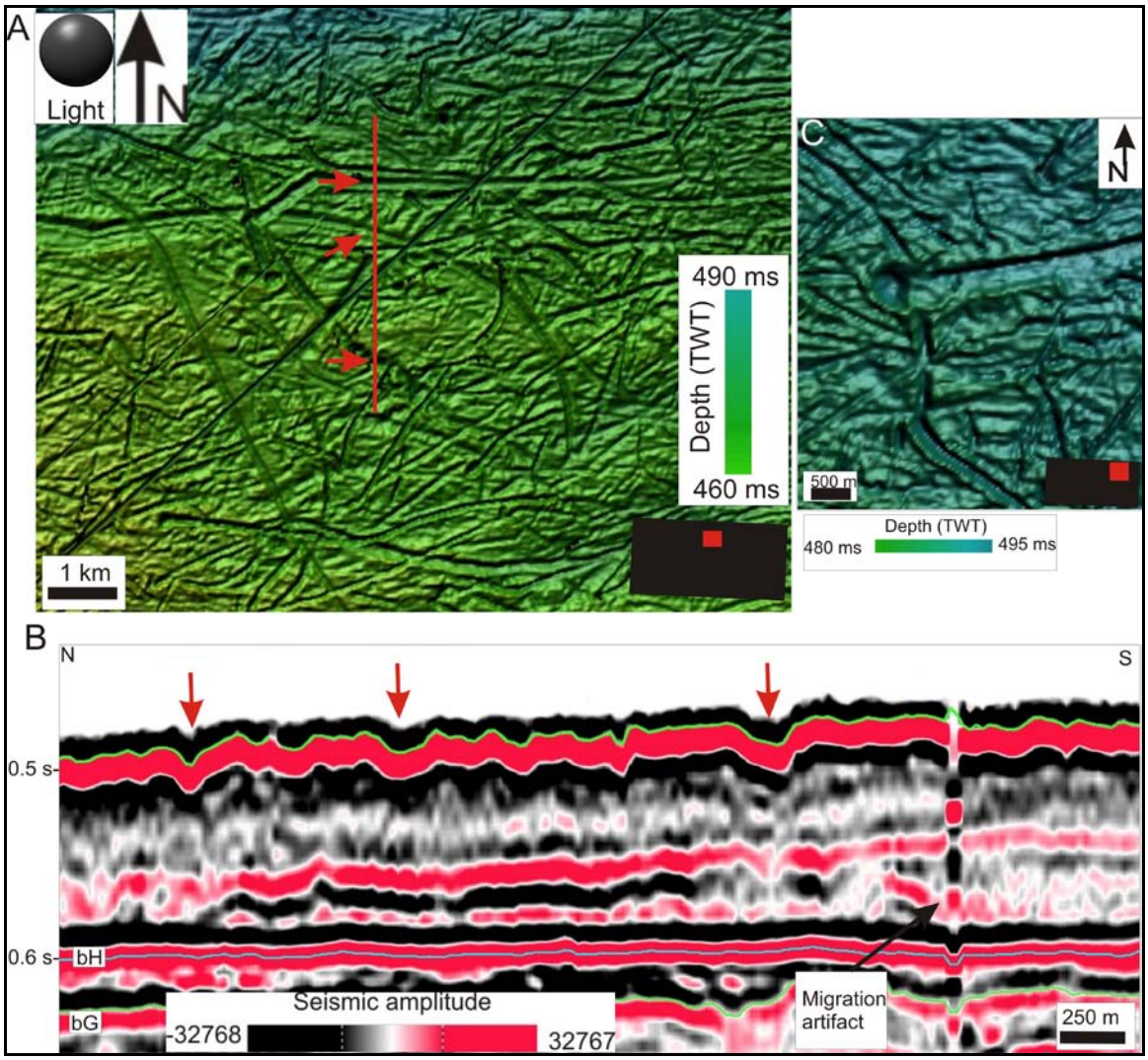

Figure 4.50: A. Shaded relief image of the seafloor focusing on iceberg ploughmarks. The red line indicates the location of seismic profile in B. The small red box in the lower right corner indicates the location of the image within the 3D study area. **B.** Seismic profile across several of the iceberg ploughmarks. The red arrows indicate three of these ploughmarks. **C.** Shaded relief image of the seafloor focusing on an iceberg ploughmarks with a rounded termination.

NE-SW orientated *ridges and grooves on the seafloor*

The southernmost part of the seafloor is characterized by four ridges (I-IV in fig.4.49) and four grooves between them. The ridges are parallel to each other and have a NE-SW orientation. The ridges are between 15 and 30 km long (probably longer because they seem to continue outside the study area), between 1 and 5 km wide and 17, 19, and 24 and 23 ms (TWT) thick respectively. All the ridges have symmetric profiles (fig.4.51). Their elongation ratios are 15:1. Between the ridges, the long grooves have the same

orientation as the ridges. They are at least 31 km long, up to 2.5 km wide, and 9 ms (TWT) deep (fig.4.49 and fig.4.52).

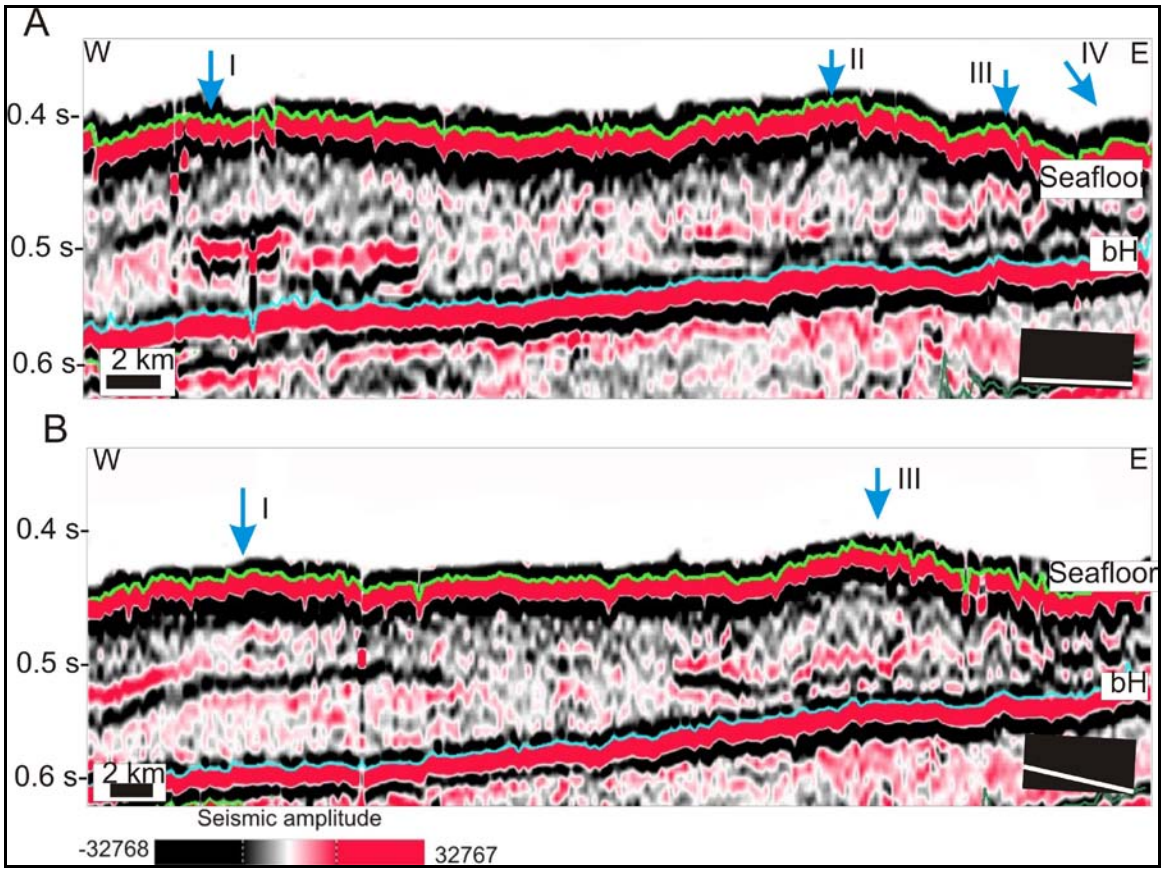

Figure 4.51: Two seismic profiles across the ridges in the seafloor. Blue arrows indicate location of the different ridges.

Interpretation of NE-SW orientated *ridges and grooves on the seafloor*

The sets of ridges and grooves observed in the Veslemøy High 3D area are morphologically similar to MSGL observed on land from satellite images of paleo-ice sheet beds (Clark, 1993; Stokes & Clark, 1999) and in marine environments in Antarctica (Canals et al., 2000; Ó Cofaigh et al., 2005), the Barents Sea (Rafaelsen et al., 2002; Ottesen et al., 2005, 2008; Andreassen et al., 2008) and Canada (Shaw et al., 2006) where they appear in areas that have been occupied by fast-flowing ice streams. The sets of ridges and grooves in the Veslemøy High 3D area are therefore interpreted as MSGLs produced by a fast-flowing grounded ice stream (fig.4.53).

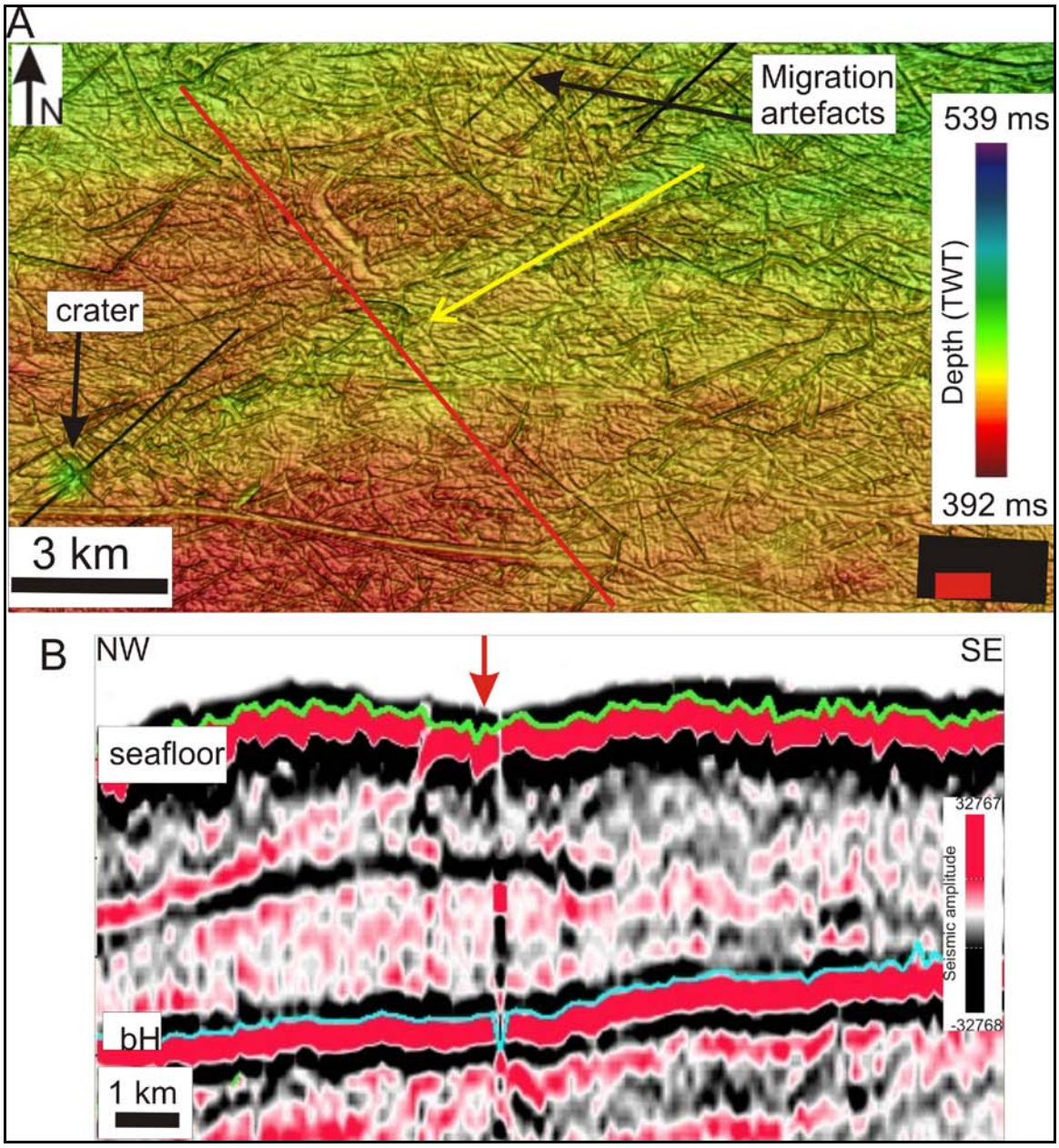

Figure 4.52: A. Shaded relief map of the seafloor. The yellow arrow shows the orientation of the ridges and grooves. **B.** Seismic profile across two ridges and a groove as indicated with a red line in figure A.

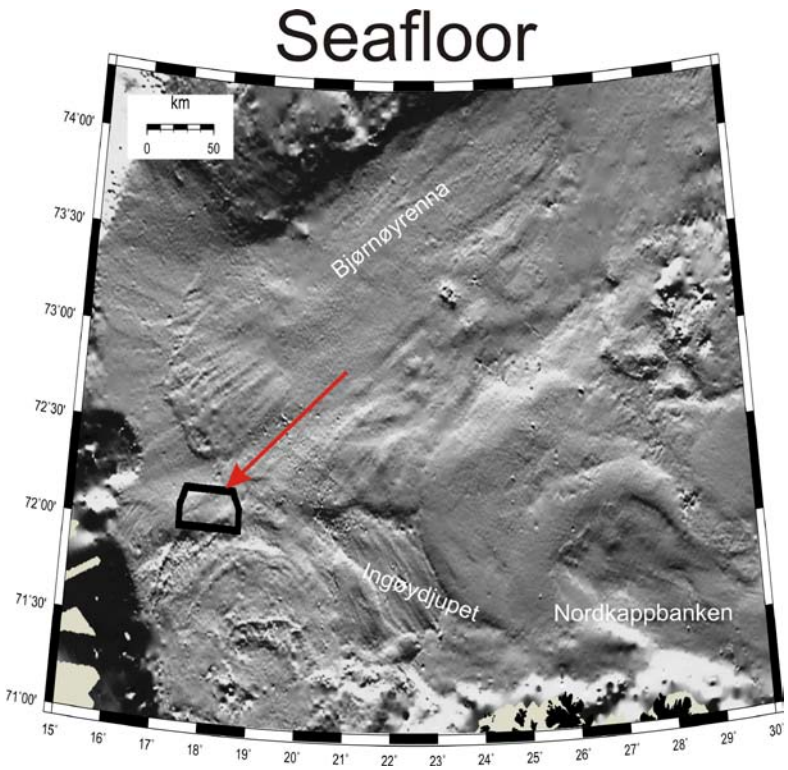

Figure 4.53: Inferred ice stream in the seafloor of the study area on a shaded relief map of the southwestern Barents Sea seafloor.

5. DISCUSSION

In this thesis, six seismic units and eight erosional surfaces have been studied. Seismic units C, E, F, G and H show evidence of an ice sheet which reached the shelf break in the last 1.5 Ma (fig.5.1). On the other hand, unit A has been interpreted to be distal glacimarine facies. Unit A has been interpreted to represent paleo-slope sediments, while the younger units have been interpreted to represent paleo-shelf sediments.

5.1. Submarine channels at the base of unit A

The base of unit A is characterized by the presence of downslope oriented channels located on the paleo-slope (fig.5.2). The presence of channels on the paleo-slope may indicate that they were formed by turbidity currents originating from meltwater released from a temperate ice sheet (Eyles & Eyles, 1992; Laberg et al., submitted). On the ODP site 986, west of Svalbard (fig.1.1), turbidites were identified in sediments of the same age, but not channels; however, the sediments were inferred to derive from glaciers that did not reach sea level (Forsberg et al. 1999). Numerical modeling (Butt et al., 2002) and studies of borehole data (Knies et al., 2009) also indicate that glaciers terminated on land at this time. In conclusion, the channels are inferred to have been formed by turbidity currents originating from glacial meltwater from an ice sheet that did not reach the shelf break.

5.2. Features formed by glacier erosion

Andreassen et al. (2004) showed evidence of grounded ice reaching the shelf edge in the SW Barents Sea from reflector R5 age. MSGL and depressions on the younger reflectors in the study area show evidence of glacial erosion towards the continental shelf edge (i.e. fig.5.3, fig.5.4, fig.4.12). On the seafloor the features described are interpreted to reflect a combination of erosion and deposition (fig.5.5) and on glacially affected paleo-surfaces they are interpreted as erosive features (fig.5.4). This reflects the subsequent glacial

erosion of positive features on paleo-surfaces, for example the hill part of the hill-hole pairs (fig.5.6) or because positive features are too small to be resolved.

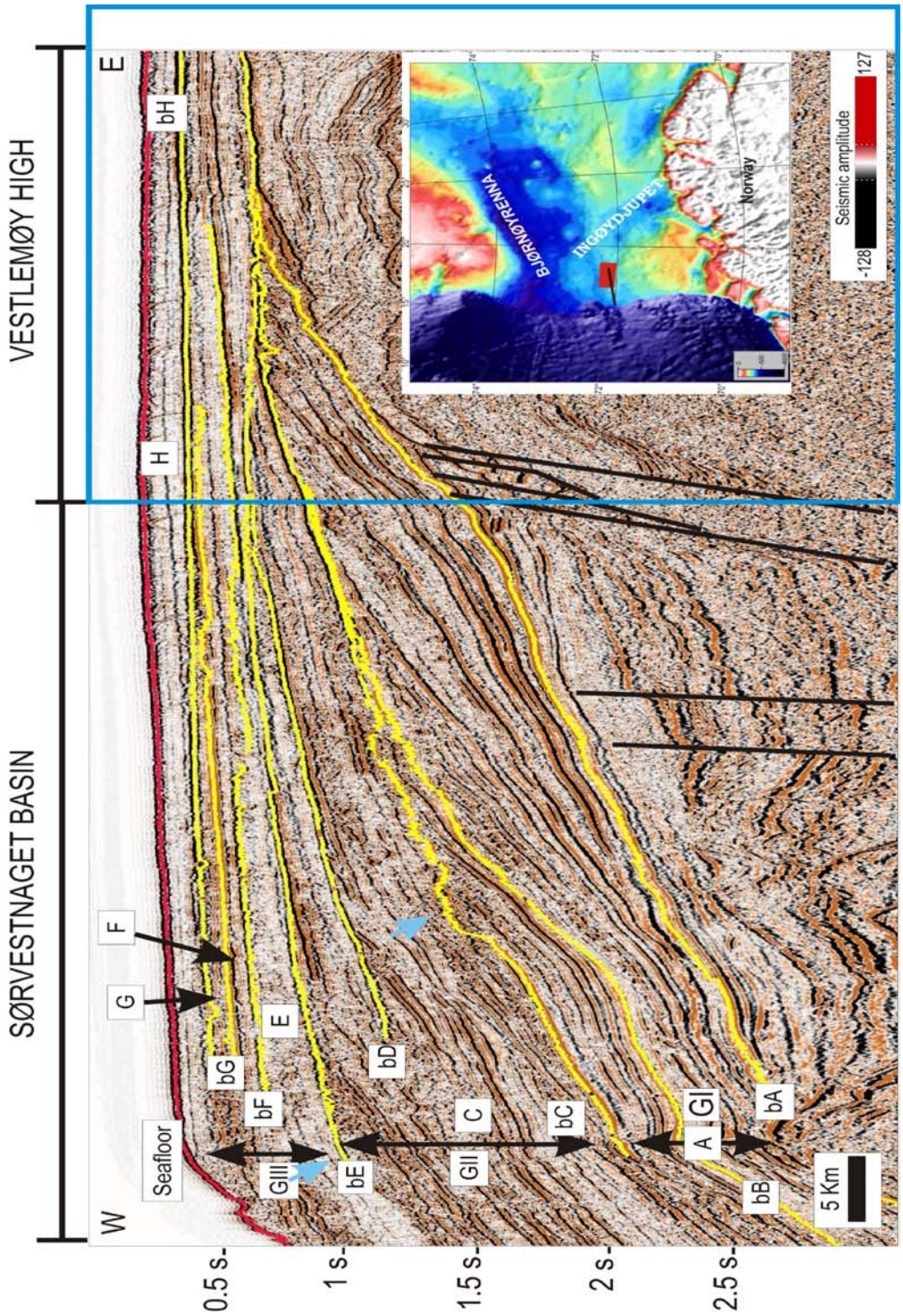

Figure 5.1: Seismic stratigraphy in the SW Barents Sea. Seismic units GI-GIII are the main glacial seismic packages (Faleide et al., 1996) while the seismic reflectors bA-bH are the interpreted seismic unconformities. Blue arrows indicate the location of the paleo-shelf break. The 3D study area is enframed with a blue box.

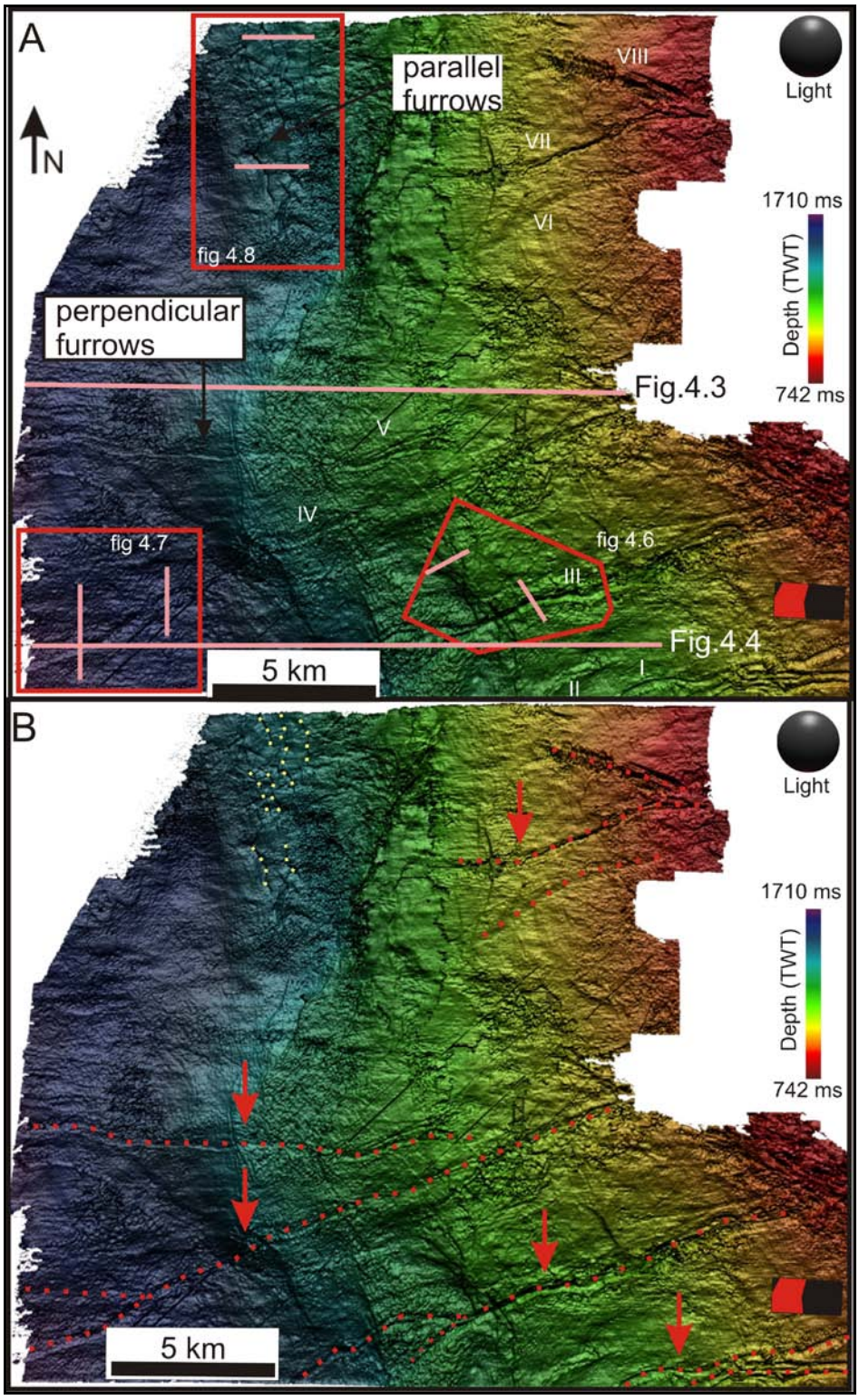

Figure 5.2: Shaded relief image of the paleo-surface bA. Paleo-channels with a WSW orientation are marked from as I-VII, while the paleo-channel with a WNW orientation is marked as VIII. The red squares indicates the location of the figures 4.6-4.8, the pink lines show the location of seismic profiles shown in these figures. The small red boxes in the lower right corner show the location of the map within the 3D area.

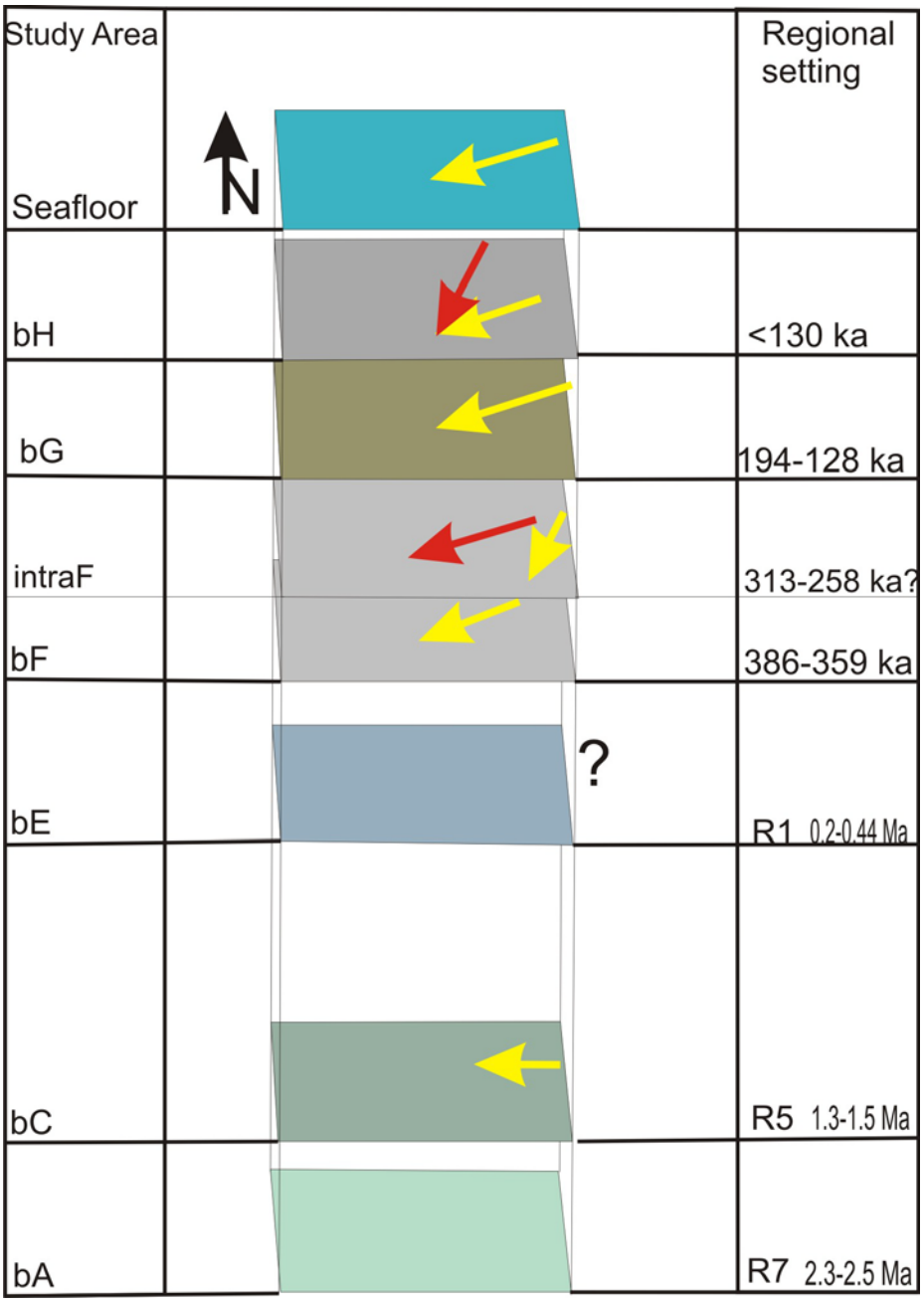

Figure 5.3: Schematic view of orientation of MSGL in the study area. Dating is taken from table 1.1.

In seismic units C and F, accumulations of high amplitude anomalies have been interpreted as sediment blocks (fig.5.6A, fig.4.37). The traditional explanation for transportation of glacial megablocks is by freezing onto the base of the glacier (Aber, 1989) caused by fast downward advection of cold surface ice (Christoffersen & Tulaczyk, 2003). The study area is also affected by gas migration and accumulation and

anomalies may be related to this phenomenon (this is beyond the scope of this Master Thesis).

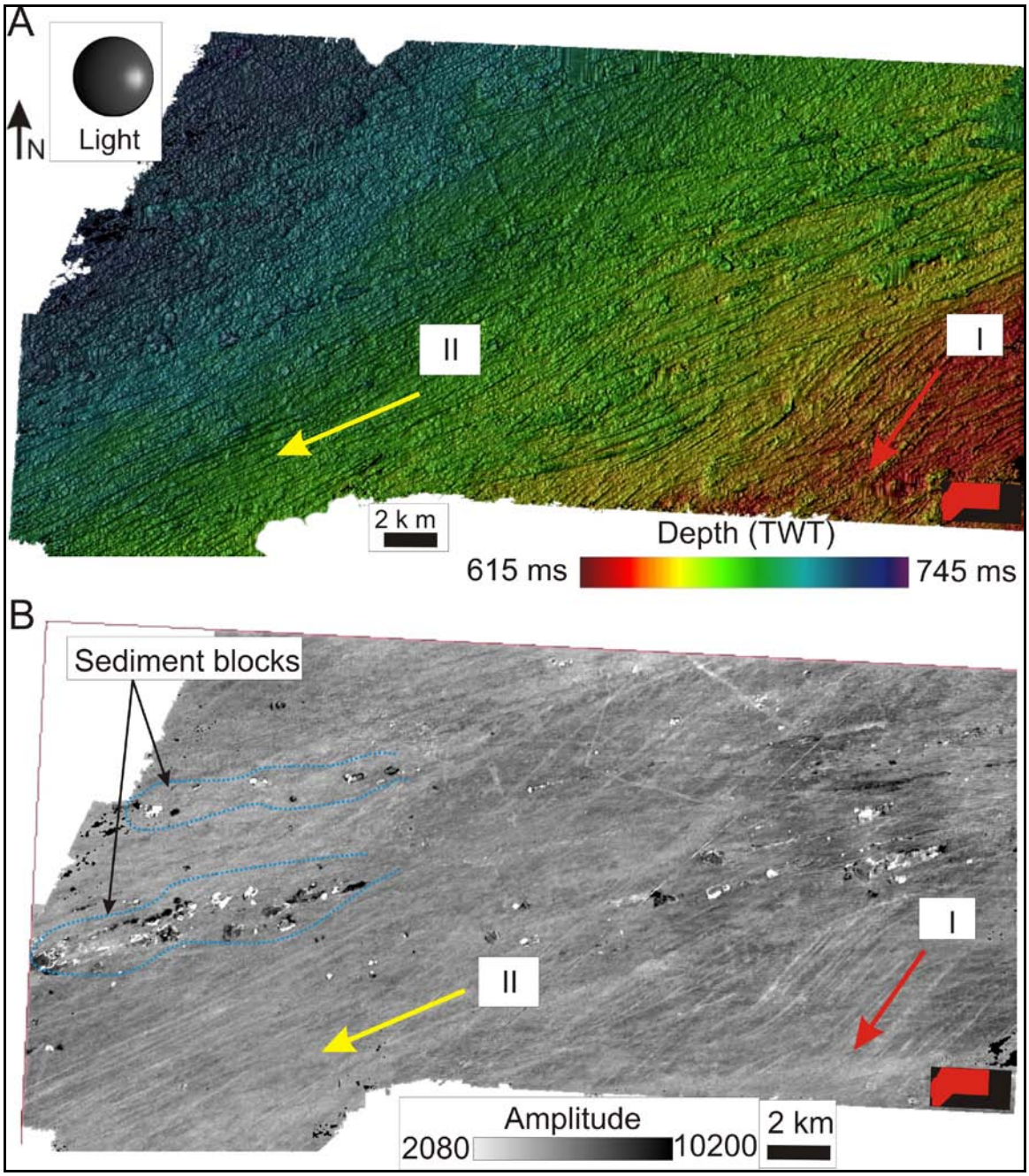

Figure 5.4: A. Shaded relief map of horizon intraF. Two sets of megascale glacial lineations can be inferred (red and yellow arrows). **B.** Surface based amplitude map of the horizon intraF. The small red box in the lower right corner shows the location of the map within the 3D dataset. Sediment blocks have been interpreted in fig. 4.38.

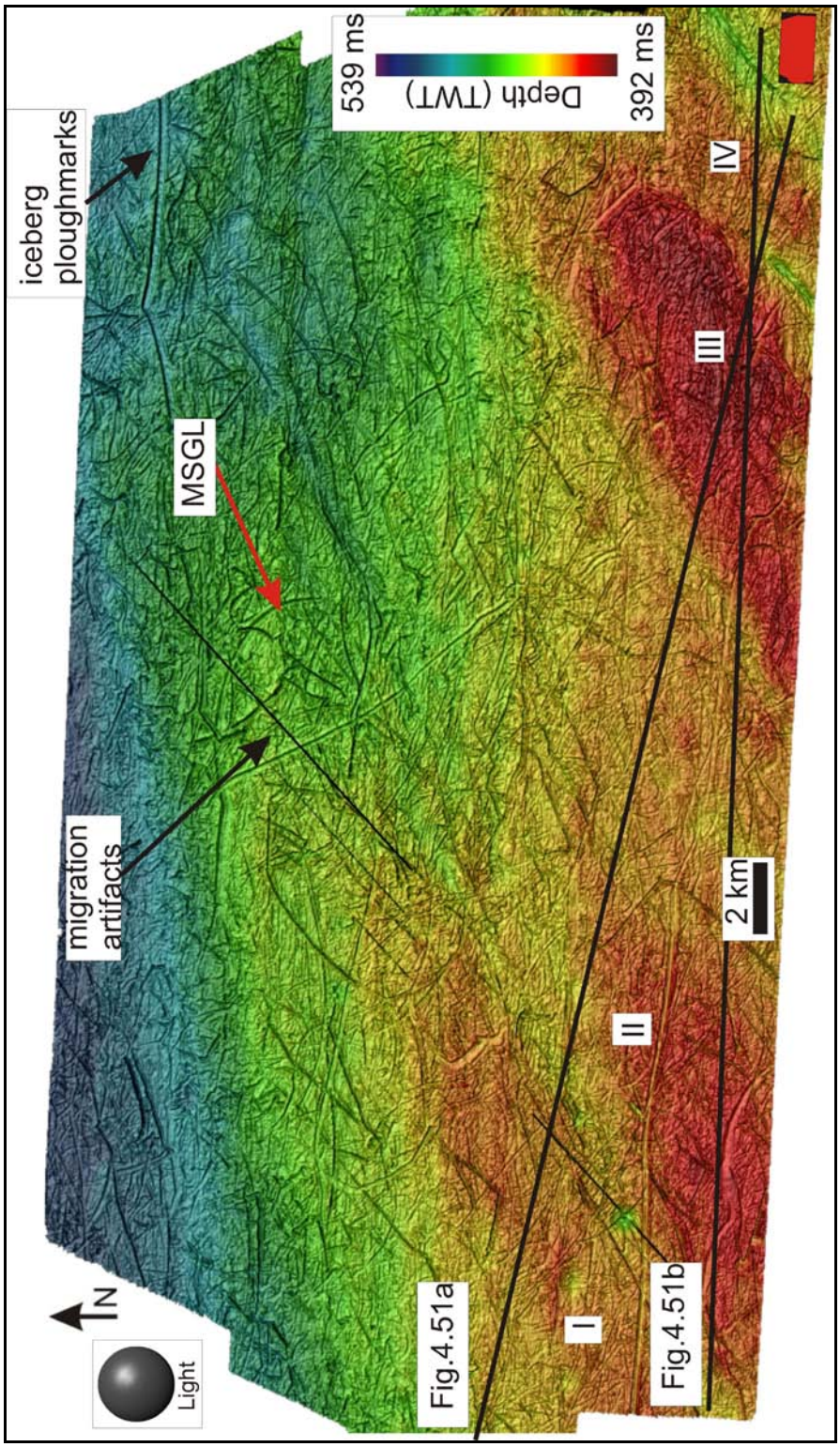

Figure 5.5: Shaded relief map of the seafloor. Red arrow indicates the orientation of MSGLs on the seafloor. The small red box in the lower right corner shows the location of the map within the 3D dataset. NE-SW orientated ridges are numbered as I-IV.

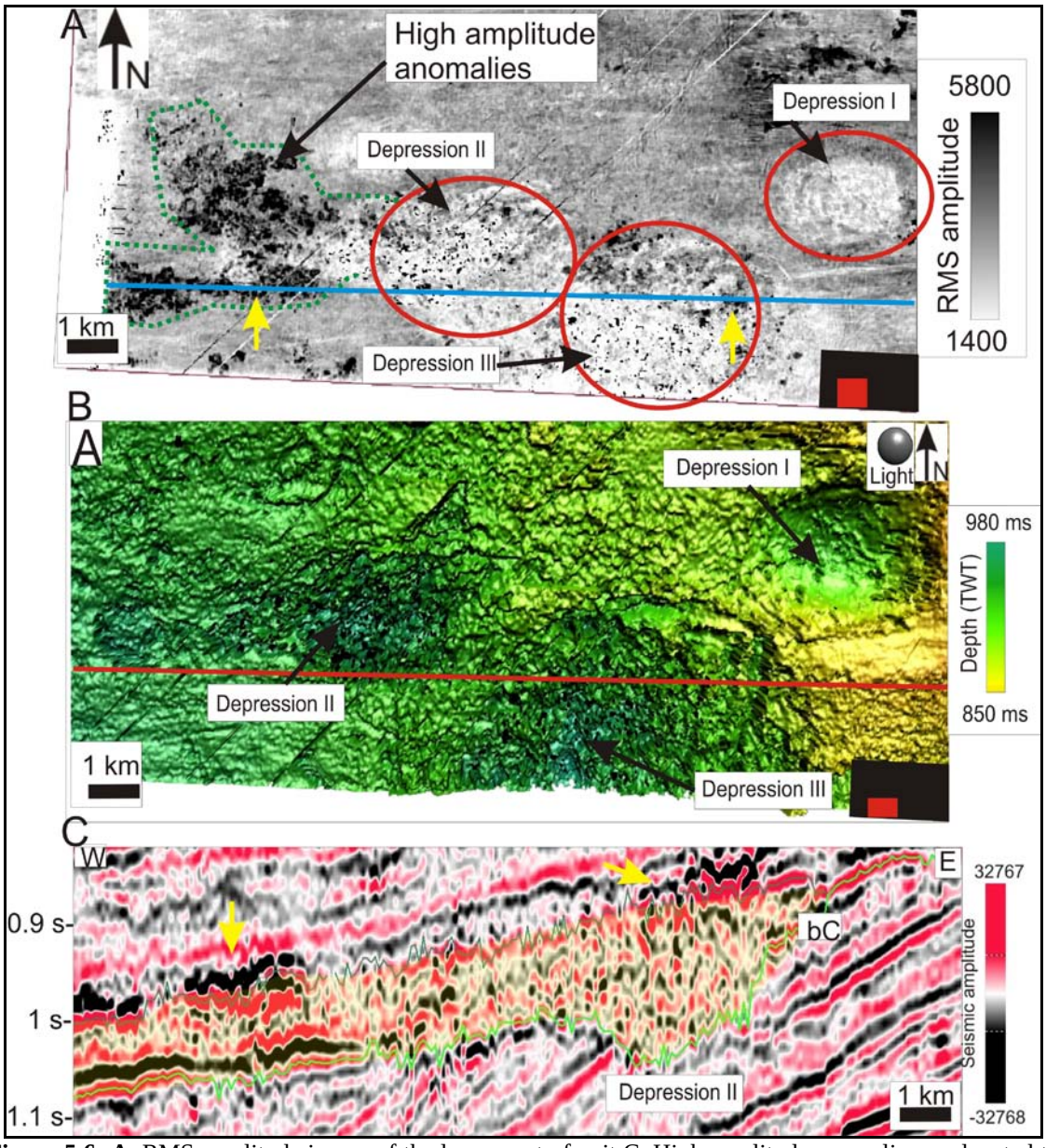

Figure 5.6: A. RMS amplitude image of the lower part of unit C. High amplitude anomalies are located to the west of the depressions on reflector bC. The volume for the RMS volume is shown in C. The red box in the lower right corner shows the location of the image within the 3D dataset. The blue lines shows the location of the seismic profile in C. **B.** Shaded relief image of reflector bC showing the location of the depressions I, II, III. The small red box in the lower right corner shows the location of the image within the 3D dataset. **C.** Seismic profile across the high amplitude anomalies in the south. The yellow shadowed area show the volume used for the RMS map shown in A.

5.2.1.- Megascale glacial lineations

Megascale glacial lineations have been observed on land from satellite images of paleo-ice sheets beds (Clark, 1993; Stokes & Clark, 1999; Clark et al., 2003), in marine environments in Antarctica (Canals et al., 2000; Ó Cofragh et al., 2002; 2005), in the

Barents Sea (Andreassen et al, 2004; 2007; 2008; Ottesen et al, 2005). These features are used to identify paleo-ice streams; however it is not agreed whether MSGL are positive features (Clark, 1993; Canals et al., 2000) or erosive features (Tulaczyk et al., 2001; Clark et al., 2003; Andreassen et al., 2004, 2007). Here, investigation of MSGLs on buried surfaces supports the theory of MSGL as being erosive features (fig.5.4), but the MSGL interpreted on reflector bH and the seafloor suggest that they are a combination of ridges and grooves (fig.5.5) as will be further discussed below.

One hypothesis for the formation of the MSGLs is that they result from basal erosion of soft-wet till underneath the ice stream (Tulaczyk et al., 2001; Clark et al., 2003). This hypothesis is based on work done on a drumlinized field in Canada where the ridges, rather than having formed by some relief amplification process, are seen as residual accumulations of sediments, whose form is consequence of carving of intervening grooves. In this process, sediment can be transported laterally and form ridges between the erosional grooves, MSGL are therefore identified as ridges (Tulaczyk et al., 2001; Clark et al., 2003). Clark et al. (2003) hypothesized that MSGL formed by large bumps in the base of the ice sheet which act as keels and plough through soft sediments, carving elongated grooves and squeezing sediments up into intervening ridges (fig.5.7). Shear strength of till is an important factor in determinating the shape of the MSGLs. Clark et al. (2003) predict that grooves and ridges will form in wet and slippery till, whereas only grooves will form in drier and stronger tills. In this study, the MSGLs on the seafloor are formed as sets of ridges and grooves with a NE-SW orientation. The ridges have been interpreted as accumulations with intervening eroded grooves. These observations support to Tulaczcyk's et al. (2001) theory of MSGL as erosional forms with residual accumulations to the sides. Assuming this theory as valid, there are three possible explanations for the lack of ridges in most parts of the interpreted reflectors in the Veslemøy High 3D area. 1) It is expected that the accumulations have low resistance to erosion and that they are easy to erode by later glacier advances, 2) The sediments on the seafloor have lower shear strength than in deeper reflectors as Clark et al. (2003) predicted and 3) that the accumulations are too small to be resolved.

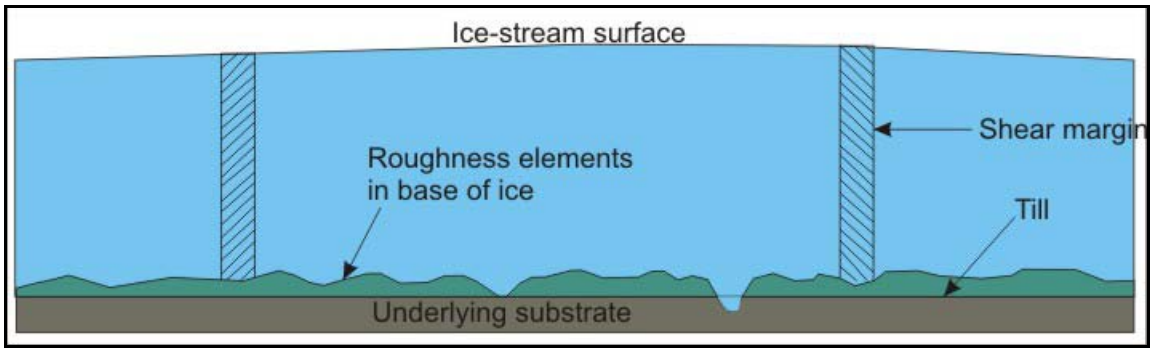

Figure 5.7: Schematic ice-stream cross section illustrating how bumps at the base of the ice carve and mould the till into groove-ridge systems characteristic of MSGLs. The diagram (not to scale) is modified from Clark et al. (2003).

Megascale glacial lineations are interpreted to be formed under conditions of fast ice flow such as ice streams or surge events (Clark et al., 2003) and interpreted as indicators of paleo-ice streams (Clark et al., 1993, 1999; Stokes & Clark, 1999; Andreassen et al., 2004, 2007). Ice streams are described as part of an ice sheet in which ice flows more rapidly, and not necessary in the same direction as, the surrounding ice (Swithinbank, 1954). Bennett (2003) added that the ice should be surrounded by ice rather than rock and that the ice should be grounded rather than floating.

5.2.3. Hill-hole pairs on reflector bC

Hill-hole pairs consist of an ice-scooped basin and related hill (Sættem et al., 1990). Aber (1988) described the hill-hole pair as, "a combination of ice-scooped basin and ice-pushed hill". This type of glacitectonic features has been previously described in central North Dakota (Bluemle, 1970, 1984; Clayton and Moran, 1974) and Denmark (Jessen, 1931), on the Norwegian Continental Margin (Ottesen et al., 2005), in the Barents Sea (Sættem, 1990, 1994) and offshore Svalbard (Ottesen et al., 2005)**.** Bluemle & Clayton (1984) described the hill-holes pairs as "a discrete hill of ice-thrust material, often slightly crumpled, situated a short distance downglacier from a depression and of similar size and shape". However, hills without associated depressions (Moran et al. 1980, Harris et al. 1997) and anomalous depressions without associated hills (Ruszczynska-Szenajch 1976, 1978**;** Sættem, 1990) are also known from the literature. In the Veslemøy High 3D

area, the depressions are not associated with an obvious hill; however, inferred sediment accumulations are associated with the hill (see chapter 4; fig.4.23 and fig.5.6).

The shape of the depressions on reflector bC is relatively similar to holes that have been studied in detail in the margin of the former Laurentide Ice Sheet in the Canadian Prairies (Moran et al., 1980). It is therefore expected that the processes that eroded the depressions in the study area have a similar origin. The Laurentide hill-hole pairs are interpreted to be eroded by compressive subglacial stress, leading to tectonism (Moran et al., 1980). Aber et al. (1989) suggests that high horizontal stress generated by vertical ice load pressure may develop along the margin of an ice sheet and Sættem (1990) added that this will most probably occur in cold based ice because warm based ice would slide over the sediments. Pedersen (2000) also suggests that the glacier has to be very thick in order to cause enough stress to erode such a large amount of sediment.

Model for formation of hill-hole pairs

Sættem's (1990) model for the formation of hill-hole pairs in the nearby Fugløybanken is favored here to explain the formation of the depressions in reflector bC (fig.5.6B). Consolidation of sediments in front of an ice sheet is related to an increase in effective load (ice load less the water pressure at the base of the ice) which forces porewater to drain (Mathews & Mackay, 1960) (fig.5.8.1 and fig.5.8.2). The movement of the ice and an increase in pore pressure will lead to thrust faulting (fig.5.8.3) under the ice (Pedersen, 2000). These will lead to the displacement of sediments (fig.5.8.4D) and deposition of a chain of imbricated structures (Aber et al., 1989). The imbricated structures described west of depression I (fig.5.8.5) are interpreted to be caused by this displacement of sediments. It is unclear that hill-hole pairs as those know from the seafloor offshore Svalbard (Ottesen et al., 2008) or Fugløybanken (Sættem, 1994) occurred in the Veslemøy High, but it is possible that the same ice which displaced the sediments could have transported towards the paleo-shelf break. To the west of these holes, high amplitude anomalies have been interpreted to be part of the hills associated with the pairs (fig.5.6). In the Sørvestnaget Basin 3D area, small depressions in two of the reflectors

within unit GIII have been interpreted as the source of chains of sediments found towards the west (Ødegaard, 2005). On RMS volume maps, it is observed that sediments located within some of the depressions have the same amplitude as the sediments located to the west of the depressions (fig.5.6C); this is consistent with the depressions being the source of the sediment blocks.

5.2.3- Sediment blocks

High amplitude anomalies within seismic units C and F in the Veslemøy High 3D area have been interpreted as sediment blocks of a different type of sediment to the surrounding sediments (i.e. fig.5.6, fig.4.37). In unit C (fig.5.6), the sediment blocks have are randomly distributed, although two possible chains have a NE-SW orientation. On unit F (fig.4.37) the sediments are clearly distributed in chains with a NE-SW orientation.

Glacial megablocks and rafts are common in formerly glaciated areas, and may be aligned in chains (Aber et al., 1989; Rafaelsen et al., 2002; Andreassen et al., 2004). Sediment blocks are interpreted to be transported and deposited subglacially (Aber et al., 1989). In my study area all chains of sediments are located within the paleo-shelf, and they all show an orientation towards the west. The traditional explanation for the transport of the sediment blocks is by freezing onto the base of the glacier (Aber et al., 1993; Andreassen et al., 2004). Paleo- ice streams may have undergone periods of basal freezing (Christioffersen & Tulaczyk, 2003) causing the porewater extraction and overconsolidation of subglacial fine grained sediments (Sættem, 1990; 1994). Basal freezing has been suggested as the process by which the sediment blocks are eroded and subglacially transported.

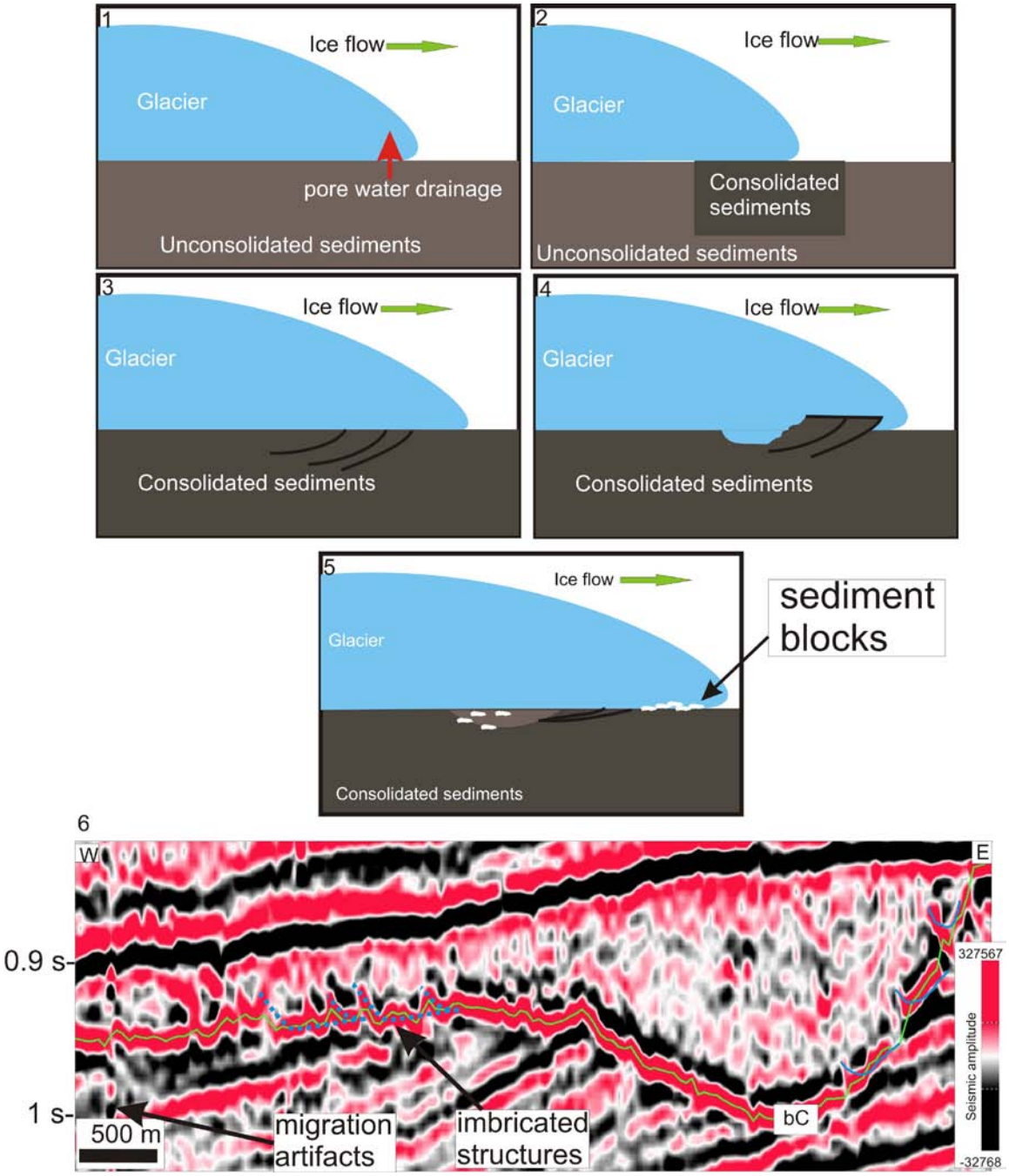

Figure 5.8: Schematic model for the formation of hill-hole pairs and later erosion by glacier. **1**. Advance of glacier and pore water drainage under the ice. **2**. Consolidated sediments are formed due to water drainage. **3.** Thrust faulting occurs. **4.** Glacier displaces sediments. **5.** Glacier deposits sediment blocks in front of the glacier. The white areas represent sediment blocks displaced from the substrate (not to scale). **6**. Seismic profile along the depression on reflector bC showing the imbricate structures interpreted as blocks.

5.3. Paleo-ice streams in the Veslemøy High area

MSGLs in the Veslemøy High 3D area (fig.6.3) and sediment blocks with a preferred E-W orientation have been interpreted within unit C and F (fig.5.6, fig.4.37). These provide clear evidence that grounded ice has reached the study area since at least reflector bC age. This interpretation is in agreement with Andreassen et al. (2004), who showed similar features in the Sørvestnaget Basin 3D area, west of the study area.

Paleo-ice streams at base of unit C (1.3-1.5 Ma)

On reflector bC, MSGLs and depressions associated with sediment blocks within unit C (fig.5.10) indicate ice flow in a E-W direction. Based on the orientation of these features, two possible sources for the ice can be inferred:

1) Ice Stream draining out Ingøydjupet from the Scandinavian Ice Sheet.
2) Ice Stream draining out Bjørnøyrenna from the Barents Sea and Svalbard Ice Sheet.

On a map showing depth to URU (fig.5.10), there is evidence of a high north of Djuprenna (paleo-Nordkappbanken), which makes it difficult to elucidate whether the ice streams drained out of Ingøydjupet or Bjørnøyrenna. Previous work carried out in the Sørvestnaget 3D area points towards the interpretation of an ice stream draining out the Bjørnøyrenna (Andreassen et al., 2004); however MSGL in the Veslemøy High 3D area do not show clear proof of that ice stream, although the presence of a high north of Djuprenna, make it probable that an ice stream was active at this time draining from the Scandinavian Ice Sheet. This interpretation is based on the morphology of URU and the presence of the high north of Djuprenna. Further work on 3D seismic datasets within Ingøydjupet is needed to confirm whether this trough was occupied by an ice stream from the Scandinavian Ice Sheet at this time.

Paleo-ice streams in unit GIII

After the formation of URU (reflector bE), it is interpreted that the main ice streams draining out the study area were from the Barents Sea and Svalbard Ice Sheet (fig.5.10). The variation in the orientation in MSGLs orientation reflects the dynamic nature of the ice streams, probably related to changes in the temperature conditions. Reflector intraF shows the clearest evidence of this dynamic behaviour of the ice streams where two divergent sets of MSGL are interpreted to be formed by two different ice flows.

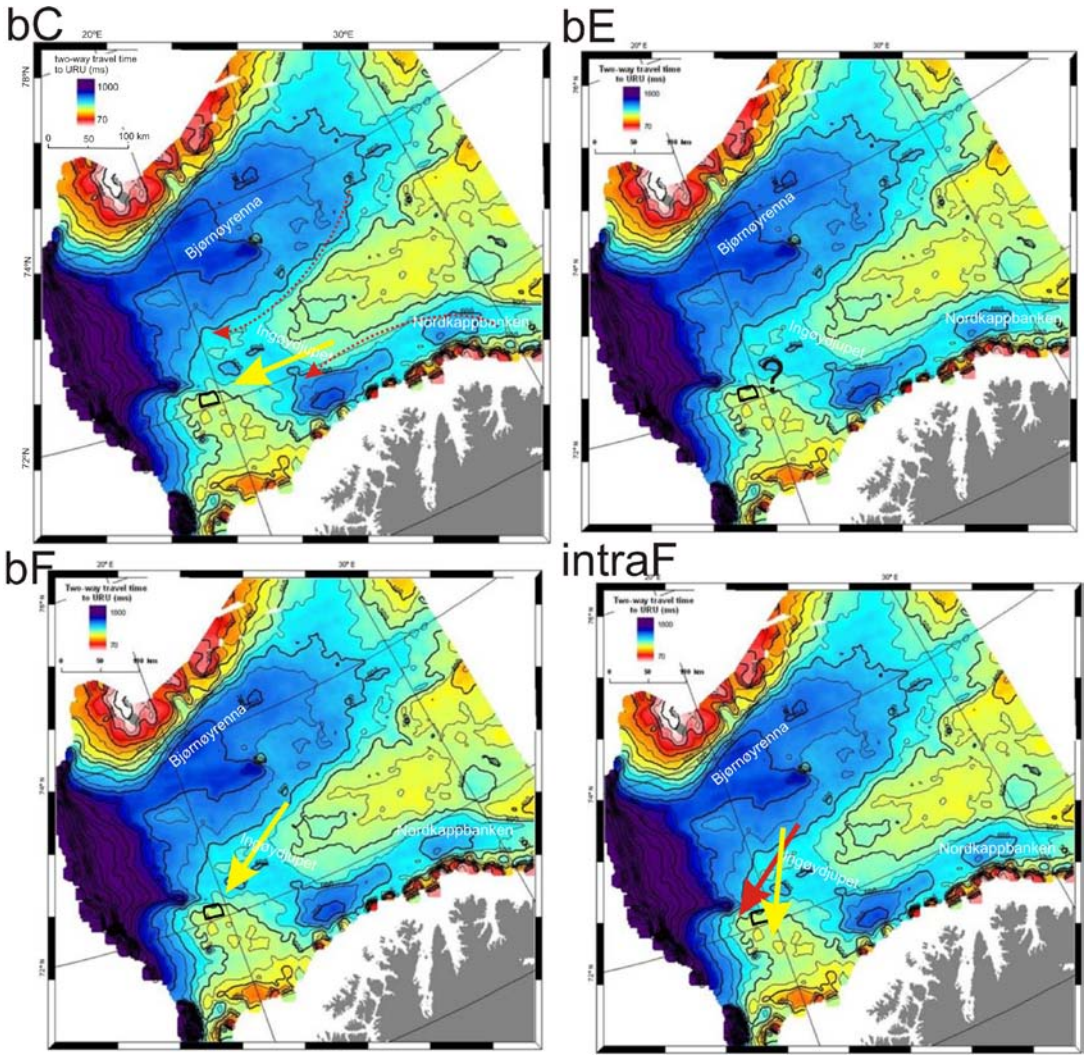

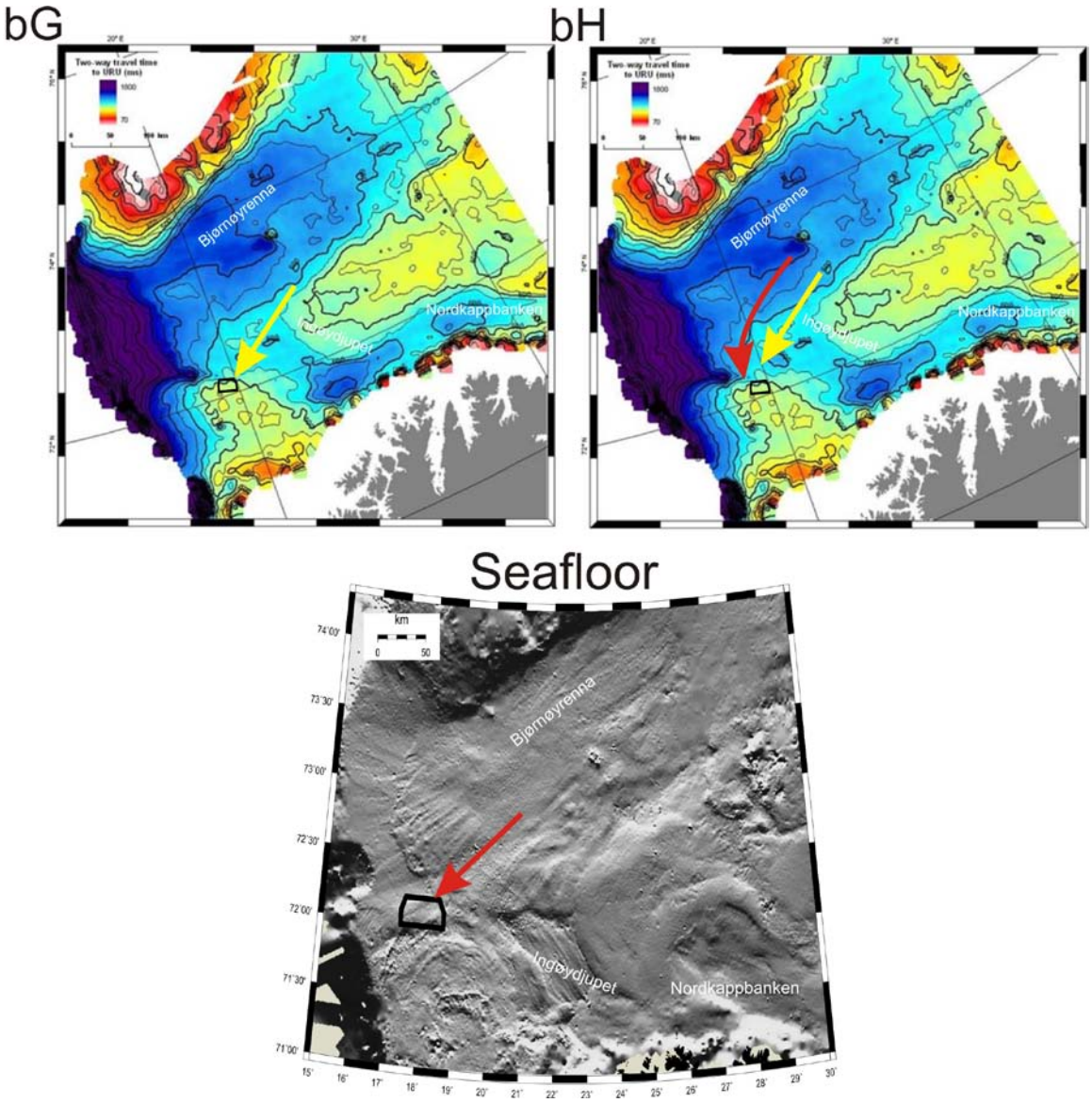

Figure 5.10: Inferred ice flow orientation during glaciations in all the interpreted horizons. Black rectangle shows the 3D dataset and the arrows indicate the inferred orientation of the ice flows. Figures bC-bH show the orientation of MSGL on a map showing depth in ms to URU (Andreassen et al., in prep.). Seafloor is a shaded relief map of the southwestern Barents Sea seafloor based on a 2D seismic grid modified from Andreassen et al. (2008).

6. CONCLUSIONS

This Master Thesis is based on the interpretation of a semiregional survey of three-dimensional (3D) seismic data on the Veslemøy High area and supported by some industry two-dimensional (2D) seismic data from the southwestern Barents Sea (fig.1.1 and 2.1). The study focused on the main seismic unconformities and seismic units within the Late Plio-Pleistocene sediments. The main conclusions from this work are:

1) The Plio-Pleistocene in the Veslemøy High area is divided into six sediment units. These units are separated by glacially eroded paleo-surfaces.

2) In the Veslemøy High 3D area, sedimentary package GI represents sediments from the paleo-slope, while sedimentary package GII and GIII represent sediments from the paleo-shelf.

3) Submarine channels with a downslope (E-W) orientation at the base of unit A are inferred to have been formed by turbidity currents originating from glacial meltwater.

4) From reflector bC to the seafloor, megascale glacial lineations have been mapped on all the seismic reflectors (except bE). This is interpreted as evidence of grounded ice, which reached the study area at least six times since the time of formation of bC.

5) Investigation of the megascale glacial lineations indicates that they were formed by basal erosion of soft-wet till underneath an ice-stream with residual accumulation of sediment at the sides. This is consistent with the theory of Tulazcyk et al. (2001) and Clark et al. (2003).

6) 3D attribute maps show evidence of sediment blocks in two seismic units. Some of these sediment blocks are aligned with the same orientation as MSGL at the base of the units where the blocks are seen in. The same ice stream that formed the megascale glacial

lineation is interpreted to have eroded the sediment blocks, transported them and deposited them in small chains orientated with ice flow direction.

7) Three large depressions at the base of unit C associated with sediment blocks accumulated west of the depressions are interpreted as part of hill-hole pairs. A model for glaciotectonism related to a consolidated sediment layer caused by subglacial freezing proposed by Sættem (1990) is used to explain the formation of the hill-hole pairs. Imbricate structures downstream of the depressions are inferred to reflect the thrust faulting during the formation of the hill-holes pairs.

8) All the erosional surfaces within seismic unit GIII indicate that an ice stream draining out of Bjørnøyrenna dominated the Veslemøy High area during this period. Seismic reflector bC has evidence of a E-W oriented ice stream activity, however it is not possible to elucidate whether this ice stream drained out of Bjørnøyrenna or Ingøydjupet.

REFERENCES

Aber, J.S. 1988: Spectrum of constructional glacitectonic landforms. In. Golthwait & Matsch (eds.). *Genetic classification of Glacigenic Deposits.*281-292. Balkema, Rotterdam.

Aber J.S., Croot, D. G. & Fenton, M. M. 1989: *Glacitectonic landforms and structures.* 201 pp. Kluwer Academic Publisher, Dordrecht.

Andreassen, K., Nilssen, L.C., Rafaelsen, B., Kuilman, L. 2004: Three-dimensional seismic data from the Barents Sea margin reveal evidence of past ice streams and its dynamics. *Geology* 32, 729-732.

Andreassen, K., Ødegaard, C.M. & Rafaelsen, B. 2007a: Imprints of former ice streams, imaged and interpreted using industry three-dimensional seismic data from the south-western Barents Sea. In Davies, R.J., Posamentier, H.W., Wood, L.J. & Cartwright, J.A (eds.): *Seismic Geomorphology: Applications to Hydrocarbons Exploration and Production*. *Geological Society, London, Special publication 277,* 151-169.

Andreassen, K., Nilssen, E. G. & Ødegaard, C. 2007b: Analysis of shallow gas and fluid migration within the Plio-Pleistocene sedimentary succession of the SW Barents Sea continental margin using 3D seismic data. *Geo-Mar Letters* 27, 155-171.

Andreassen, K., Laberg, J.S. and Vorren, T.O., 2008: Seismic seafloor geomorphology of the SW Barents Sea and its glaci-dynamics implications. *Geomorphology* 97, 157-177.

Astakhov, V.I., Kaplynaskaya, F.A., Tarnogradsky, V.D. 1996: Pleistocene permafrost of West Siberia as a deformable glacier bed. *Permafrost and periglaciar processes 7,* 165-191.

Bacon, M., Simm, R. & Redshaw, 2007: *3-D Seismic Interpretation*. 225 pp. Cambridge University Press.

Badley, M.E. 1985: *Practical Seismic Interpretation*. 266 pp. Boston, International Human Resources Development Corporation.

Benn, D. I & Evans, D. J. A. 1998: Glaciers and Glaciation. 734 pp. Arnold.

Bennet, 2003: Ice streams as the arteries of an ice sheet: their mechanics, stability and significance. *Earth-Science Reviews 61,* 309-339.

Bluemle, J.P. 1970: Anomalous hills and associated depressions in Central North Dakota. *Geological Society of America. Abstracts with Programs* 2, 325-326.

Bluemle, J.P. & Clayton, L. 1984: Large-scale glacial thrusting and related processes in North Dakota. *Boreas* 13, 279-299.

Branney, M.J. 1995: Downsag and extension at calderas: new perspectives on collapse geometries from ice-melt, mining, and volcanic subsidence. *Bulletin of Vulcanology57,* 303-318.

Branney, M.J. & Gilbert, J.S. 1995: Ice-melt collapse pits and associated features in the 1991 lahar deposits of Volcán Hudson, Chile: criteria to distinguish eruption-induced glacier melt. *Bulletin of vulcanology* 57, 293-302.

Breivik, A.J., Faleide, J.I., Gudlaugsson, S.T. 1998: Southwestern Barents Sea margin: late Mesozoic sedimentary basins and crustal extension. *Tectonophysics 293,* 21-44.

Brown, A.R., 2003: Interpretation of three-dimensional seismic data. 541 pp. *Tulsa, American Association of Petroleum Geologists, 6th Edition.*

Bulat, J. & Long, D., 2001: Images of the seabed in the Faroe-Shetland Channel from commercial 3D seismic data. *Marine Geophysical Researches* 22, 345-367.

Bulat, J., 2005: Some considerations on the interpretation of seabed images in the Faroe-Shetland Channel from commercial 3D seismic data. *Marine geophysical Research* 22, 345-367.

Butt, F.A., Elverhøi, A., Solheim, A., C.F. Forsberg, C.F., 2000: Deciphering Late Cenozoic

development of the western Svalbard Margin from ODP Site 986 results. *Marine Geology* 169, 373-390.

Butt, F.A., Drange, H., Elverhøi, A., Otterå, O.H., Solheim, A. 2002: Modeling Late Cenozoic isostatic elevation changes in the Barents Sea and their implications for oceanic and climatic regimes: preliminary results. *Quaternary Science Reviews* 21, 1643-1660.

Canals, M. Urgeles, R., & Calafat, A. M. 2000: Deep sea-floor evidence of past ice streams off the Antarctic Peninsula. *Geology* 28, 31-34.

Cartwright, J. & Huuse, M., 2005: 3D seismic technology: the geological "Hubble". *Basin Research* 17, 1-20.

Christoffersen, P. & Tulaczyk, S. 2003: Response to subglacial sediments to basal freez-on: I. Theory and comparation to observations from beneath the west Antarctic ice sheet. *Journal of Geophysical Research-Solid Earth 18*

Clark, C.D. 1993: Mega-scale glacial lineations and cross-cutting ice-flow landforms. *Earth surface processes and landforms* 18, 1-19.

Clark, C.D., Tulaczyk, S. M., Stokes, C. R., Canals, M. 2003: A groove-ploughing theory for the production of mega-scale glacial lineations, and implications for ice-stream mechanics. *Journal of Glaciology* 49, 240-256.

Clayton, L. & Moran, S.R. 1974: A glacial process-form model. In Coates, D.R. 8d.): Glacial Geomorphology. SUNY- *Birghampton Published in Geomorphology. Birghampton, New York*, 89-119.

Conway, H., Catania, g., Raymond, C.F., Gades, A.M., Scambos, T.A., Engelhardt, H. 2002: Switch of flow direction in an Antarctic ice stream, *Nature 419*, 465-467.

Dahlgren, K. I. T., Vorren, T.O., Stoker, M.S., Nielsen, T., Nygård, A., Sejrup, H.P. 2005: Late Cenozoic prograding wedges on the NW European continental margin: their formation and relationship to tectonics and climate. *Marine and Petroleum Geology* 22, 1089-1110.

Denton, G.H. & Hughes, T.J. 1981: The Arctic Ice Sheet: An outrageous hypothesus. In: Denton, G.H. & Hughes, T.J (eds.), *The Last Great Ice Sheets*, Wiley, New York.

Doré, A.G., Lundin, E.R., Jensen, L.N., Birkeland, Ø., Eliassen, P.E., Fichler, C. 1999: Principal tectonic events in the evolution of the northwest European Atlantic Margin. In: Fleet, A.J., Boldy, S.A.R. (eds.), *Petroleum Geology of Northwest Europe: Proceedings of the Fifth conference*, pp.41-61.

Dowdeswell, J.A., Villinger, H., Whittington, R.J., Marienfeld, P. 1993: Iceberg scouring in Scoresby Sund and on the East Greenland continental shelf. *Marine Geology*, 111. 37-53.

Dowdeswell, J.A., Elverhøi, A. & Spielhagen, R. 1998: Glacimarine Sedimentary Processes and facies on the polar north Atlantic Margins. *Quaternary Science Reviews* 17, 243-272.

Dowdeswell, J.A. & Elverhøi, A. 2002: The timing of initiation of fast-flowing ice streams during a glacial cycle inferred from glacimarine sedimentation. *Marine Geology 188*, 3-14.

Dowdeswell, J.A. & Bamber, J.L. 2007: Keel depths of modern Antarctic icebergs and implications for seafloor scouring in the geological record. *Marine Geology* 243. 120-131.

Eidvin, T. and Riis, F. 1989: Nye dateringer av de tre vestligste borehullene i Barentshavet. Resultater og konsekvenser for den Tertiære hevningen. *Norwegian Petroleum Direktoratet Contibution No* 27, 54 pp.

Eidvin, T., Jansen, E., Riis, F. 1993: Chronology of Tertiary fan deposits off the Western Barents Sea: Implications for the uplift ad erosion history of the Barents Shelf. *Marine Geology* 112, 109-131.

Eldholm, O., Faleide, J.I., Myrhe, A.M. 1987: Continental-ocean transition at the western Barents Sea/Svalbard continental margin. *Geology* 15, 1118-1122.

Elverhøi, A., Dowdeswell. J.A., Fundel, S., Mangerud, J., Stein, R. 1998: Late Cenozoic Erosion and sediment yield from the Svalbard-Barents Sea region: Implications for understanding erosion of glacierized basins. *Quaternary Science Reviews* 17, 209-241.

Eyles, N. & Eyles, C.H. 1992: Glacial depositional systems. In Walker, R.G. & James, N.P. (eds.), *Facies models. Response to sea level change.* Geological Association of Canada, Canada, pp 73-100.

Faleide, J.I., Gudlaugsson, T. & Jacquart, G. 1984: Evolution of the western Barents Sea. *Marine and Petroleum Geology* Vol. 1, 123-150.

Faleide, J.I., Myhre, A.M., Eldholm, O. 1988: Early tertiary volcanism at the western Barents Sea margin. In: Morton, A. C. & Parson, L. M. (eds.): *Early Tertiary Volcanism and the opening of the NE Atlantic.*135-146. *Geological Society. London Special Publications.*

Faleide, J.I., Vågnes, E. & Gudlaugsson, T. 1993: Late Mesozoic-Cenozoic evolution of the south-western Barents Sea in a regional rift-shear tectonic setting. *Marine and Petroleum Geology* 10, 186-214.

Faleide, J.I., Solheim, A., Fiedler, A., Hjelstuen, B.O., Andersen, E. S., Vanneste, K. 1996: Late Cenozoic Evolution of the Western Barents Sea-Svalbard continental margin. *Global and Planetary Change* 1, 53-74.

Faleide, J. I., Tsikalas, F., Breivik, A. J., Mjelde, R., Ritzmann, O., Enger, Ø., Wilson, J., Eldholm, O. 2008: Structure and evolution of the continental margin off Norway and the Barents Sea. *Episodes, vol.31,* No. 1. *1-10.*

Fiedler, A. & Faleide, J.A. 1996: Cenozoic sedimentation along the southwestern Barents Sea margin in relation to uplift and erosion of the shelf. *Global and Planetary Change 12,* 75-93.

Forsberg, C.F., Solheim, A., Elverhøi, A., Jansen, E., Channell, J.E.T., Andersen, E.S. 1999: The depositional environment of the western Svalbard margin during the late Pliocene and the Pleistocene: Sedimentary facies changes at Site 986. In: Raymo, M., Jansen, E., Blum, p., Herbert, T.D. (eds): *Proceeding Ocean Drilling Program. Scientific results, vol. 162*. 233-246. Ocean Drilling Program, College Station, TX.

Gabrielsen, R.H., Færseth, R.B., Jensen, L.N., Kalheim, J.E., Riis, F. 1990: Structural elements of the Norwegian continental shelf. Part I: The Barents Sea Region. NPD-Bulletin no 6. Oljedirektoratet. 33 pp.

Harland, W.B. 1965: The tectonic evolution of the Arctic-North Atlantic region. *Royal Soc. London Philos. Trans.* 258, 59-75.

Harris, C., Williams, G., Brabham, P., Eaton, G., McCarroll, D. 1997: Glacitectonized Quaternary sediments at Dinas Dinlle, Gwynedd, North Wales, and their bearing on the style of deglaciation in the eastern Irish Sea. *Quaternary Science Reviews* 16, 109-127.

Jakobsson, M., Macnab, R. & Members of the Editorial Board, IBCAO. International Bathymetric Chart of the Arctic Ocean.

Jansen, E. & Sjøholm, J. 1991: Reconstruction of glaciations over the past 6 Myr from ice-borne deposits in the Norwegian Sea, *Nature* 349, 600-603.

Jansen, E., Raymo, M.E., Blum, P. et al. 1996: Proceedings of the Ocean Drilling Program, *Initial reports,162, Ocean Drilling Program*. College Station, TX.

Jessen, A. 1931: Londstrup klint. *Danmarks Geologisk Undersogelse,* IV raekke 2 (8), 26 pp.

Junttila, J., Lathinen, T., Strand, K. 2008: Provenance and sea-ice transportation of Mid-Pliocene and Quaternary sediments, Yermak Plateau. Arctic Ocean (ODP Site 911). *Boreas* 37. 273-285.

Kleman, J. & Stroeven, A.P. 1997: Preglacial surface remnants and Quaternary glacial regimes in northwestern Sweden. *Geomorphology 19,* 35-54.

Knies, J., Matthiessen, J., Vogt, C., Stein, R. 2002: Evidence of Mid-Pliocene (~ 3 Ma) global warmth'

in the eastern Arctic Ocean and implications for the Svalbard/Barents Sea ice sheet during the late Pliocene and early Pleistocene (~ 3-1.7 Ma). *Boreas* 31. 82-93.

Knies, J., Matthiessen, J., Vogt, C., Laberg, J.S., Hjelstuen, B. O., Smelror, M., Larsen, E., Andreassen, K., Eidvid, T., Vorren, T.O. 2009: The Plio-Pleistocene glaciation of the Barents Sea-Svalbard region: a new model based on revised chronostratigraphy. Quaternary Science Reviews, 28, 812-829.

Kuvaas, B. & Kristoffersen, Y. 1996: Mass movements in glacimarine sediments on the Barents Sea continental slope. *Global and Planetary Change* 12, 287-307.

Laberg, J.S. & Vorren, T.O. 1995: Late Weischselian submarine debris flow deposits on the Bear Island Trough Mouth Fan. *Marine Geology* 127, 45-72.

Laberg, J.S. & Vorren, T.O. 1996: The Middle and Late Pleistocene evolution of the Bear Island Trough Mouth Fan. *Global and Planetary Change* 12, 309-330.

Laberg, J.S., Andreassen, K., Knies, J., Vorren, T.O., Winsborrow, M. (submitted): Late Pliocene-Pleistocene development of the Barents Sea Ice Sheet.

Landvik, J.Y., Bondevik, S., Elverhøi, A., Fjeldskaar, W., Mangerud, J., Salvigsen, O., Siegert, M. J., Svendsen, J. I., Vorren, T. O. 1998: The Last Glacial Maximum of Svalbard and the Barents Sea area: Ice Sheet extent and configuration. *Quaternary Science Reviews* 17, 43-75.

Larsen, E., Andreassen, K., Nilssen, L. & Raundalen, S. 2003: The prospectively of the Barents Sea: Ice ages, erosion and tilting of traps. *NGU Report* 102, 60 pp.

Larsen, E., Kjaer, K.H., Demidov, I.N., Funder, S., Grosfjeld, K., Houmark, N.M., Jensen, M. Linge, H. & Lysa, A., 2006: Late Pleistocene glacial and lake history of northwestern Russia. *Boreas* 25, 394-434.

Lien, R. 1983: Pløyemerker etter isfjell på norsk kontinentalsokkel. *Doktorgradsoppgave. Institutt for kontinentalsokkelundersøkelser 109*, 147 pp.

Longva, O. & Thorsnes, T. (1997): Skagerrak in the past ant at the present – an integrated study of geology, chemistry, hydrography and microfossil ecology. *Norsk Geologisk Undersøkelsen Special Publication 8.*

Mathews, W.H. & Mackay, F.R.S.C. 1960: Deformation of soils by glacier ice and the influence of pore pressure and permafrost. *Transactions of the Royal Society of Canada* 54-3, 27-36.

Marfurt, K.J., Scheet, R.M., Sharp., J.A., Harpert, M.G. 1998: Suppression of the acquisition footprints from seismic sequence attribute mapping. *Geophysics 62*, 1774-1778.

Mangerud, J., Jansen, E., Landvik; J.Y. 1996: Late Cenozoic history of the Scandinavian and Barents Sea ice sheets. *Global and Planetary Change, 12*, 11-26

Mangerud, J., Dokken, T., Hebbeln, D. Heggen, B., Ingólfsson, Ó, Landvik, J. Y., Mejdahl, V., Svendsen, J. I., Vorren, T. O. 1998: Fluctuations of the Svalbard-Barents Sea Ice Sheet during the Last Glacial Maximum. *Quaternary Science Reviews* 17, 11-42.

Moran, S.R., Clayton, L., Hooke, R. LeB., Fenton, M.M, Andriasheck, L.D. 1980: Glacier-bed landforms of the prairie region of North America. *Journal of Glaciology* 25, 457-476.

Mudelsee, M. & Raymo, M.E. 2005: Slow dynamics of the Northern Hemisphere glaciation. Paleoceanography 20, PA4022, doi:10.1029/2005PA001153

Myhre, A.M., Eldholm, O., Sundvor, E. 1982: The margin between Senja and Spitsbergen Fracture Zones: implications from plate tectonics. *Tectonophysics 89*, 33-50.

Nilssen, L.C. 2000: Studier av kenozoiske erosjonflater på den sørvestlige Barentshav marginen. *Unpublished Cand. Scient. Oppgave i Geologi.* Universitet i Tromsø. 156 pp.

Nyland, B., Jensen, L. N., Skagen, J., Skarpnes, O. and Vorren, T. O. 1992: Tertiary uplift and erosion in the Barents Sea: magnitude, timing and consequences. In Larsen, R. M., Brekke, H., Larsen, B. T. & Talleraas, E. (eds.): Structural and tectonic modeling and its applications to

petroleum Geology, 153-162. Elsevier, Amsterdam.

Nøttvedt, A., Berglund, T., Rasmussen, E., and Steel, R. 1988: Some aspects of Tertiary tectonics and sediments along the Western Barents Shelf. In: Early Tertiary Volcanism and the opening of the NE Atlantic in A. C. Morton and L. M. Parson (eds.) *Geological Society Special Publications* 39, 421-425.

Ó'Cofaigh, C., Pudsey, C.J., Dowdeswell, J.A., Morris, P., 2002: Evolution of subglacial bedforms along a paleo-ice stream, Antarctica Peninsula continental shelf. *Geophysical Research Letters 29*, 1199.

Ó'Cofaigh, C., Dowdeswell, J.A., Allen, C.S., Hiemstra, J.F., Pudsey, C.J., Evans, J., Evans, D. J. A. 2005: Flow dynamics and till genesis associated with a marine-based Antarctica paleo-ice stream. *Quaternary Science Review* 24, 709-740.

Ottesen, D., Dowdeswell, J. A. & Rise, L., 2005: Submarine landforms and the reconstruction of fast-flowing ice streams within a large Quaternary ice sheet: The 2500-km-long Norwegian-Svalbard margin (57º-80ºN). *GSA Bulletin* 117, 1033-1050.

Ottesen, D., Dowdeswell, J.A., Benn, D.I., Kristensen, L., Christiansen, H.H., Christensen, O., Hansen, L., Lebesbye, E., Forwick, M., Vorren, T.O. 2008: Submarine landforms characteristic of glacier surges in two Spitsbergen fjords. *Quaternary Science Reviews 27*, 1583-1599.

Pedersen, S.A.S., 2000: Superimposed deformation in glacitectonics. *Bulletin of the Geological Society of Denmark* 46, 125-144.

Rafaelsen, B., Andreassen, K., Kuilman, L., Lebesbye, E., Hogstad, K., Midtbø M. 2002: Geomorphology of buried glacigenic horizons in the Barents Sea from three-dimensional seismic data. In Dowdeswell, J. A. & Ó Cofaigh, C. (eds.) *Glacier-influenced sedimentation on high-latitude continental margins.* London, Geological Society, Special Publications 203, 259-276.

Rafaelsen, B., Andreassen, K., Hogstad, K., Kuilman, L. W. 2007: Large-scale glacitectonic-imbricated thrust sheets on three-dimensional seismic data: facts or artifacts? *Basin Research* 19. 87-103.

Rasmussen, E. & Fjeldskaar, W. 1996: Quantification of the Pliocene-Pleistocene erosion of the Barents Sea from present-day bathymetry. *Global and Planetary Change* 12, 119-133.

Richardsen, G., Henriksen, E, Vorren, T.O. 1991: Evolution of the Cenozoic sedimentary wedge during rifting and seafloor spreading west of the Stappen High, western Barents Sea. *Marine Geology 101*, 11-30.

Riis & Fjeldskaar, W. 1992: On the magnitude of the late tertiary and Quaternary erosion and its significance for the uplift of Scandinavia and Barents Sea. In: Larsen, R.M., Brekke, H.,Larsen, B.T., Talleraas, E. (eds.): *Structural and tectonic modeling and its application to Petroleum Geology, NPF Special Publications* 1,163-185. Elsevier, Amsterdam.

Rowley, D.B. & Lottes, A.L. 1988: Plate-Kinematic reconstructions of the North Atlantic and Arctic: Late Jurassic to present. *Tectonophysics* 155, 73-120.

Røthlisberger, H. & Iken, A. 1981: Plucking as an effect of water pressure variations at the glacier bed. *Annals of Glaciology 2*,57-62.

Ruszczynska-Szenajch, H. 1976: Glacitectonic depressions and glacial rafts in mid-eastern Poland. *Studia Geologica Polonica* 1, 87-106.

Ruszczynska-Szenajch, H. 1978: Glacitectonic origin of some lake-basins in areas of Pleistocene glaciations. *Polish Archiwum Hydrobiologii*, 25 (1/2), 373-381.

Ryseth, A., Auguston, J.H., Charnock, M., Haugerud, O., Knutsen, S. M., Midbøe, P. S., Opsal, J.G., Sundbø, G. 2003: Cenozoic stratigraphy and evolution of the Sørvestnaget Basin,

southwestern Barents Sea. *Norwegian Journal of Geology* 83, 107-130.

Sejrup, H. P., Hjelstuen, B. O., Dahlgren, K. I. T., Haflidason, H., Kuijpers, A., Nygård, A., Praeg, D., Stoker, M. S., Vorren, T. O. 2005: Pleistocen Glacial History of the NW European continental margin. *Marine and Petroleum Geology* 22, 1111-1129.

Shaw, J., Piper, D.J.W., Fader, G.B.J., King, E.L., Todd, B.J., Bell, T., Batterson, M.J., D.J.E. Liverman, 2006: A conceptual model of the deglaciation of Atlantic Canada. *Quaternary Science Reviews* 25, 2059-2081.

Sheriff, R., 1980: Seismic Stratigraphy. 227 pp. *Boston, International Human Resources Development Corporation.*

Solheim, A. & Kristoffersen, Y. 1984: Sediments above the upper regional unconformity: thickness, seismic stratigraphy and outline of the glacial history. Nor. Polarinst. Skr., 179B, 26 pp.

Solheim, A., Russwarm, L., Elverhøi, A., Nyland Berg, M. 1990: Glacial geomorphic features: direct evidence for grounded ice in the northern Barents Sea and implications for the pattern of deglaciation and late glacial sedimentation. In: Dowdeswell, J.A. & Scouse, J.D. (eds.) *Glacimarine Environments: Processes and Sediments. Geological Society, London, Special Publication 53*, 253-268.

Solheim, A., Andersen, E. S., Elverhøi, A., Fiedler, A. 1996: Late Cenozoic depositional history of the western Svalbard continental shelf, controlled by subsidence and climate. *Global Planetary Change* 12, 135-148.

Solheim, A., Faleide, J.I., Andersen, E.S. et al. 1998: Late Cenozoic seismic stratigraphy and glacial geological development if the East Greenland and Svalbard-Barents Sea continental margin. *Quaternary Science Reviews* 17, 155-184.

Spencer, A.M., Home, P.C., Berglund, L.T. 1984: Tertiary structural development of the western Barents Shelf: Troms to Svalbard. 119-209. Graham & Trotman, London.

Stokes, C. R. & Clark, C. D. 1999: Geomorphological criteria for identifying Pleistocene ice streams. *Annals of Glaciology* 28, 67-75.

Stokes, C. R. & Clark, C. D. 2001: Paleo-ice streams. *Quaternary Science Review* 20, 1437-1457.

Stokes, C. R. & Clark, C. D. 2002: Are long subglacial bedforms indicative of fast ice flow? *Boreas* 31, 239-249.

Stoker, M.S. 2002: Late Neogene development of the UK Atlantic margin. In: Doré, A.G.D., Cartwright, J., Stoker, M.S., Turner, J.P., White, N. (eds.), *Exhumation of the North Atlantic Margin: Timing, Mechanisms and Implications for the Petroleum Exploration Special Publications 196*. Geological Society, London, 313-329.

Stoker, M.S., Praeg, D., Shannon, P.M., Hjelstuen, B.O., Laberg, J.S., Nielsen, T., van Weering, T.C.E., Sejrup, H.P., Evans, D. 2005: Neogene evolution of the Atlantic continental margin of NW Europe (Lofoten Islands to SW Ireland): anything but passive. In Doré, A.G., Vining, B. (eds.), Petroleum Geology of Northwest Europe. *Proceedings of the Sixth Conference. Geo Society London*, pp. 1057-1076.

Svendsen, J. I., Alexanderson, H., Astakhov, V. I., Demidov, I., Dowdeswell, J. A., Funder, S., Gataullin, V., Henriksen, M., Hjort, C., Houmark-Nielsen, M., Hubberten, H. W., Ingólfsson, Ó., Jakobsson, M., Kjær, K. H., Larsen, E., Lokrantz, H., Lunkka, J. P., Lysså, A., Mangerud, J., Matiouchkov, A., Murray, A., Möller, P., Niessen, F., Nikolskaya, O., Polyak, L., Saarnisto, M., Siegert, C., Siegert, M. J., Spielhagen, R. F., Stein, R. 2004: Late Quaternary ice sheet history of northern Eurasia. *Quaternary Science Reviews* 23, 1229-1271.

Swithinbank, C.W.M. 1954: Ice streams. *Polar record 7*, 185-186.

Syvitski J.P.M., Stein, A.B., Andrews, J.T., 2001. Icebergs and the Sea Floor of the East Greenland

(Kangerlussuaq). Continental Margin. *Arctic, Antarctic, and Alpine Research* 33, 52-61.
Sættem, J, 1990: Glacitectonic forms and structures on the Norwegian continental shelf: observations, processes and implications. *Norsk. Geologisk Tidsskrift* 70, 81-94.
Sættem, J., Poole, D. A. R., Ellingsen, L., Sejrup, H. P. 1992: Glacial Geology of outer Bjørnøyrenna, southwestern Barents Sea: preliminary results. *Norsk Geologisk Tidsskrift 71*, 173-177.

Sættem, J., Poole, D. A. R., Ellingsen, L., Sejrup, H. P. 1992: Glacial Geology of outer Bjørnøyrenna, southwestern Barents Sea. *Marine Geology* 103, 233-325.
Sættem, J., Bugge, T., Fanavoll, S., Goll, L.M., Mørk, A., Mørk, M. B. E., Smelror, M., Verdenius, J. G. 1994: Cenozoic margin development and erosion of the Barents Sea: Core evidence from southwest of Bjørnøya. *Marine Geology* 118, 257-281.
Sættem, J. 1994: Glacitectonic structures along the southern Barents shelf margin. In. Warren & Croot (eds.): *Formation and Deformation of Glacial Deposits*. 19 pp. Balkema, Rotterdam.
Talwani, M. & Eldholm, O. 1977: Evolution of the Norwegian-Greenland Sea. *Geological Society of America. Bulletin* 88, 969-999.
Thiede, J., Eldholm, O., Taylor., E. 1989: Variability of Cenozoic Norwegian- Greenland Sea paleoceanography and northern hemisphere paleoclimate, in: Eldholm, O., Thiede, J., Taylor, E., et al. (eds): *Proceeding Ocean Drilling Program, Scientific Results* 104, 1067-1118.
Tulaczyk, S. M., Scherer, R. P., Clark, C. D. 2001: A ploughing model for the origin of weak tills beneath ice streams: a qualitative treatment. *Quaternary International* 86, 59-70.
Vorneberger, P.L. & Whillians, I.M. 1986: Surface features of ice stream B, Marie Byrd Land, West Antarctica. *Annals of Glaciology 8*, 168-170.
Vorren, T.O. & Laberg, J.S. 1997: Trough mouth fans – Paleoclimate and ice sheet monitors. *Quaternary Science Reviews 16*, 865-881.
Vorren, T.O., Hald, M., Lebesbye, E. 1988: Late Cenozoic environments in the Barents Sea. Paleoceanography 3 No.5, 601-612.
Vorren, T.O., Lebesbye, E., Andreassen, K., Larsen, K.B. 1989: Glacigenic sediments in the southern Barents Sea. In Dowdeswell, J.A.& Scourse, J.D. (eds): *Glacimarine environments: processes and sediments, 53.* Geological Society Special Publications, 269-288.
Vorren, T.O., Richardsen, G., Kutsen, S.M., Eriksen, H. 1991: Cenozoic erosion and sedimentation in the western Barents Sea. *Marine and Petroleum Geology* 8, 317-340.
Vorren, T.O., Laberg, J.S., Blaume, F., Dowdeswell, J. A., Kenyon, N. H., Mienert, J., Rumohr, J., Werner, F. 1998: The Norwegian-Greenland Sea continental margins: Morphology and Late Quaternary Sedimentary Processes and environment. *Quaternary Science Reviews* 17, 273-302.
Wood, R.J., Edrich, S.P, Hutchinson, I. 1990: Influence of the North Atlantic tectonics on the large-scale uplift of the Stappen High, western Barents Shelf. In: Tankard, A.J. and Balkwill, H.R. (eds.): *Extensional Tectonics and Stratigraphy of the North Atlantic Margins. AAPG Memories*, 46, 559-566.
Ziegler, P.A. 1978: North-Western Europe: tectonics and basins development, in: Van Loon, A.J. (Ed.): *Key-notes of the MEGS-II*, 589-626. Geolog. Mijnbouw 57, Amsterdam.
Ødegaard, C., 2005: 3D-seismisk geomorfologisk studie av paleoisstrømavsetninger på den sørvestlige Barentshav margin. *Unpublished Master thesis*. Universitetet i Tromsø. 143 pp.